



FEASIBILITY OF REHABILITATING TIMBER BRIDGES WITH MECHANICALLY FASTENED FRP STRIPS

Project 08-02
June 2008

Midwest Regional University Transportation Center
College of Engineering
Department of Civil and Environmental Engineering
University of Wisconsin, Madison



Authors:

Schorer, Alyssa E.; Bank, Lawrence C.; Oliva, Michael G.
University of Wisconsin, Madison WI
Wacker, James P.; Rammer, Douglas R.
Forest Products Laboratory, Madison WI

Principal Investigator: Lawrence Bank;
Professor, Department of Civil and Environmental Engineering, University of Wisconsin, Madison

DISCLAIMER

This research was funded by the Midwest Regional University Transportation Center. The contents of this report reflect the views of the authors, who are responsible for the facts and the accuracy of the information presented herein. This document is disseminated under the sponsorship of the Department of Transportation, University Transportation Centers Program, in the interest of information exchange. The U.S. Government assumes no liability for the contents or use thereof. The contents do not necessarily reflect the official views of the Midwest Regional University Transportation Center, the University of Wisconsin, the Wisconsin Department of Transportation, or the USDOT's RITA at the time of publication.

The United States Government assumes no liability for its contents or use thereof. This report does not constitute a standard, specification, or regulation.

The United States Government does not endorse products or manufacturers. Trade and manufacturers names appear in this report only because they are considered essential to the object of the document.

EXHIBIT B

Technical Report Documentation Page

1. Report No. MRUTC 08-02	2. Government Accession No.	3. Recipient's Catalog No. CFDA 20.701	
4. Title and Subtitle Feasibility of Rehabilitating Timber Bridges Using Mechanically Fastened FRP Strips		5. Report Date June, 2008	
		6. Performing Organization Code	
7. Author/s Alyssa E. Schorer, Lawrence C. Bank, Michael G. Oliva, James P. Wacker, Douglas R. Rammer		8. Performing Organization Report No. MRUTC 08-02	
9. Performing Organization Name and Address Midwest Regional University Transportation Center University of Wisconsin-Madison 1415 Engineering Drive, Madison, WI 53706		10. Work Unit No. (TRAIS)	
		11. Contract or Grant No. DTRS99-G-0005	
12. Sponsoring Organization Name and Address Wisconsin Department of Transportation Hill Farms State Transportation Building 4802 Sheboygan Avenue Madison, WI 53707		13. Type of Report and Period Covered Final Report [03/01/07 – 06/30/08]	
		14. Sponsoring Agency Code	
15. Supplementary Notes Project completed for the Midwest Regional University Transportation Center with support from the Wisconsin Department of Transportation.			
16. Abstract Many timber trestle railroad bridges in Wisconsin have experienced deterioration and are in need of rehabilitation. In addition, the railroad industry is increasing the weights of cars. The combined effect of heavier loads and deterioration threatens to cut short the service life of timber bridges. One of the most critical problems that has been identified was the overloading of timber piles in bridges, which can be remedied by creating a stiffer pile cap. The goal of this investigation was to show that mechanically fastened fiber reinforced polymer (MF-FRP) strips fastened to timber with screws can be used to create composite action between two beams in flexure or truss action between two deep beams. Ultimately this may help redistribute the loads to piles when FRP strips are used as struts on cap beams over short spans. Several test series were conducted with beams in flexure, deep beams over short spans, and full scale specimens to determine the manner in which FRP strips improved the members' performance. Tests were conducted over various widths of beams and lengths of spans to investigate how the geometry affected the strengthening's ability to create composite action. Next, the MF-FRP was tested on deep beams to determine if composite action was maintained. Lastly, full scale tests simulating a pile cap over 5 piles were run to see if composite action improved load distribution to piles. Mechanically fastened FRP strips were found to be effective in developing composite action in slender beams in flexure, meaning the stiffness of the system was increased by using MF-FRP strips. This MF-FRP method showed great potential for creating composite, stiffer double pile caps.			
17. Key Words Timber bridge, fiber reinforced polymer (FRP), mechanically fastened, pile cap, bridge rehabilitation, timber strengthening with composites		18. Distribution Statement No restrictions. This report is available through the Transportation Research Information Services of the National Transportation Library.	
19. Security Classification (of this report) Unclassified	20. Security Classification (of this page) Unclassified	21. No. Of Pages 192	22. Price -0-

Executive Summary

Feasibility of Rehabilitating Timber Bridges Using Mechanically Fastened FRP Strips

Project Summary

Many timber trestle railroad bridges in Wisconsin have experienced deterioration and are in need of rehabilitation. The goal of this investigation was to show that mechanically fastened fiber reinforced polymer (MF-FRP) strips fastened to timber with screws can be used to create composite action between two beams in flexure or truss action between two deep beams. Ultimately this may help redistribute the loads to piles when FRP strips are used as struts on cap beams over short spans. Tests were conducted to determine the effect of variables such as beam width and depth on composite action. Mechanically fastened FRP strips were found to be effective in developing composite action in slender beams in flexure, meaning the stiffness of the system was increased by using MF-FRP strips. This MF-FRP method showed great potential for creating composite, stiffer double pile caps.

Background

Timber railroad bridges in Wisconsin are often over 50 years old and have experienced deterioration. In addition, the railroad industry is increasing the weights of cars. The combined effect of heavier loads and deterioration threatens to cut short the service life of timber bridges. One of the most critical problems that has been identified was the overloading of timber piles in bridges, which can be remedied by creating a stiffer pile cap.

The technique of mechanically fastening FRP strips to timber members using screws is a new technology that had not previously been investigated thoroughly for wood. The MF-FRP technique has been used successfully on reinforced concrete members to strengthen them in flexure; this project investigated whether composite behavior could be attained between two timber members using the MF-FRP technique to bond the beams together. Successful composite action has the potential to improve the behavior of pile caps on timber trestle bridges. The implications of using the MF-FRP technique on timber members extends beyond pile caps and can benefit many aspects of the industry where strengthening is needed.

Process

Wood specimens used were Douglas Fir rough sawn lumber and Douglas Fir creosote treated timbers. The composite material was SAFSTRIP manufactured by Strongwell. Tests were completed over a 12 month span from June 2007 to June 2008 at the Forest Products Laboratory in Madison, WI.

The project was divided into two phases of testing. The two phases were developed by combining types of tests so that similar tests could be executed more quickly and

efficiently, and so that the results of the first phase might be helpful in the implementation of the second phase.

Test Phase 1: Width and Depth Series. Tests were conducted on small sized beams in flexural bending over two span lengths: 10'-6" and 5'. Specimens employed a variety of methods for simulating degrees of composite action: single members, stacked members, epoxied members, and members with MF-FRP strips fastened to the sides. Both the widths and depths of specimens were varied separately. The objectives were (1) to determine whether the width or depth of a beam affected the composite nature of MF-FRP beams, and (2) to determine whether the distance between supports affected the accuracy of results.

Test Phase 2: Full Scale and Dynamic Series. Tests were conducted on full-sized specimens close to actual pile cap size, which were provided by WSOR and were typical of the in-situ condition of a timber railroad bridge. Five supports were used to replicate the support condition of the piles. Static testing was completed on a variety of MF-FRP configurations and dynamic testing to 1 million cycles was completed on one MF-FRP configuration. The objectives were (1) to determine whether benefits of the MF-FRP method were applicable to continuous deep beams over multiple short spans, (2) to determine if loads could be redistributed using MF-FRP strips, and (3) to examine the behavior of the beam and determine whether it acts in accordance with design equations.

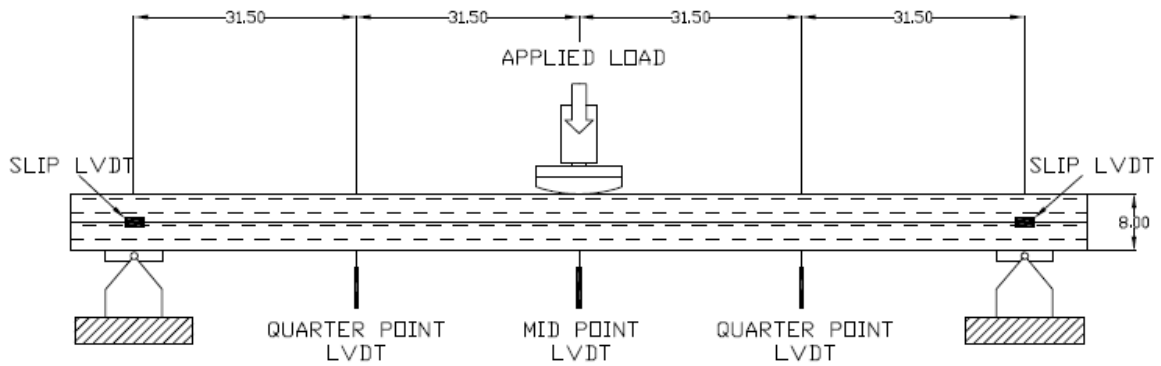
The test setup for Phase 1 was typical of a 3 point bending test for wood specimens. LVDTs, which use change in voltage to measure displacements, were used to collect deflection data, and strain gauges were utilized on the FRP. Data was collected using LabView. Phase 2 utilized a unique setup that was custom designed for this project. There were no supports or machines equipped to specifically replicate a beam with 5 pile-like supports and 2 point loading, so special parts were designed to fit the existing test area at the Forest Products Lab. LVDTs were used once again to measure deflections, and strain gauges were utilized on the FRP. All data was collected using LabView.



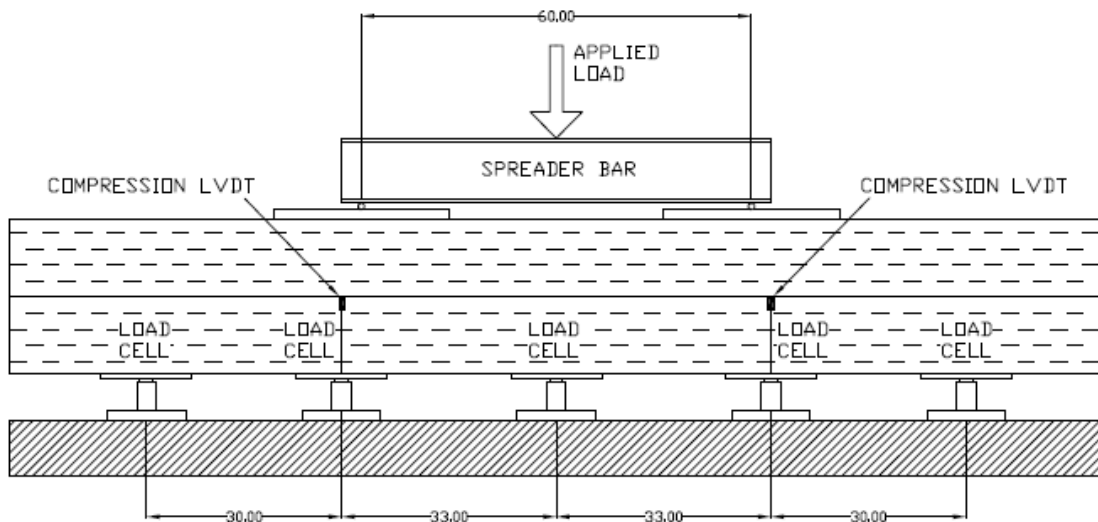
Douglas Fir timber specimens used in Phase 1 Tests.



Douglas Fir creosote treated timber specimens used in Phase 2 tests.



Test setup for Phase 1.



Test setup for Phase 2. Note the special loading condition of 2 plates and the 5 supports.

Findings and Conclusions

The results of this study conclude that (1) MF-FRP strips did not significantly improve load distributions to piles, but showed potential to do so by creating a stiffer composite pile cap, (2) MF-FRP strips increase the flexural stiffness of timber beams in bending with large span to depth ratios, (3) composite action between two timber members can be achieved with mechanically fastened FRP strips, and (4) while composite action may be achieved between two members, this is not enough to significantly improve the load distribution of double cap beams on timber trestle bridges which have severe overloading of piles. Where composite action is most likely to come into use on a trestle bridge is after one or more piles settles and is no longer in contact with the pile cap, causing the cap to span a longer distance between piles still in contact.



Mechanically fastened FRP strips on two stacked timbers.

A cost benefit analysis was not in the scope of this project, however it can be stated that MF-FRP strips can be applied with minimal amounts of labor, skills, or equipment. All specimens in this report were fabricated by students using drills, levels, and clamps. In addition, there is no epoxy mixing or application required, and the only hardware needed is screws. This provides an economical and quick solution, but a cost comparison to other methods is not available in this report.

The results in this report pertain specifically to beams in flexure and timber trestle bridge pile caps. The implications of the MF-FRP technique go beyond this application and extend into any timber strengthening needs in the industry. Any stacked combination of beams can be made composite through the MF-FRP method, improving the systems flexural stiffness. This may be useful for other members in timber bridges, or for rehabilitating other timber structures, like piers or decks.

Recommendations for Further Actions

This report describes the benefits available with the mechanically fastened FRP strip system. It is recommended that Wisconsin and Southern Railroad and WisDOT evaluate which bridges would be candidates for MF-FRP rehabilitation. This method is best used on double caps, and the FRP can be fastened either on site or the entire system can be prefabricated elsewhere and installed on a bridge as one piece. All double capped bents could receive MF-FRP strip treatment, or just the bents which are in the poorest condition; the decision is up to the discretion of the organization responsible for the railroad bridge maintenance.

Due to ease of installment, no special guides or specifications are required for the MF-FRP technique. It is recommended that a group or person is made familiar with the assessment of deteriorated pile caps and the MF-FRP installation technique so that it might be efficiently used. The materials used in this report were selected due to availability and to limit variables in the research. While other types of FRP strips and screws may be available on the market, the results of using these are not guaranteed by this report. It is recommended that the material specifications and installation instructions are read for all materials used.

It is recommended that further studies be conducted to determine other methods for redistributing the loads that fall on the piles in a bent, possibly through use of FRP dowels or springs between piles and pile caps.

Abstract

Many timber trestle railroad bridges in Wisconsin have experienced deterioration and are in need of rehabilitation. In addition, the railroad industry is increasing the weights of cars. The combined effect of heavier loads and deterioration threatens to cut short the service life of timber bridges. One of the most critical problems that has been identified was the overloading of timber piles in bridges, which can be remedied by creating a stiffer pile cap. The goal of this investigation was to show that mechanically fastened fiber reinforced polymer (MF-FRP) strips fastened to timber with screws can be used to create composite action between two beams in flexure or truss action between two deep beams. Ultimately this may help redistribute the loads to piles when FRP strips are used as struts on cap beams over short spans. Several test series were conducted with beams in flexure, deep beams over short spans, and full scale specimens to determine the manner in which FRP strips improved the members' performance. Tests were conducted over various widths of beams and lengths of spans to investigate how the geometry affected the strengthening's ability to create composite action. Next, the MF-FRP was tested on deep beams to determine if composite action was maintained. Lastly, full scale tests simulating a pile cap over 5 piles were run to see if composite action improved load distribution to piles. Mechanically fastened FRP strips were found to be effective in developing composite action in slender beams in flexure, meaning the stiffness of the system was increased by using MF-FRP strips. This MF-FRP method showed great potential for creating composite, stiffer double pile caps.

Contents

1.	Chapter 1: Introduction	1
1.1.	Problem Statement and Background.....	1
1.2.	Objectives	6
1.3.	Scope of Project	6
1.4.	Test Objectives.....	7
2.	Chapter 2: Literature Review	10
2.1.	Timber Railroad Bridges.....	10
2.1.1.	History of Timber Bridges	10
2.1.2.	AREMA Methods for Timber Railroad Bridge Analysis	11
2.2.	Fiber Reinforced Polymer (FRP) Strengthening of Timber	15
2.3.	Mechanically Fastened FRP (MF-FRP) Method of Strengthening	16
3.	Chapter 3: FRP Material	17
3.1.	Physical and Material Description of FRP.....	17
3.2.	Laboratory Tests of FRP	18
4.	Chapter 4: Wood Material	24
4.1.	Physical and Material Description of Douglas Fir.....	24
5.	Chapter 5: Phase 1 – Width Series Tests	28
5.1.	Phase 1: Width Series Test Setup	31
5.2.	Phase 1: Width Series Specimen Fabrication	35
5.3.	Phase 1: Width Series Test Procedure	39
5.4.	Phase 1: Width Series Test Results.....	42
5.5.	Phase 1: Width Series Test Discussion.....	45
6.	Chapter 6: Phase 1 - Depth Series Tests	54
6.1.	Phase 1: Depth Series Test Setup.....	56
6.2.	Phase 1: Depth Series Specimen Fabrication.....	58
6.3.	Phase 1: Depth Series Test Procedure	59
6.4.	Phase 1: Depth Series Test Results.....	61

6.5.	Phase 1: Depth Series Test Discussion	62
7.	Chapter 7: Phase 2 Tests	67
7.1.	Phase 2: Test Setup	67
7.2.	Phase 2: Specimen Fabrication	70
7.3.	Phase 2: Test Procedure	71
7.4.	Phase 2: Test Results	76
7.5.	Phase 2: Test Discussion.....	82
7.6.	Phase 2: Dynamic Test Setup and Procedure	86
7.7.	Phase 2: Dynamic Test Results.....	87
7.8.	Phase 2: Dynamic Test Discussion	88
8.	Chapter 8: Conclusion.....	90

List of Figures

Figure 1: A 286 kip railcar (Westbrook 2006).....	1
Figure 2: Wisconsin & Southern 286 kip railcar load pattern.	2
Figure 3: Bridge F-134 on WSOR operated line showing a single pile cap.....	3
Figure 4: Bridge F-134 on WSOR operated line showing a double cap.	3
Figure 5: Typical Cross Section, Standard Drawings H-6140 & H-6160 (Westbrook 2006)..	4
Figure 6: Rehabilitation of a timber bent for a bridge on the WSOR line in the Reedsburg subdivision. The deck was jacked up, and any deterioration in the piles was removed by sawing their tops off. A new pile cap is shown being placed over the piles. In the case of bridges which are double capped, a second pile cap would be stacked with the first (Wisconsin & Southern 2008).	5
Figure 7: A completed rehabilitation project of bridge F-76 on the WSOR line in the Monroe Subdivision. Note some of the bents have been double capped – the first bent in the foreground and the 4 th bent (Wisconsin & Southern 2008).....	5
Figure 8: AREMA Graph for Pile Load Distribution (AREA 1996).....	13
Figure 9: WSOR 286 kip Railcar Load (Westbrook 2006).	15
Figure 10: SAFSTRIP by Strongwell (a) shows that SAFSTRIP can be pre-drilled to accommodate installation needs. Note the lighter and darker longitudinal lines which are caused by the different materials (carbon fiber, glass fiber, resin) present in the product. (b) shows SAFSTRIP as it is delivered in rolled lengths (Strongwell 2008).....	17
Figure 11: (a) Extensometer placed at the mid point of the FRP strip. The extensometer measures elongation between its arms spaced 1 inch apart (b) Strain Gauge placed at the mid point of the FRP strip. The strain gauge measures microstrain in the FRP (c) FRP tensile test failure. The failure was sudden; note the rupture and separation of fibers in the strip. While most fibers separated and ruptured, some of the carbon fibers (darker fibers) in the center remained intact.....	18
Figure 12: Data from FRP 1. Strain in this graph was measured using the stroke divided by the original length of the strip. The steeper slope at the beginning represents the “settlement” process of the test when there was some slippage before the grips fully engaged.	19
Figure 13: Data from FRP 2. Strain was measured with an Extensometer.....	20

Figure 14: Data from FRP 3. Strain was measured with an Extensometer.....	20
Figure 15: Data from FRP 4. Strain was measured with an Extensometer. Note the irregularity at the beginning of the graph. This was caused by improper instrumentation setup. The test was paused and the instrumentation fixed. The data is still useful because the remainder of the graph presents a defined slope.....	20
Figure 16: Data from FRP 5. Strain was measured with a 350 ohm strain gauge.....	21
Figure 17: Data from FRP 6. Strain was measured using a 350 ohm strain gauge.	21
Figure 18: Data from FRP 7. Strain was measured using an Extensometer.	21
Figure 19: Data from FRP 8. Strain was measured with an Extensometer.....	22
Figure 20: Data from FRP 9. Strain was measured using an Extensometer. Note the kink in the graph due to instrumentation slip.....	22
Figure 21: Data from FRP 10. Strain was measured using an Extensometer.	22
Figure 22: Rough sawn Douglas Fir specimens out of storage at the Forest Products Lab in Madison, WI.	24
Figure 23: Full sized 12" x 12" creosote treated specimen.	26
Figure 24: Single member specimen – 4" x 4"	29
Figure 25: Stacked member specimen – 4" x 4" over 4" x 4"	29
Figure 26: Epoxied member specimen – 4" x 8" over 4" x 8"	30
Figure 27: Two members from the width series stacked and fastened with FRP strips and screws.....	30
Figure 28: Test setup for Phase 1: Width Series, long span. Drawing shows two stacked 4" deep beams. Dimensions in inches.	32
Figure 29: Test setup for Phase 1: Width Series, short span. Drawing shows two stacked 4" deep beams. Dimensions in inches.	32
Figure 30: Detail showing roller support and wood buffer for FRP X braced beams.	33
Figure 31: Mid span LVDT held in place at the center of the beam thickness by a clamp and stand.	34
Figure 32: Slip LVDT. The mounting bracket and LVDT itself were on the lower beam, while the tab which causes the LVDT to move was located on the upper beam.....	34

Figure 33: Quarter span LVDT held in place at the center of the beam thickness by a clamp and stand.	35
Figure 34: Detail of Width Series load head. The point of contact is made of hardwood mounted to a steel plate and then the load cell.	35
Figure 35: Pre-drilled bolt pattern in FRP strips for Phase 1 MF-FRP specimens.....	37
Figure 36: MF-FRP Specimen fabrication. 1.75” wide FRP strips were attached to timber specimens using Spax self tapping lag screws. This did not require any special training or equipment, and could be done easily by students using simple tools.....	38
Figure 37: FRP strips attached before being trimmed. Each beam was 4” deep and the system was a total of 8” deep.....	38
Figure 38: FRP X-braced specimen finished product. Each beam was 4” deep and the system was a total of 8” deep. Note a missing screw at the top where strips overlapped; in some cases the hole was too close to the edge of the beam and would cause splintering if drilled, or a knot in the wood prevented a screw from being placed.....	39
Figure 39: Lateral roller supports used for safety precautions.	41
Figure 40: Comparison of Mid Point Deflections for 4” width specimens on 10.5’ span.....	43
Figure 41: Comparison of Mid Point Deflections for 4” width specimens on 5’ span.....	43
Figure 42: Comparison of Mid Point Deflections for 8” width specimens on 10.5’ span.....	44
Figure 43: Comparison of Mid Point Deflections for 8” width specimens on 5’ span.....	44
Figure 44: Comparison of Mid Point Deflections for 12” width specimens on 10.5’ span....	45
Figure 45: Comparison of Mid Point Deflections for 12” width specimens on 5’ span.....	45
Figure 46: Graph to obtain E_bI and G_bA for 4” width series.	49
Figure 47: Graph to obtain E_bI and G_bA for 8” width series.	50
Figure 48: Graph to obtain E_bI and G_bA for 12” width series.	51
Figure 49: Two members from the depth series stacked and fastened in a V formation with FRP strips and screws. Each beam was 14” deep and the entire system was 28” deep. The FRP strips were 4” wide.	55
Figure 50: Two members from the depth series stacked and fastened in an X formation with FRP strips and screws. Each beam was 14” deep and the entire system was 28” deep. The FRP strips were 4” wide.	55

Figure 51: Test setup for Phase 1: Depth Series. Drawing shows two stacked 14” deep members. Dimensions in inches.	57
Figure 52: Test setup for depth series.	57
Figure 53: LVDT measuring transverse compression in wood.	58
Figure 54: Strain gauges on depth series beams.	58
Figure 55: Crushing near the load head of specimen X14.	60
Figure 56: Steel and wood plates to remedy stress concentrations at both (a) the load head and (b) supports.	60
Figure 57: Load vs. Deflection curve for Depth Series.	61
Figure 58: Load vs. strain data from the X14 depth series specimen.	62
Figure 59: Test setup for Phase 2 tests. Drawing shows two stacked full scale beams. Dimensions in inches.	68
Figure 60: Phase 2 test setup, with the 3 center supports visible.	68
Figure 61: Detail of left loading plate. The I beam is the spreader bar, and the load is channeled through this spreader to a steel dowel point load to a steel plate resting on top of the specimen. The cables which are visible around the spreader bar and plate are for safety reasons.	69
Figure 62: Detail of load cell at support.	70
Figure 63: MF-FRP specimen fabrication. 12” x 12” stacked beams had 4” strips applied with lag screws directly in the test set up. Note that not all of the pre-drilled holes are being used.	71
Figure 64: Ideal and Poor spacing as identified by the Westbrook report.	72
Figure 65: Diagonal compression strips.	73
Figure 66: Diagonal tension strips.	74
Figure 67: Vertical compression strips.	74
Figure 68: Horizontal strips at double cap interface.	75
Figure 69: Combination of compression and tension strips.	75
Figure 70: X-brace strips.	76
Figure 71: Strain gauges attached to FRP X-braced full scale specimen.	76
Figure 72: Load distributions for single cap tests with prescribed spacing.	77

Figure 73: Load distributions for double cap tests with prescribed spacing.....	77
Figure 74: Load distributions for double cap tests with worst spacing	78
Figure 75: Percentage of load on individual piles for MF-FRP tests on NB12-1 over NB12-4.	79
Figure 76: Percentage of load on individual piles for MF-FRP tests on NB12-2 over NB13-3.	80
Figure 77: Percentage of load on individual piles for MF-FRP tests on NB12-2 over NB12-3 for 150 kip loads	80
Figure 78: Compression strip top surface strain readings.....	81
Figure 79: Tension strip top surface strain readings.....	82
Figure 80: Compression strip top and bottom surface readings, and their sum.....	82
Figure 81: Load on center pile for 150 kip static tests at increments during 1,000,000 load cycles.....	87
Figure 82: Compression strain in FRP strip for 150 kip static tests at increments during 1,000,000 load cycles.....	88

List of Tables

Table 1: Percent load on piles for prescribed pile spacing	13
Table 2: Results from FRP coupon tensile tests	23
Table 3: Bending stresses for Phase 1 specimens	25
Table 4: Modulus of elasticity for Phase 1 specimens.....	25
Table 5: Bending and shear stresses for Phase 2 Specimens	26
Table 6: Modulus of elasticity for Phase 2 specimens.....	27
Table 7: Phase 1 Width Series Test Specimen Configurations.....	28
Table 8: Description of labeling convention for test specimens.....	31
Table 9: Values of maximum allowable force on different specimens	40
Table 10: Record of all tested specimens in width series	42
Table 11: E values calculated from 10.5' and 5' spans	46
Table 12: FRP X-braced EI values shown as a percentage of EI from same sized epoxied beams	46
Table 13: X and Y coordinates for evaluation of E_bI	48
Table 14: E_bI Values	51
Table 15: E_aI and E_bI value comparison (units in 10^8 lbs-in ²).....	52
Table 16: Phase 1 Depth Series Test Specimen Configurations.....	54
Table 17: Description of labeling convention for test specimens.....	56
Table 18: Record of all tested specimens in the Depth Series	60
Table 19: Slope calculations for curves in.....	63
Table 20: E_a calculations based on data in.....	64
Table 21: FRP X-braced EI values shown as a percentage of EI from same sized epoxied beams	65
Table 22: Descriptions of specimens tested in Phase 2	72
Table 23: Percentage of total load on each pile – prescribed spacing	83
Table 24: Percentage of total load on each pile – worst spacing	84

1. Chapter 1: Introduction

1.1. Problem Statement and Background

The state of Wisconsin has a large number of timber railroad bridges which are owned by the Wisconsin Department of Transportation (WisDOT) Bureau of Rails and Harbors; some of the bridges are leased by private railroad companies such as Wisconsin & Southern Railroad (WSOR). A 286,000 pound railcar is the current normal traffic car for rail lines, however a 315,000 pound car is expected to be more common in the coming years according to industry professionals (Kevin Halpin, 2008). A 286 kip railcar is a car like the one in Figure 1 which weighs 86,000 pounds when empty and carries up to a 100 ton load. Figure 2 shows the loading pattern for a WSOR 286 kip railcar.



Figure 1: A 286 kip railcar (Westbrook 2006).

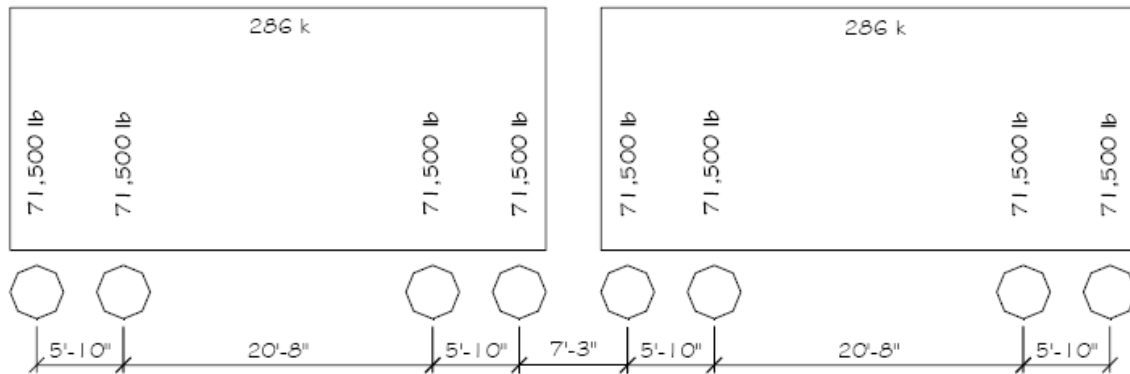


Figure 2: Wisconsin & Southern 286 kip railcar load pattern.

Recently, WisDOT commissioned a report by Westbrook Associated Engineers Inc. and E80 Plus Constructors LLC which examined 26 bridges in the Milwaukee and Monroe Subdivisions, all on lines operated by WSOR. Of these 26 bridges investigated, 20 were constructed solely of timber. The purpose of the report was to assess the impact of 286,000 pound railcars on the bridges, determine the bridges' load carrying capacity, and make any recommendations for rehabilitation where it was needed (Westbrook 2006).

The timber bridges under examination were pile trestles, all built between 1900 and 1965. The bridge type dealt with in this research is a 5 pile trestle, with bent spacing at either 14 feet o/c or 16 feet o/c. Each bent consisted of 5 piles spanned by a pile cap with dimensions of 14 inches \times 14 inches \times 14 feet. Some bents were double capped, having two pile caps stacked one on top of the other. Stringers ran between the bents, supporting ties and the rails themselves.

Figure 3 and Figure 4 show a typical 5 pile trestle bridge from underneath, while Figure 5 shows the original standard design drawings. The piles were originally designed for soil bearing capacity of 25 tons, or 50,000 pounds (Westbrook 2006).



Figure 3: Bridge F-134 on WSOR operated line showing a single pile cap.



Figure 4: Bridge F-134 on WSOR operated line showing a double cap.

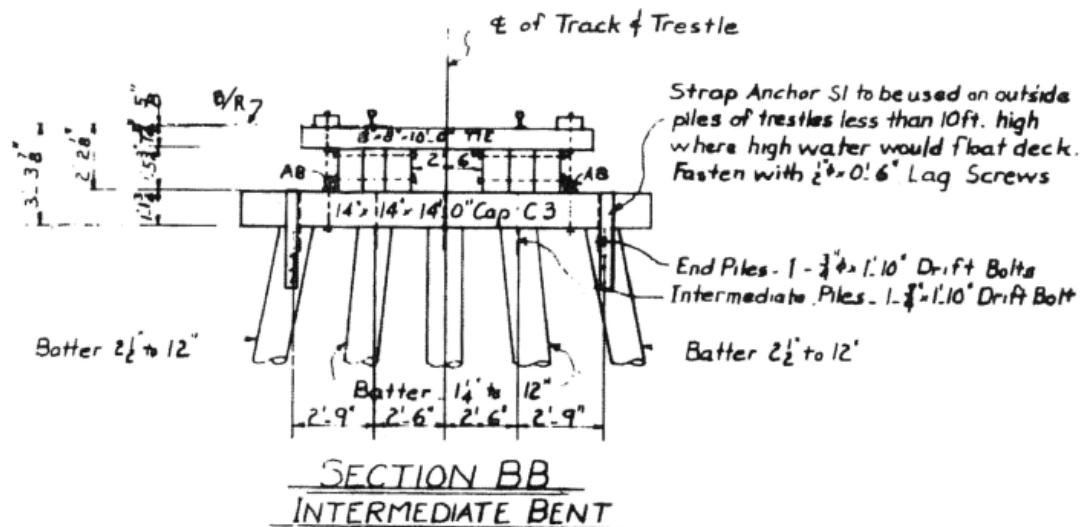


Figure 5: Typical Cross Section, Standard Drawings H-6140 & H-6160 (Westbrook 2006).

The Westbrook report summarizes the findings of two-man inspection crews utilizing on-site examinations and existing plans:

“Two specific deficiencies are noted: first, the ability of the stringers to carry the load with respect to bending; second, and more critically, the ability of the piling to transfer the load to the ground. Analysis shows that loads applied to the piling are very near their intended design capacities. Furthermore, actual pile capacities could be less than stated, and in many cases poor pile spacing noted in the field has created an increase in load distributed to the center piles. This has manifested in the form of pile settlement” (2006).

Many of the bridges which have already shown deterioration in the form of pile settlement have received temporary repair by having pile caps replaced or having double caps installed. This entailed having the tops of piles sawn off and a second pile cap stacked directly under the first, lying flush over the newly-cut piles. A single pile cap is shown in Figure 3 and a double pile cap is shown in Figure 4. Double capping a bent has the advantage of creating a stiffer pile cap, which in turn can offer better load distribution to piles. Figure 6 shows the construction for rehabilitation of a bent and Figure 7 shows the

finished product; both were photographed from bridges on WSOR lines from 2007 rehabilitation projects.



Figure 6: Rehabilitation of a timber bent for a bridge on the WSOR line in the Reedsburg subdivision. The deck was jacked up, and any deterioration in the piles was removed by sawing their tops off. A new pile cap is shown being placed over the piles. In the case of bridges which are double capped, a second pile cap would be stacked with the first (Wisconsin & Southern 2008).



Double caps

Figure 7: A completed rehabilitation project of bridge F-76 on the WSOR line in the Monroe Subdivision. Note some of the bents have been double capped – the first bent in the foreground and the 4th bent (Wisconsin & Southern 2008).

This project focused its resources on the issues pertaining to load transfers from the pile caps to the piles by utilizing Mechanically Fastened Fiber Reinforced Polymer (MF-FRP) strips. “Mechanically fastened” refers to strips that are connected to another material with

dowel type fasteners (screws, nails, etc) penetrating through the strip and anchored into the main member. The MF-FRP method is preferred to using adhesives because there is minimal surface preparation and can be done quickly and with unskilled labor (Lamanna et al, 2001; Bank and Arora, 2007). In addition, the MF-FRP technique has been used for shear strengthening of timber stringers (Akbiyik et al, 2007) and flexural strengthening of timber beams (Dempsey and Scott, 2006).

1.2. Objectives

The objectives of this project are (1) to improve the ability of the piling to transfer the load to the ground, (2) to study techniques to strengthen and stiffen beams using mechanically fastened FRP strips, (3) to achieve composite action through mechanically fastened composite materials, and (4) to optimize the composite behavior of a timber double cap beam for an open deck railroad trestle bridge.

1.3. Scope of Project

The possibilities for resolving the issues with poor load distribution to piles are numerous. For example, pile caps could be replaced by a stiffer material like steel or reinforced concrete, or springs could be installed between piles and pile caps to help even out load distribution. This project attempts to narrow the focus to one specific method in an attempt to find an economical and rapid method for rehabilitation of timber trestle railroad bridges. The following constraints were chosen with the intention of limiting the study variables so that conclusive results could be drawn while keeping the repair method affordable:

1. Method of composite action – composite action was implemented through the mechanical fastening of fiber reinforced polymer strips on either outer surface of stacked beams. The FRP strips used were Strongwell SAFSTRIP® 4 inch wide

carbon and glass reinforced strips. These strips have been used successfully in previous studies (Bank and Arora 2007).

2. Method of load distribution – when using full scale timber specimens the method being investigated for improving load distribution was limited solely to different patterns of MF-FRP strips. Limiting the stiffening to a single method ensured that rehabilitation would be economical and simpler to install. Methods using FRP dowels or plate, or springs on top of piles are recommended for further study in another project since they will require additional budget and time for thorough investigation.
3. Type of fastener – the fastener type was limited to Spax ¼ inch × 2 inch self tapping lag screws. These were of a small enough diameter to fit several across the width of an FRP strip and required no special skill or equipment to install.
4. Loads – since the pile design capacity is 25 tons the goal of the project will be to ensure that pile loads will not exceed 25 tons. Additionally, it was the goal that loads would be distributed more evenly across the piles to avoid settlement in single piles.

1.4. Test Objectives

The project was divided into two phases of testing. The two phases were developed by combining types of tests so that similar tests could be executed more quickly and efficiently, and so that the results of the first phase might be helpful in the implementation of the second phase. Following is a description of the testing phases and their objectives:

Test Phase 1: Width and Depth Series

Description – tests were conducted on small sized beams in flexural bending over two span lengths: 10'-6" and 5'. Specimens employed a variety of methods for simulating degrees of composite action: single members, stacked members, epoxied members,

and members with MF-FRP strips fastened to the sides. Both the widths and depths of specimens were varied separately.

Objectives

- (1) to determine whether the width or depth of a beam affected the composite nature of MF-FRP beams
- (2) to determine whether the distance between supports affected the accuracy of results

Anticipated Results – it was anticipated that using MF-FRP strips on the sides of stacked beams would increase their stiffness to achieve nearly composite action. It was expected that as beam width increased, some of the composite effect would be lost. It was expected that as beam depth increased, some of the composite effect would also be lost. It was expected that beams which behaved mostly in flexure and not in shear (i.e. a longer span) would give the most accurate representation of the system's stiffness.

Test Phase 2: Full Scale and Dynamic Series

Description – tests were conducted on full-sized specimens (actual pile caps) which were provided by WSOR and were typical of the in-situ condition of a timber railroad bridge. Five supports were used to replicate the support condition of the piles. Static testing was completed on a variety of MF-FRP configurations and dynamic testing to 1 million cycles was completed on one MF-FRP configuration.

Objectives

- (1) to determine whether benefits of the MF-FRP method were applicable to continuous deep beams over multiple short spans

(2) to determine if loads could be redistributed using MF-FRP strips

(3) to examine the behavior of the beam and determine whether it acts in accordance with design equations

Anticipated Results – it was anticipated that the MF-FRP system would create composite action in continuous deep beams over multiple short spans and that this would make stiffer stacked pile caps. It was expected that loads could be redistributed more evenly to the piles. It was also expected that tests would show results consistent with design equations presented in railroad manuals.

2. Chapter 2: Literature Review

2.1. Timber Railroad Bridges

2.1.1. History of Timber Bridges

Though timber was historically the principal material for bridge building, today only about 7% of the bridges listed in the National Bridge Index (NBI) are timber bridges (Radford et al 2002 and Duwadi and Ritter 1997). Of these, many are used for railroad traffic, including main transcontinental lines (Radford et al 2002). Most new bridges over the past 50 years have been made of concrete or steel, though some timber bridges have been constructed on secondary roads since timber has remained a prevalent resource in some parts of the country (Duwadi and Ritter 1997). Today, departments of transportation, local highway officials, and private engineers are faced with the decision of whether or not to use timber for highway and railroad projects. A study conducted by the United States Department of Agriculture (USDA) surveyed over 1300 highway officials, including those in Wisconsin, and found that timber was perceived to be the poorest bridge material due to maintenance, difficulty of design, short life, and low relative strength. The initial cost of a timber bridge is relatively high compared with concrete. Benefits of timber included resistance to deicing chemicals, low relative life cycle cost, aesthetics, and ease of installation and repair (USDA 1995). A main complaint by highway officials was that timber bridges' lifespan is only 25 to 30 years, and decay, especially in the substructure, requires rehabilitation (USDA 1995). The USDA report also concluded that Wisconsin is one of five states that have actually had an increase in timber bridges since 1986, possibly attributed to existing standard timber plans and heavy marketing by timber companies (1995). Due to the benefits unique to timber, such as resistance to deicing chemicals, there have been several initiatives in the past 20 years to

encourage use of timber for transportation structures. Currently, collaborative research initiatives between various departments of transportation, the Forest Products Lab (FPL), the Federal Highway Administration (FHWA), and other institutions are investigating design properties, preservative treatments to improve resistance to decay, and rehabilitation methods for timber (Duwadi and Ritter 1997), the latter on which this report focuses. Previous repair methods have included timber replacement, fiberglass wrapping of damaged areas, and epoxy repair to name a few; most of these methods require structural members to be removed from the bridge. Due to economic and personnel demands, replacing bridges is often difficult or impossible, and repairs are made on a schedule by priority basis. Therefore it is ideal to find methods of rehabilitation which do not require the removal of timbers and which can be done in a timely manner and also be cost effective (Radford et al 2002).

2.1.2. AREMA Methods for Timber Railroad Bridge Analysis

Chapter 7 of the AREMA Manual for Railway Engineering outlines specific processes for determining appropriate materials, design, and construction of timber railroad bridges. Among these are several design tools to predict the load distribution on a given bent. Before becoming AREMA, the organization which published the railway standard was the American Railway Engineering Association, or AREA. Both the 2007 AREMA version and 1996 AREA version of the manual contain a set of equations which appear to be derived from the flexibility method (also called the redundant force method) to determine what percent of the load applied to the bent would fall on center, intermediate, and outer piles. The 2007 version supplies equations to be used for 7 and 8 pile bents, which can also be modified to include 5 and 6 pile bents (AREMA 2007). The 1996 version supplies equations for 5 and 6 pile bents which can be modified to include 7 and 8 pile bents (AREA 1996). Unfortunately, both

manuals present the equations in the form of poor quality photocopies, and the 1996 version has several known errors to these equations, making them difficult and time consuming to use. The Forest Products Laboratory in Madison, WI keeps vaults of old manuals and codes; a 1953 version of the AREA Railway Manual was found in its original form bound as one book, with the equations and figures handwritten. This version proved to be much clearer and also supplied equations to accommodate 5 pile bents (AREA 1953). Easy to solve by hand or with a common math software package, these equations provide a guideline for the theoretical load distributions. Transverse compression of the cap and shortening of the piles are taken into account. The pile distributions obtained from these equations will never accurately represent a bent in the field – there is too much variability in the wood and they rely on the material properties being constant throughout the member. Note that the percentages in the AREMA equations represent the portion of the load R on any given pile. The load R is the load resulting from one rail on the bent, equivalent to (Total Applied Load)/(2 rails). Note that the load distribution percentages calculated for the double cap specimens used the same equations. The equations were updated so that the moment of inertia, $I_{\text{double cap}}$, was $2 \times I_{\text{single cap}}$ since there is twice as much material resisting the load. Also, the cross sectional area, $A_{\text{double cap}}$, was also $2 \times A_{\text{single cap}}$. Appendix C contains MathCAD representations of the equations as they appear in AREA 1953 and with the updated I and A values.

To accompany these load distribution equations, AREMA developed charts containing graphs for some pre-set common values of pile spacing plugged into the given equations. This is useful for quickly determining a load distribution and the equations are only

necessary when the dimensions are not typical. Please refer to Figure 8 for an example of the AREMA chart.

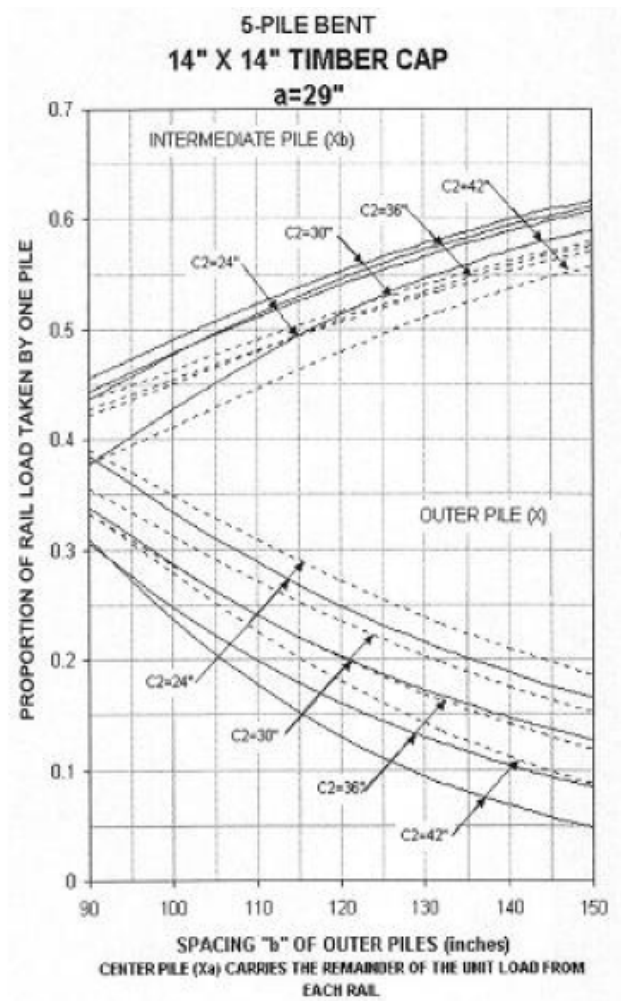


Figure 8: AREMA Graph for Pile Load Distribution (AREA 1996).

Table 1: Percent load on piles for prescribed pile spacing

Equation	Pile Cap Type	Center Pile	Intermediate Pile	Outer Pile
AREMA ¹ 5 Pile Bent Equation	Single 12" x 12"	24.4%	29.7%	8.1%
AREMA ¹ 5 Pile Bent Equation	Double 12" x 12" stacked	25.7%	27.1%	10.1%
AREMA ¹ 5 Pile Bent Equation	12" x 24" fully composite	22.9%	23.6%	14.8%

1. For the AREMA equation presented in Appendix C, a=29". Percentages from equations have been divided by 2 to represent percentage of TOTAL applied load.

Table 1 compares the AREMA equation results for different pile cap combinations with piles spaced correctly as they were designed. The last entry in the chart shows a prediction for a fully composite section between two pile caps using the AREMA method; it is apparent that the fully composite sections would provide a huge improvement on load distribution by utilizing the outer piles for more of the load and taking some off the center and intermediate piles.

AREMA Chapter 7 gives one provision for live load on a single-track open deck bridge: “The live load per track shall consist of that Cooper loading which will produce a loading effect equivalent to that caused by the heaviest engine or train load expected to be moved over the completed structure during its expected life” (AREMA 2007). A Cooper rating is a loading scheme that identifies the carrying capacity of a bridge using an arrangement of axles and serves as a convenient way to compare one bridge to another. The Cooper rating is back calculated from the maximum moment created by the heaviest engine, which in this case is a 286 kip rail car (Westbrook 2006 and Halpin 2008). The Westbrook report also shows a 286 kip rail car being equal to an 8,000 pound per foot uniformly distributed load. Using the 8 kip/ft load over a tributary area of 14 feet (distance between bents) a total applied load of 112 kips falls on a single bent. Using a simple structural analysis program, the axle loads in Figure 9 were placed in several patterns over two 14 foot spans to get the critical load at the bent. The resulting load was 197 kips on the bent.

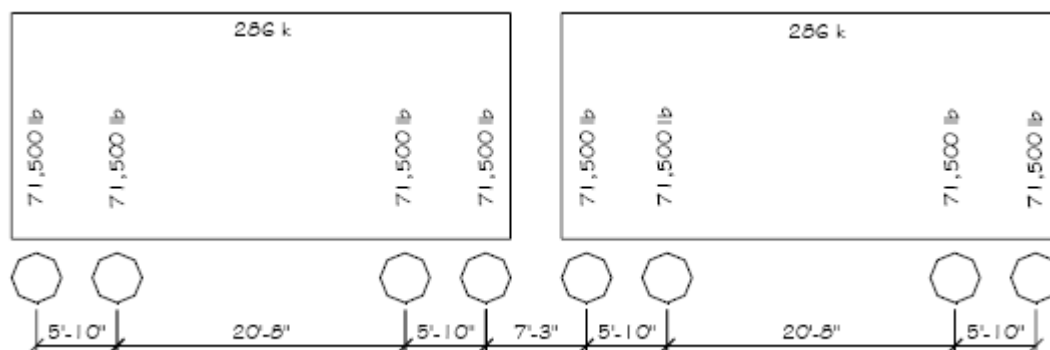


Figure 9: WSOR 286 kip Railcar Load (Westbrook 2006).

The Westbrook report also identifies the load on each pile for several pile spacings and the summed totals are 168 kips and 170 kips (2006). To be conservative, the 197 kips was used in assessing bent adequacy. For a total bent load of 197 kips, each rail would be supplying half of that load, or 98.5 kips, and the load distribution percentages are taken from this number if the AREMA equations are used.

2.2. Fiber Reinforced Polymer (FRP) Strengthening of Timber

FRP has successfully been used to strengthen timber in the form of pultruded shear spikes (Radford et al 2002), pultruded shape reinforcement (Corradi 2006), bonded laminates or fabric wraps (Triantafillou 1997), and of cylindrical shells for pile repair (Lopez-Anido 2004). Reinforcing wraps and plates can only be applied to exposed timber surfaces, which makes these methods particularly ineffective for timber bridges since there are many hidden surfaces. In addition, any preservative treatment has been shown to degrade the quality of adhesives used. Drilling holes and embedding pultruded shear spikes proved very effective since they are bonded to the untreated inside of the beam and promote composite behavior between laminates of wood (Radford et al 2002). FRP sheets have also been used as shear strengthening or repair to damaged beams (Akbiyik et al 2007).

2.3. Mechanically Fastened FRP (MF-FRP) Method of Strengthening

Composite materials have been used to strengthen timber members, as noted above, but also are widely used to strengthen reinforced concrete members. One method of attaching the composite material to the main member is through mechanical fastening. Mechanically fastened FRP (MF-FRP) has successfully strengthened both timber and concrete specimens. Using adhesives to bond FRP to materials has been thoroughly investigated, and ACI even provides a guideline for the adhesive process in ACI 440.1R-03. MF-FRP methods are less thoroughly investigated and there are no guidelines or provisions for mechanically fastened strengthening methods (Martin and Lamanna 2008). Mechanically fastening FRP strips or plates with screws was found to be an effective form of strengthening timber in flexure, though wood quality and moisture content were variables identified to have a large impact on results (Dempsey and Scott 2003). The process of producing an MF-FRP member may or may not include pre-drilling of the FRP and the material to be strengthened. Akbiyik et al used MF-FRP plates to strengthen timbers and did not pre-drill the wood (2007) while Martin and Lamanna used MF-FRP strips to strengthen concrete beams, having pre-drilled both the strips and the concrete beams (2008). Pre-drilling has been shown to reduce spalling in concrete (Bank and Arora 2007). The MF-FRP method is preferred to using adhesives because there is minimal surface preparation and can be done quickly and with unskilled labor (Lamanna et al, 2001; Bank and Arora, 2007) and avoids any deterioration that oil based wood treatment can cause to FRP/wood bonded interfaces (Tascioglu et al 2003).

3. Chapter 3: FRP Material

3.1. Physical and Material Description of FRP

The carbon and fiberglass reinforced polymer materials, called SAFSTRIP®, were produced by Strongwell (Chatfield, MN). The FRP strips came on 100 foot continuous rolls, each 4 inches wide and 1/8 inch thick. Refer to Figure 10 for SAFSTRIP® images. The SAFSTRIP® consists of carbon tows surrounded by layers of glass fiber mats and rovings, all impregnated with a vinyl ester resin. There is also a synthetic surfacing veil which serves to protect against UV degradation. The FRP strip is highly resistive to corrosion. This particular FRP material was designed to be mechanically fastened to other structural members, and are referred to as Mechanically Fastened Fiber Reinforced Polymer (MF-FRP) strips (Strongwell 2008). This is advantageous over externally bonded FRP with epoxies because the timbers of the bridges in question have a creosote treatment which is not conducive to adhesive bonding. In addition, using fasteners rather than an epoxy bonding allows the FRP strips to be installed with relatively unskilled labor in almost any condition.



Figure 10: SAFSTRIP by Strongwell (a) shows that SAFSTRIP can be pre-drilled to accommodate installation needs. Note the lighter and darker longitudinal lines which are caused by the different materials (carbon fiber, glass fiber, resin) present in the product. (b) shows SAFSTRIP as it is delivered in rolled lengths (Strongwell 2008).

The properties reported in the Strongwell SAFSTRIP® brochure (2008) are given for both Average Values and Design Values. The Design Values (determined by Average Values minus 3 standard deviations) are as follows: Tensile Strength, $\sigma_t = 92,902$ psi and Tensile Modulus, $E_t = 9.02 \times 10^6$ psi.

3.2. Laboratory Tests of FRP

The FRP was tension tested in 1 inch \times 14 inch coupons roughly in accordance with ASTM D 3039. The data was collected using a LabView program. An extensometer was placed at the middle of the strip to measure elongation, and select specimens were fitted with 350 ohm 1/8 inch strain gauges. Refer to Figure 11 for images of the testing setup and strip failure. The clear span between wedge grips was 8.25 inches, and the smallest grip force possible, around 900 pounds per square inch, was used to prevent crushing of the FRP material.



Figure 11: (a) Extensometer placed at the mid point of the FRP strip. The extensometer measures elongation between its arms spaced 1 inch apart (b) Strain Gauge placed at the mid point of the FRP strip. The strain gauge measures microstrain in the FRP (c) FRP tensile test failure. The failure was sudden; note the rupture and separation of fibers in the strip. While most fibers separated and ruptured, some of the carbon fibers (darker fibers) in the center remained intact.

Initial tests showed that the coupons failed in the range of 17 – 19 kips, so the extensometer was removed at 11 kips to be sure no damage to the equipment occurred. Therefore, the strain data represents readings up until 60% of the ultimate load. Failure was brittle and sudden; the resin, fiberglass, and some of the carbon portions of the strips were completely severed at the site of failure, while some of the carbon tows remained intact.

Plots of the stress vs. strain for each specimen were created, and from these an average longitudinal modulus of elasticity, $E_{FRP} = 9.28 \times 10^6$, was derived with a standard deviation of 0.448×10^6 . This confirms that Strongwell's material property data were in fact conservatively reported. Figure 12 through Figure 21 show the data obtained from the coupon tensile tests.

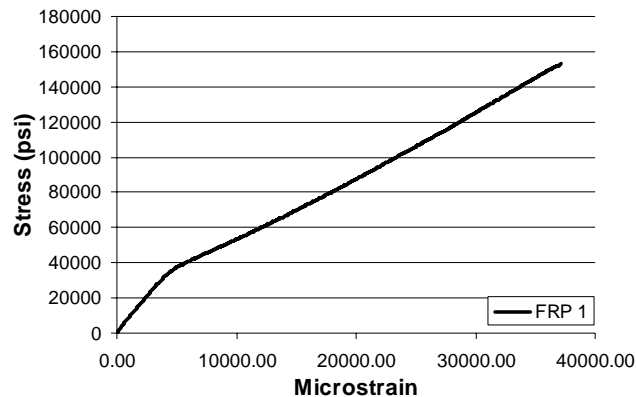


Figure 12: Data from FRP 1. Strain in this graph was measured using the stroke divided by the original length of the strip. The steeper slope at the beginning represents the “settlement” process of the test when there was some slippage before the grips fully engaged.

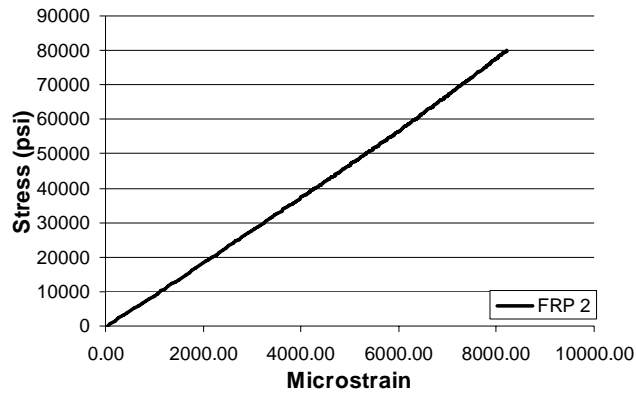


Figure 13: Data from FRP 2. Strain was measured with an Extensometer.

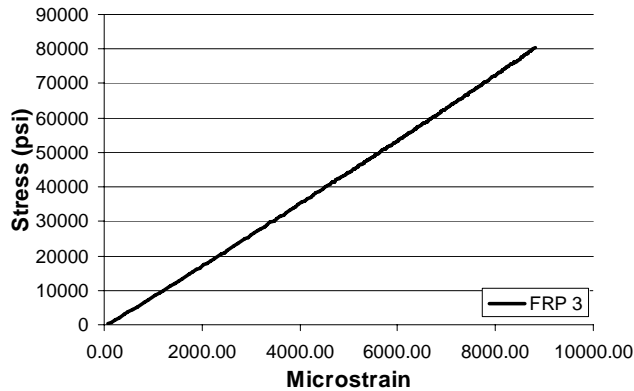


Figure 14: Data from FRP 3. Strain was measured with an Extensometer.

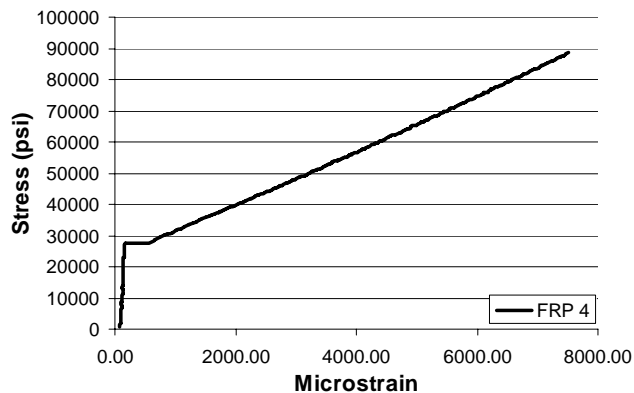


Figure 15: Data from FRP 4. Strain was measured with an Extensometer. Note the irregularity at the beginning of the graph. This was caused by improper instrumentation setup. The test was paused and the instrumentation fixed. The data is still useful because the remainder of the graph presents a defined slope.

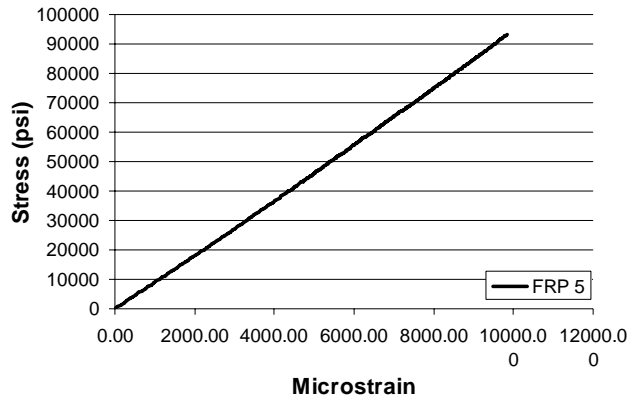


Figure 16: Data from FRP 5. Strain was measured with a 350 ohm strain gauge.

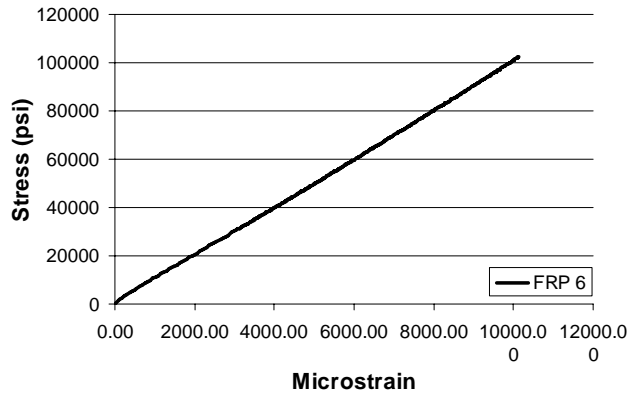


Figure 17: Data from FRP 6. Strain was measured using a 350 ohm strain gauge.

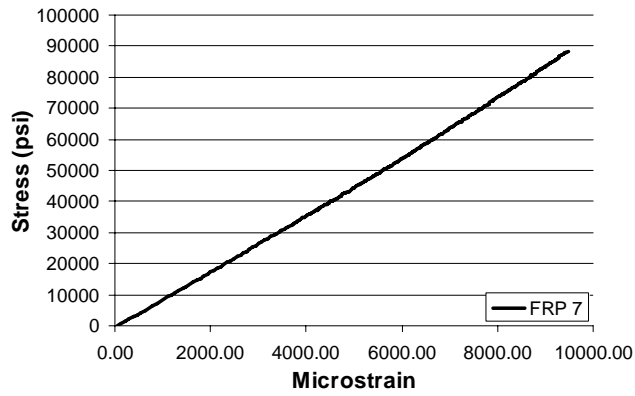


Figure 18: Data from FRP 7. Strain was measured using an Extensometer.

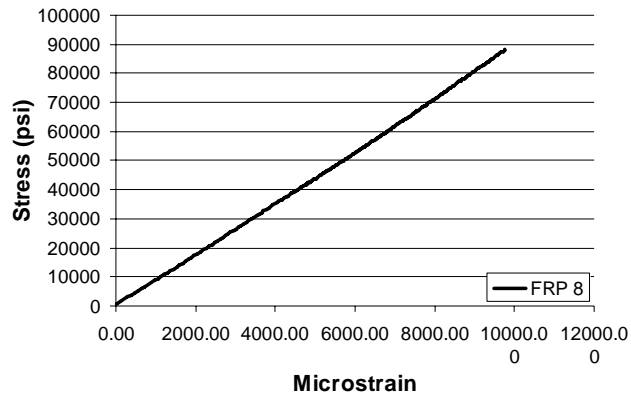


Figure 19: Data from FRP 8. Strain was measured with an Extensometer.

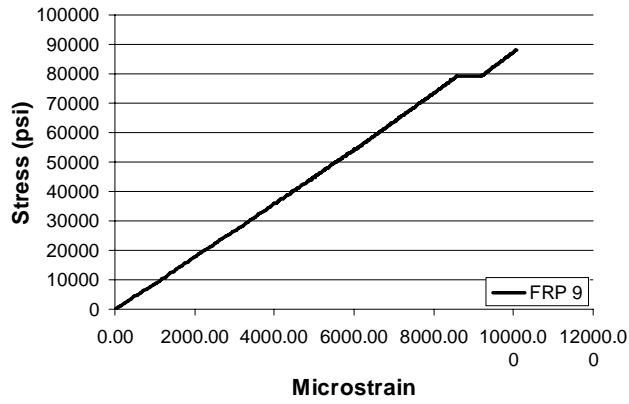


Figure 20: Data from FRP 9. Strain was measured using an Extensometer. Note the kink in the graph due to instrumentation slip.

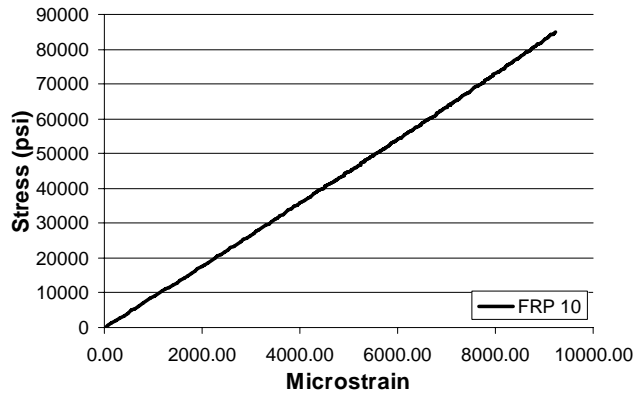


Figure 21: Data from FRP 10. Strain was measured using an Extensometer.

The first FRP test strain data was based on strain calculated from stroke displacement divided by the original clear span of the strip between grips because no strain instrumentation was used. This is a less accurate method for calculating strain since the length is constantly changing and the grips may have slip at the ends. Table 2 shows the tensile test results, and it is clear that the slope calculated in FRP 1 is not similar at all to the slopes of the data collected with either an extensometer or strain gauge. The slope should be representative of the modulus, and in the calculation of E_{FRP} , the data from FRP 1 was not included and considered an outlier.

Table 2: Results from FRP coupon tensile tests

Coupon Name	E (slope) 10⁶ Psi	σ_{ult} Psi	P_{ult} Lbs	Δ_{ult} (stroke) in
FRP 1	3.65	152,920	19,115	0.372
FRP 2	9.77	146,750	18,343	0.385
FRP 3	9.21	143,573	17,946	0.339
FRP 4	8.54	144,927	18,115	0.359
FRP 5	9.51	137,208	17,151	0.340
FRP 6	10.01	145,200	18,150	0.382
FRP 7	9.40	156,136	19,517	0.391
FRP 8	8.99	141,272	17,659	0.346
FRP 9	8.92	142,544	17,818	0.351
FRP 10	9.21	154,328	19,291	0.381
Average	9.28¹	146,486	18,311	0.36
Standard Dev.	0.45¹	6123.37	765.47	0.02
1. FRP 1 was left out of the average and standard deviation calculations and considered an outlier because the method used to get E was much less accurate than the remaining samples, as discussed in text above.				

4. Chapter 4: Wood Material

4.1. Physical and Material Description of Douglas Fir

Specimens for the first phase tests were rough sawn Douglas Fir timber beams that were surplus from a testing project at the Forest Products Laboratory. They had been stored inside and had moisture contents ranging from approximately 9% to 13%, and their grading was Select Structural. The members' original rough sawn size was 4" wide \times 12" high and 4" wide \times 8" high. For testing purposes, smaller 4" \times 4" members were cut from the larger members. Specimens were all 12' long. All dimensions given are nominal and the actual sizes vary with each specimen. Figure 22 shows wood specimens stacked as they were in storage.



Figure 22: Rough sawn Douglas Fir specimens out of storage at the Forest Products Lab in Madison, WI.

The specimens for Phase 1 qualify as dimension lumber 2 inches to 4 inches thick and at least 2 inches wide (NDS 2005). Both AREMA 2007 and the National Design Specification for Wood Construction 2005 give material properties of wood in the form of reference design stresses, denoted F . In order to obtain a correct allowable stress, denoted F' , adjustment factors are used to modify the chart value. Some of these include a temperature adjustment, a

moisture condition adjustment, or an incising factor. It is assumed that for the Douglas Fir specimens used in this project all factors are equal to 1.0 unless noted otherwise. The bending stresses and moduli according to AREMA 2007 are as given in Table 3 and Table 4. Note the last column in Table 3 is the bending stress for the given beams with the flat use factor, which accounts for using a beam with the greatest dimension of the cross section oriented horizontally, rather than vertically. In addition, the reference stresses that AREMA gave already accounted for a moisture content of over 19% (field conditions). Since the timber has all been kept in a controlled dry environment, an allowance of a 1.18 multiplier to the stresses was allowed, as seen in the C_m column below (AREMA 2007).

Table 3: Bending stresses for Phase 1 specimens

Size	F_b	C_m	C_f	F_b'	C_{fu}	F_b'
Width (in) x Height (in)	Reference stress, psi	Dry use factor	Size factor	Dsgn stress, psi	Flat use factor	Dsgn stress with flat use factor, psi
4" x 4"	1150	1.18	1.5	2035	1.0	2035
8" x 4"	1150	1.18	1.3	1764	1.05	1852
12" x 4"	1150	1.18	1.1	1492	1.1	1641
14" x 4"	1150	1.18	1.0	1357	1.1	1492

Table 4: Modulus of elasticity for Phase 1 specimens

Size	E	C_m	E'
Width (in) x Height (in)	Modulus, ksi	Dry use factor	Dsgn Modulus, ksi
4" x 4"	1710	1.11	1898
8" x 4"	1710	1.11	1898
12" x 4"	1710	1.11	1898
14" x 4"	1710	1.11	1898

Specimens from the second phase were donated courtesy of Wisconsin and Southern Railroad. They consisted of (4) four 12" wide × 12" high × 20' long timbers, creosote treated and in the same condition as timbers used for actual bridge construction. For testing

purposes, the timbers were cut to 14' lengths to simulate the exact length of the pile caps under examination. Some of the specimens contain checks and splits.



Figure 23: Full sized 12" x 12" creosote treated specimen.

The full sized specimens classify as posts and timbers (NDS 2005) which is an approximately square cross section at least 5 inches \times 5 inches. Their grading was assumed to be Grade No. 1 since the wood was unmarked and that was the lowest grading AREMA 2007 listed values for. Table 5 and Table 6 give the material properties for the Phase 2 specimens. Note the size factor and dry use factor became 1.0 for posts and timbers, and a flat use factor could not be applied to a square cross section, so all factors are now taken as 1.0.

Table 5: Bending and shear stresses for Phase 2 Specimens

Size	F_b	F_b'	F_v	F_v'
Width (in) x Height (in)	Reference stress, psi	Dsgn stress, psi	Reference stress, psi	Dsgn stress, psi
12" x 12"	1080	1080	150	150

Table 6: Modulus of elasticity for Phase 2 specimens

Size	E	E'
Width (in) x Height (in)	Modulus, ksi	Dsgn Modulus, ksi
12" x 12"	1600	1600

5. Chapter 5: Phase 1 – Width Series Tests

For the width series in Phase 1 testing, beams of 4 inch height and varying widths were tested over a long span (10.5 feet or 126 inches) and a short span (5 feet or 60 inches). The combinations are outlined in Table 7. Figure 24 through Figure 27 illustrates the various combinations given in Table 7.

Table 7: Phase 1 Width Series Test Specimen Configurations

Width Series			
Beam Width	Beam Depth	Configuration	Description
4" 8" and 12"	4"	Single Beam	A single member
4" 8" and 12"	4"	Stacked Beams	One beam on top of the other – no composite action
4" 8" and 12"	4"	Epoxied Beams	Simulates fully composite section between two members
4" 8" and 12"	4"	FRP X-Braced Beams	FRP fastened to outer surface on either side, achieving some composite action



Figure 24: Single member specimen – 4" x 4"



Figure 25: Stacked member specimen – 4" x 4" over 4" x 4"



Figure 26: Epoxied member specimen – 4” x 8” over 4” x 8”



Figure 27: Two members from the width series stacked and fastened with FRP strips and screws.

Most combinations of the width series beams had 2 or 3 specimens in order to get several data sets over which the results could be averaged. The stacked specimens were easiest to make multiples of since they required the least amount of fabrication time.

Epoxied and x-braced combinations only had one multiple in each width due to fabrication time and material constraints. In an attempt to obtain more than one epoxy and X-braced specimen, each one was flipped upside-down and re-tested as a “new” specimen. However, the results were identical and this idea was abandoned after just a few attempts. Table 8 outlines the labeling convention used for the Phase 1 timber specimens.

Table 8: Description of labeling convention for test specimens

Label	Description
NB4-#	Not braced, single 4” x 4” beam
NB4-# over NB4-#	Not braced, stacked 4” x 4” beam over a 4” x 4” beam
E4	Epoxied 4” x 4” beam to a 4” x 4” beam
X4	FRP X-braced 4” x 4” beam over a 4” x 4” beam
NB8-#	Not braced, single 4” x 8” beam
NB8-# over NB8-#	Not braced, stacked 4” x 8” beam over a 4” x 8” beam
E8	Epoxied 4” x 8” beam to a 4” x 8” beam
X8	FRP X-braced 4” x 8” beam over a 4” x 8” beam
NB12-#	Not braced, single 4” x 12” beam
NB12-# over NB12-#	Not braced, stacked 4” x 12” beam over a 4” x 12” beam
E12	Epoxied 4” x 12” beam over a 4” x 12” beam
X12	FRP X-braced 4” x 12” beam over a 4” x 12” beam
s	An “s” before the beam label denotes the test as a “short” or 5 ft span

Thus, a beam labeled NB8-3 is the third specimen which is a combination of 4” × 8” stacked beams over a span of 10.5 ft. A beam labeled sNB8-3 is the same exact specimen tested over a span of 5 ft.

5.1. Phase 1: Width Series Test Setup

The width series was tested over two spans: a long span (10.5 feet or 126 inches) and a short span (5 feet or 60 inches). All tests were conducted at the Forest Products Laboratory in Madison, Wisconsin. The tests were completed on a hydraulic press with a 10,000 lb load cell; data acquisition was through an MTS controller and compiled with a custom program in LabView.

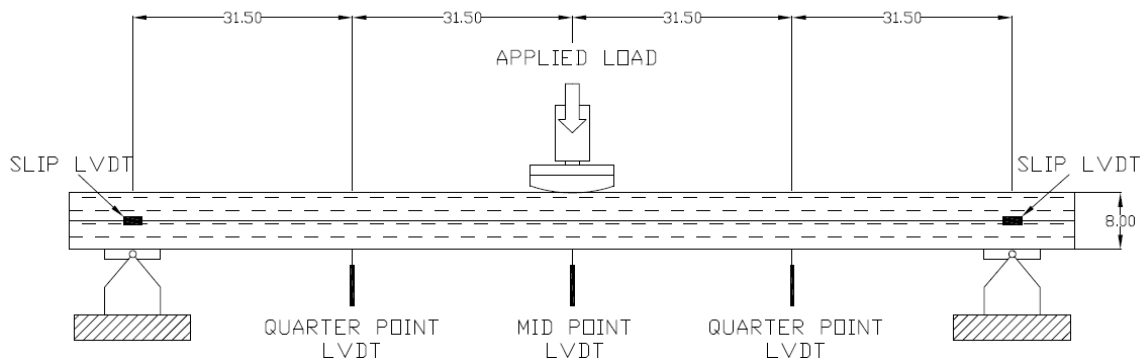


Figure 28: Test setup for Phase 1: Width Series, long span. Drawing shows two stacked 4" deep beams. Dimensions in inches.

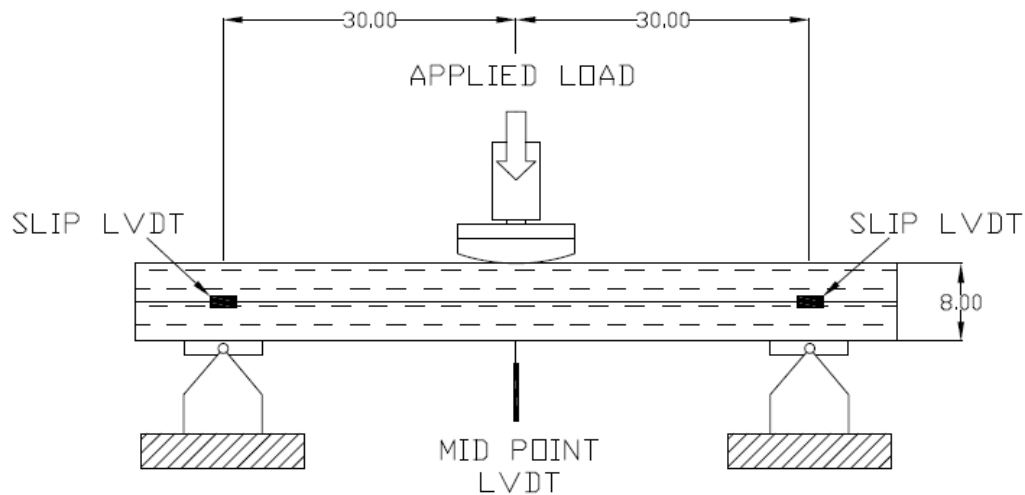


Figure 29: Test setup for Phase 1: Width Series, short span. Drawing shows two stacked 4" deep beams. Dimensions in inches.

The test setup included two roller supports, shown in Figure 30. When the width of the beams reached 12 inches they extended over the supports on either side, so a larger steel plate was fastened to the top of the support to offer an even bearing surface to the beam. In addition, when the FRP X-braced beams were tested, every effort was made to ensure that the FRP strips did not come in contact with the supports. A ½ inch thick piece of wood cut the length of the support and with width just narrower than the beam was used as a buffer

between the beam and support so that any FRP strip that may have been overhanging the beam would not have been compressed by the roller supports (Figure 30).

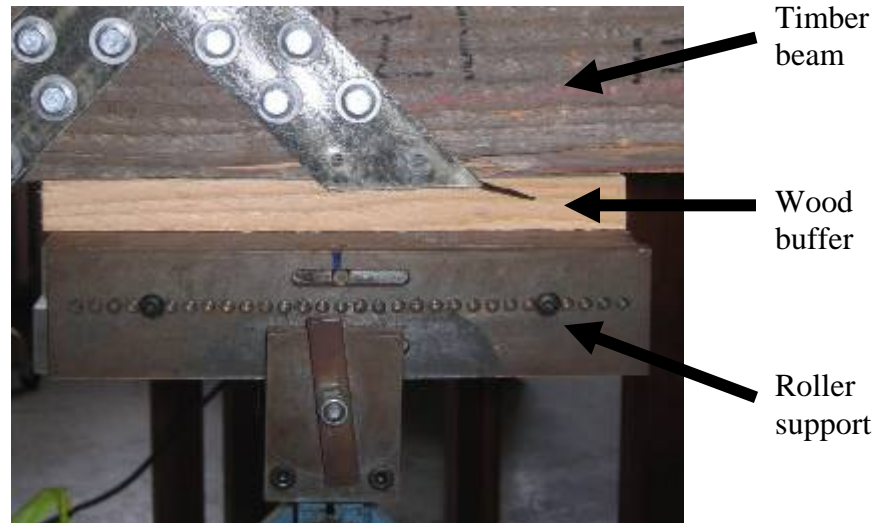


Figure 30: Detail showing roller support and wood buffer for FRP X braced beams.

Each long span beam tested had 5 LVDTs attached: one ± 0.5 inch LVDT to measure mid span deflection (Figure 31), two ± 0.5 inch LVDTs to measure quarter point deflections (Figure 32) and two ± 0.1 inch LVDTs to measure slip at either end (Figure 33). Each short span beam tested had 3 LVDTs attached: one ± 0.5 inch LVDT to measure mid span deflection and two ± 0.1 inch LVDTs to measure slip at either end. Slip is the distance one beam moves relative to the beam it is stacked on top of, and was measured directly over the supports on either side. In addition, the load cell was also read into LabView, for a total of 6 data channels per test. The two quarter point deflection channels were not used during short span tests since their deflection would be small and there was less space for instrumentation.



Figure 31: Mid span LVDT held in place at the center of the beam thickness by a clamp and stand.

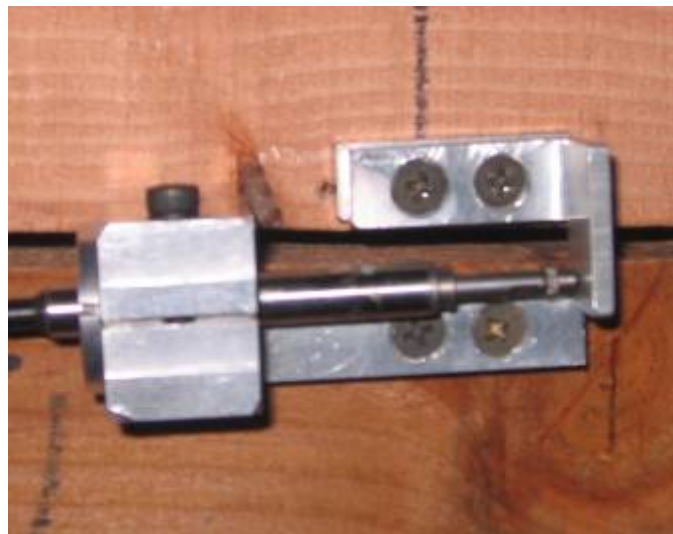


Figure 32: Slip LVDT. The mounting bracket and LVDT itself were on the lower beam, while the tab which causes the LVDT to move was located on the upper beam.



Figure 33: Quarter span LVDT held in place at the center of the beam thickness by a clamp and stand.

The load head was equipped with a hardwood head curved at the point of contact with the specimen, shown in Figure 34.



Figure 34: Detail of Width Series load head. The point of contact is made of hardwood mounted to a steel plate and then the load cell.

5.2. Phase 1: Width Series Specimen Fabrication

The stacked specimens were meant to represent the double pile caps of a timber bridge which were not interconnected whatsoever. This was achieved by simply placing one timber member on top of another, with an effort to choose surfaces which were level to be placed

against each other. As the specimens were in an uncontrolled environment for several years many of them were warped; thus often the stacked combinations contained gaps where the individual pieces were too warped to lay flush.

Epoxied specimens were meant to simulate a fully composite relationship between two beams. The two part epoxy consisted of R3500 Resin manufactured by Epic Resins, and Ancamide 2050 Curing Agent manufactured by Air Products. The epoxy was mixed in a 1:1 volumetric ratio, and thickened to mayonnaise consistency with a fumed silica filler, Aerosil R 202 manufactured by Degussa AG, Aerosil & Silanes. Complete specifications for these materials can be found in the appendices. To fabricate specimens, the thickened epoxy was spread over the surface to be bonded on the first member. A second member was placed on top of the first, and at least 100 pounds per square foot of pressure was applied to the system for a minimum of 24 hours. Excess epoxy which may have been squeezed out from the interface was wiped away so that the system would fit into the test setup smoothly and instrumentation could be attached where necessary. Some effort was made to epoxy the straightest edges together and to get two beams of corresponding size, but as discussed above, many of the beams had imperfections. The weight of the press did, however, correct any gaps that may have been present between the two beams.

MF-FRP strengthened specimens were tested in order to examine the feasibility of using FRP as a method of obtaining fully composite action by comparing it to the stacked and epoxied specimens. Phase 1 MF-FRP specimens were fabricated by first clamping two beams together to close any gaps. FRP strips were cut to 1.75 inches wide from the original 4 inch wide Strongwell SAFSTRIP® product and pre-drilled with holes for the screws. The centerline of the beams was located and marked and the strips were attached with Spax self

tapping $\frac{1}{4}$ inch \times 2 inch lag screws, beginning at the centerline of the beam and working outwards. A washer was placed under the head of each screw to prevent the screw head from biting into the FRP and creating stress concentrations. Those strips that were to be in tension during mid point loading were placed flush against the surface of the timber while the compression strips were layered to cross over these. The overhanging edges were sawn to be flush with the timber. The X pattern was created with each strip lying at a 45 degree angle to the edge of the beam. The pre-drilled bolt pattern for the width series of beams (consisting of two 4 inch deep beams stacked on top of each other) is shown in Figure 35. Figure 37 through Figure 38 illustrate stages of the FRP attachment process.

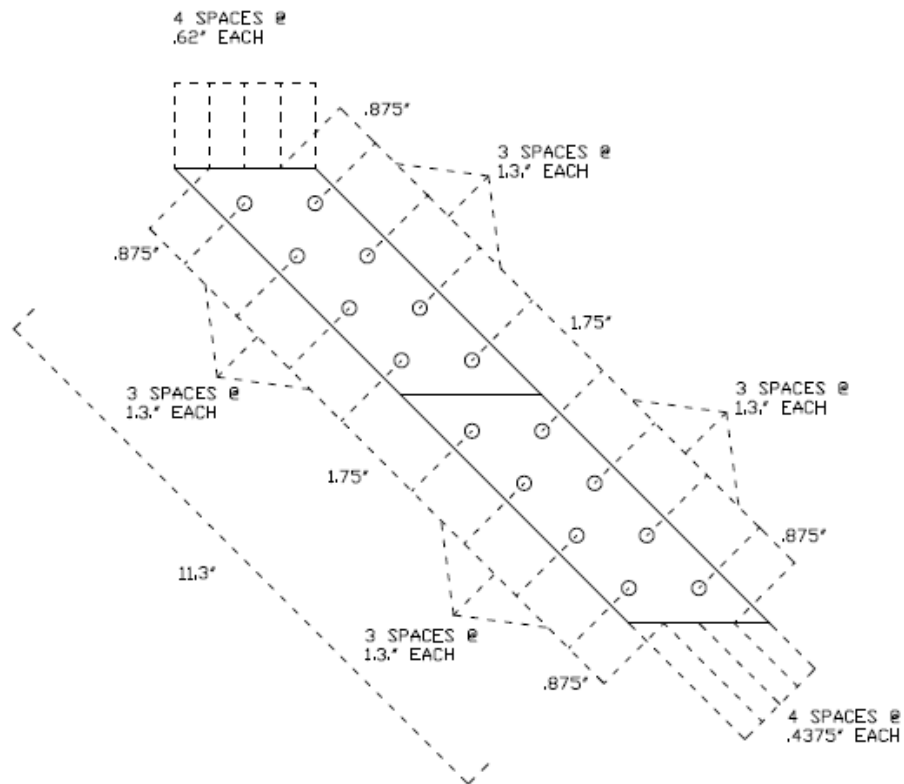


Figure 35: Pre-drilled bolt pattern in FRP strips for Phase 1 MF-FRP specimens



Figure 36: MF-FRP Specimen fabrication. 1.75" wide FRP strips were attached to timber specimens using Spax self tapping lag screws. This did not require any special training or equipment, and could be done easily by students using simple tools.



Figure 37: FRP strips attached before being trimmed. Each beam was 4" deep and the system was a total of 8" deep.



Figure 38: FRP X-braced specimen finished product. Each beam was 4” deep and the system was a total of 8” deep. Note a missing screw at the top where strips overlapped; in some cases the hole was too close to the edge of the beam and would cause splintering if drilled, or a knot in the wood prevented a screw from being placed.

5.3. Phase 1: Width Series Test Procedure

For each test, the theoretical maximum allowable load (contained in Table 9) was calculated using the nominal dimensions of the beam according to formula (1) or (2).

$$P_{\max_allow} = \frac{4IF_b}{Lc} \quad (1)$$

or

$$P_{\max_allow} = \frac{4(2I)F_b}{Lc} \quad (2)$$

Where formula (2) is used when the individual beams in a specimen are not attached (i.e. stacked combinations) and the moment of inertia is 2 x I of a single beam.

$$I = \frac{bd_2^3}{12} \quad (3)$$

$$c = \frac{d_1}{2} \quad (4)$$

b = beam width

d₁ = total depth of specimen

d₂ = depth of individual beam (if not attached to another beam)

L = specimen length

F_b = 1600 psi (bending stress of Douglas Fir Select Structural, NDS 2005)

Table 9: Values of maximum allowable force on different specimens

Beam Size	Combination		b (in)	d ₁ (in)	d ₂ (in)	L (in)	I (in ⁴)	c (in)	P max (lbs)
	Type	Span							
4" x 4"	Stacked	Long	4	8	4	126	21.33	4	541.80
		Short	4	8	4	60	21.33	4	1137.78
	Epoxyed	Long	4	8	8	126	170.67	4	2167.20
		Short	4	8	8	60	170.67	4	4551.11
	X Braced	Long	4	8	8	126	170.67	4	2167.20
		Short	4	8	8	60	170.67	4	4551.11
4" x 8"	Stacked	Long	8	8	4	126	42.67	4	1083.60
		Short	8	8	4	60	42.67	4	2275.56
	Epoxyed	Long	8	8	8	126	341.33	4	3521.69
		Short	8	8	8	60	341.33	4	7395.56
	X Braced	Long	8	8	8	126	341.33	4	3521.69
		Short	8	8	8	60	341.33	4	7395.56
4" x 12"	Stacked	Long	12	8	4	126	64.00	4	1320.63
		Short	12	8	4	60	64.00	4	2773.33
	Epoxyed	Long	12	8	8	126	512.00	4	5282.54
		Short	12	8	8	60	512.00	4	11093.33
	X Braced	Long	12	8	8	126	512.00	4	5282.54
		Short	12	8	8	60	512.00	4	11093.33

First, specimens were placed onto the testing apparatus, centered on each support. Two lateral roller supports were utilized for the long span and one for the short span, placed slightly towards mid span from the quarter points. The lateral supports were largely for safety

precautions, therefore did not bear directly on the wood, but about 1/16 to 1/8 of an inch away; some beams came into contact with one or more lateral supports during testing, but since they had rollers it did not affect the in-plane bending of the specimens. Figure 39 shows the lateral supports.

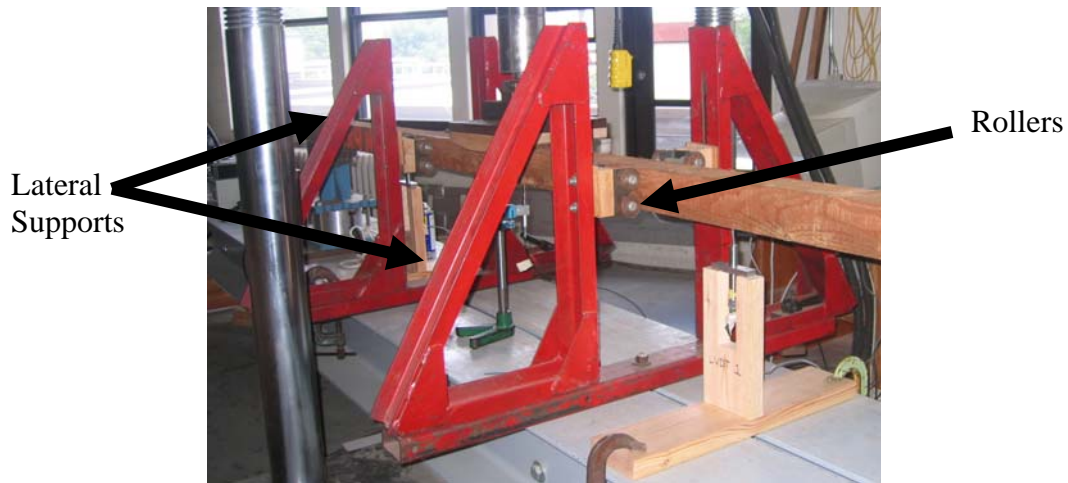


Figure 39: Lateral roller supports used for safety precautions.

A small preload was applied, around 20 lbs, in order to ensure that the beam was not being loaded eccentrically when testing commenced. Specimens were loaded in deflection control of 0.23 in/min until the maximum allowable load was reached or the LVDTs full capacity was met, whichever occurred first. In most cases, the maximum allowable load was reached first. Once the test was completed the load was removed. Each specimen was loaded and data collected three separate times. Table 10 describes each specimen tested.

Table 10: Record of all tested specimens in width series

Beam Label	Description (w x h)	Reps	Test Load 10.5' span	Test Load 5' span
NB4	4" x 4"	2		1137
NB4-2	4" x 4"	3		1137
NB4-3	4" x 4"	3		1137
NB4-4	4" x 4"	3		no test
NB4 over NB4-2	4" x 4" / 4" x 4"	3		2200
NB4-3 over NB4-4	4" x 4" / 4" x 4"	3		2200
E4	4" x 4" / 4" x 4" epoxy	2		4550
X4	4" x 4" / 4" x 4" FRP	3	2100	4550
NB8	8" x 4"	3	1085	no test
NB8-2	8" x 4"	3	1085	2300
NB8-3	8" x 4"	3		no test
NB8-4	8" x 4"		no test	
NB8-2 over NB8	8" x 4" / 8" x 4"	3	2000	
NB8-2 over NB8-3	8" x 4" / 8" x 4"	3	2100	
NB8-2 over NB8-4	8" x 4" / 8" x 4"		no test	4500
NB8-3 over NB8-4	8" x 4" / 8" x 4"		no test	4500
E8	8" x 4" / 8" x 4" epoxy	3		9100
X8	8" x 4" / 8" x 4" FRP	3	4200	9102
NB12	12" x 4"	3	1500	
NB12-2	12" x 4"	3	1600	
NB12-3	12" x 4"	3		
NB12-4	12" x 4"		no test	3400
NB12-5	12" x 4"		no test	3400
NB12-6	12" x 4"		no test	3400
NB12-2 over NB12-3	12" x 4" / 12" x 4"	3	3200	
NB12 over NB12-3	12" x 4" / 12" x 4"	3	3600	
NB12-2 over NB12	12" x 4" / 12" x 4"		3600	
NB12-5 over NB12-6	12" x 4" / 12" x 4"		no test	6800
NB12-5 over NB12-4	12" x 4" / 12" x 4"		no test	6800
E12	12" x 4" / 12" x 4" epoxy	3	6500	13700
X12	12" x 4" / 12" x 4" FRP	3	6500	13700

5.4. Phase 1: Width Series Test Results

Load vs. Mid Point Deflection curves of all specimens over both short and long spans can be found in Appendix B. Also included is Load vs. Quarter Point Deflection and Load vs. Slip for specimens which collected these data. Comparisons between Mid Point Deflections of varying width specimens on a 10'-6" span are shown in Figure 40 through Figure 44.

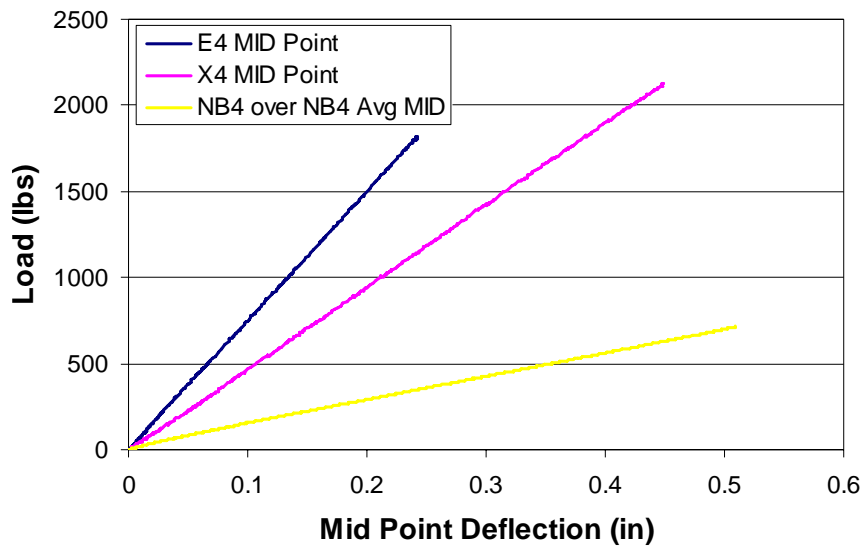


Figure 40: Comparison of Mid Point Deflections for 4'' width specimens on 10.5' span.

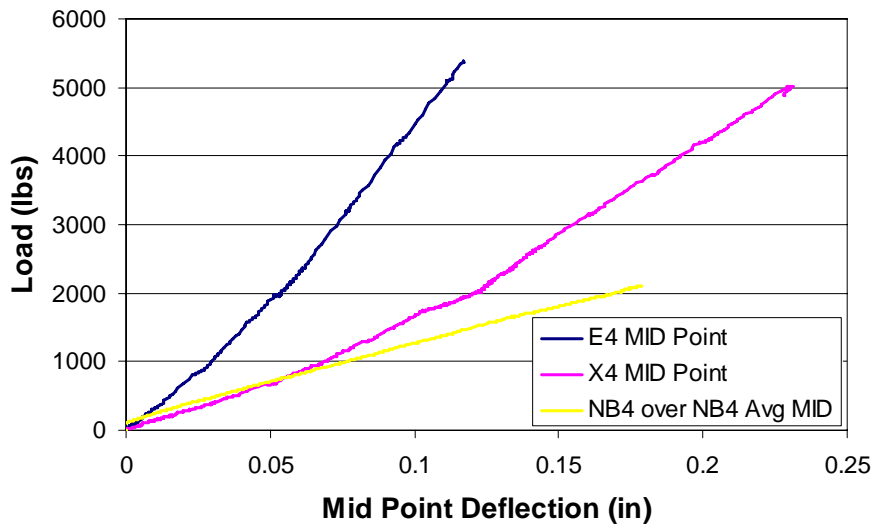


Figure 41: Comparison of Mid Point Deflections for 4'' width specimens on 5' span.

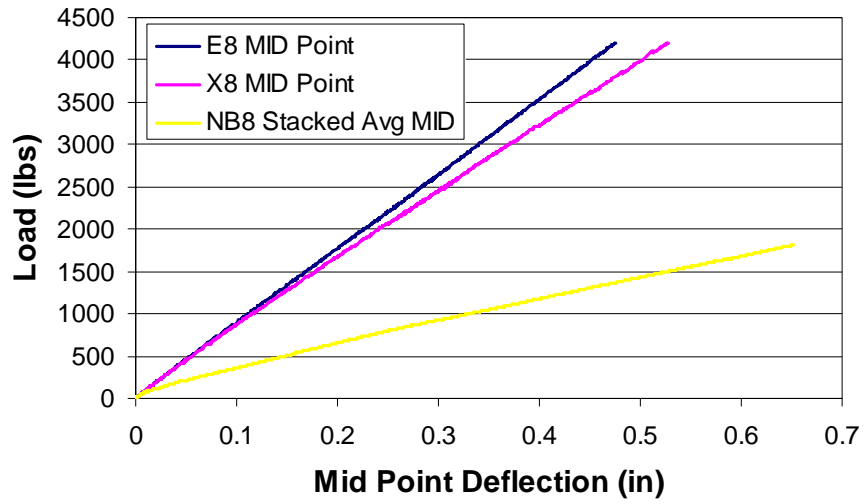


Figure 42: Comparison of Mid Point Deflections for 8” width specimens on 10.5’ span.

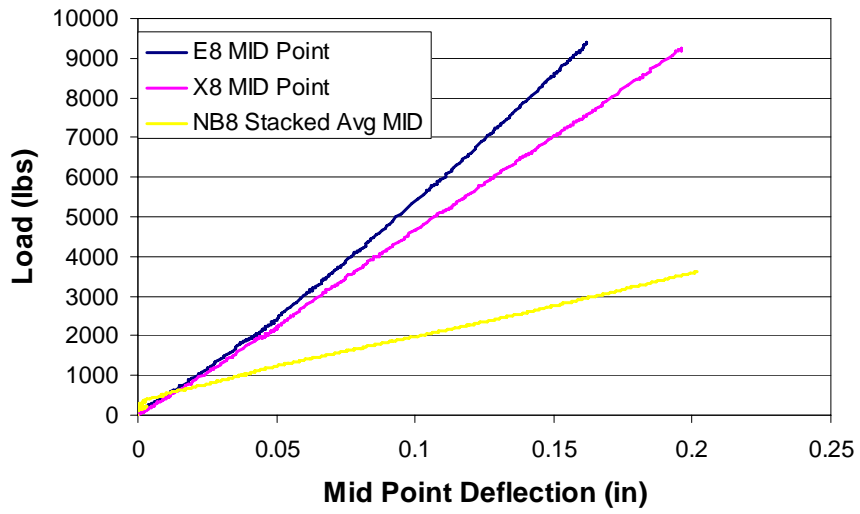


Figure 43: Comparison of Mid Point Deflections for 8” width specimens on 5’ span.

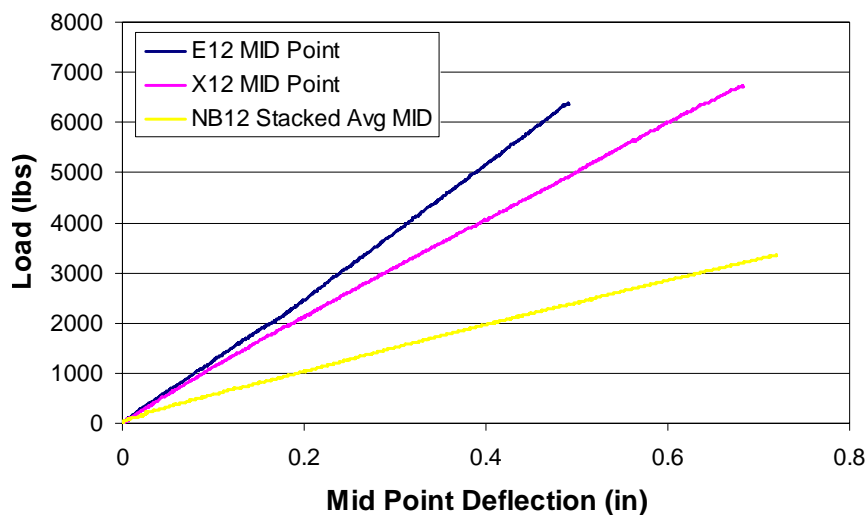


Figure 44: Comparison of Mid Point Deflections for 12'' width specimens on 10.5' span.

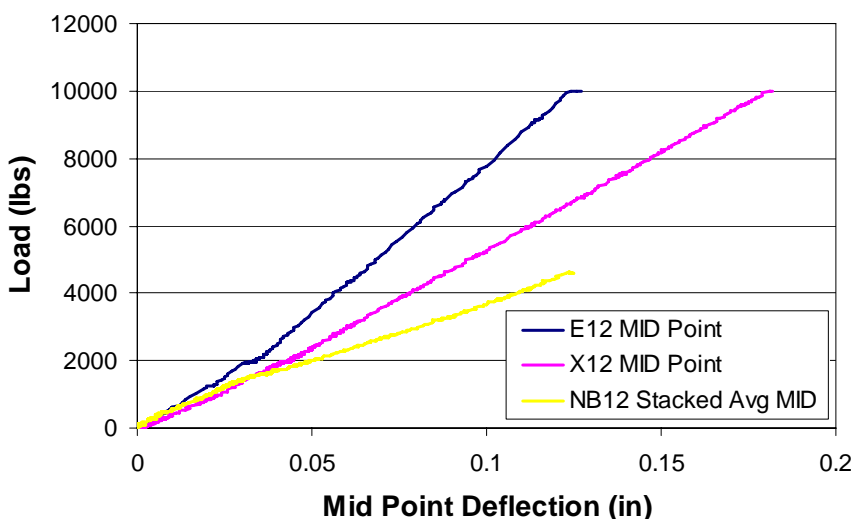


Figure 45: Comparison of Mid Point Deflections for 12'' width specimens on 5' span.

5.5. Phase 1: Width Series Test Discussion

In Figure 40 through Figure 44, note that the epoxied specimens (E4, E8, and E12) lines have the greatest slope. This simulates a fully composite section, fabricated from two timbers acting as one member. The stacked specimens (NB4 over NB4, etc) lines represent two stacked timbers, not connected at all, and their slopes are the lowest. The MF-FRP specimens (X4, etc) lie between the stacked and epoxied, indicating that they do achieve

more composite action than the stacked beams but not quite the fully composite model of the epoxied timbers. Table 11 gives flexural stiffness values (denoted $E_a I$ for EI apparent) obtained from the slopes of the above graphs.

Table 11: E values calculated from 10.5' and 5' spans

4" Widths					
Beam	Slope (lb/in)	L (in)	$E_a I$ (10^8 lb*in ²)	I_{theory} (in ⁴)	E_a (10^6 psi)
E4	7291.3	126	3.03	170	1.78
X4	6145	126	2.56	170	1.50
NB4 over NB4-2	1964.6	126	0.81	42	1.91
NB4-3 over NB4-4	1458.9	126	0.60	42	1.42
sE4	43475	60	1.95	170	1.14
sX4	26654	60	1.19	170	0.70
sNB4 over NB4-2	15136	60	0.68	42	1.59
sNB4-3 over NB4-4	13070	60	0.58	42	1.37
8" Widths					
E8	11985	126	4.99	341	1.46
X8	10031	126	4.18	341	1.22
sE8	78296	60	3.52	341	1.03
sX8	57292	60	2.57	341	0.75
12" Widths					
E12	19604	126	8.17	512	1.59
X12	12646	126	5.27	512	1.02
sE12	126879	60	5.71	512	1.11
sX12	75935	60	3.41	512	0.67

The stiffness obtained from the FRP X-braced specimens is compared to the fully composite stiffness as a ratio of the epoxied beams in Table 12.

Table 12: FRP X-braced EI values shown as a percentage of EI from same sized epoxied beams

Span	$E_a I$ Epoxied Beam (10^8 lb-in ²)	$E_a I$ - FRP X-Braced (10^8 lb-in ²)	FRP X-Braced Stiffness as % of Epoxied Stiffness
4" Width Series			
10.5' Span	3.04	2.56	84%
5' Span	1.96	1.20	61%
8" Width Series			
10.5' Span	4.99	4.18	83%
5' Span	3.52	2.58	73%
12" Width Series			
10.5' Span	8.17	5.27	64%
5' Span	5.71	3.42	59%

Having data from two different spans allows us to calculate yet another flexural stiffness value described by Bank (1989). Using shear deformation and beam theory the following process was applied:

$$\Delta = \frac{PL^3}{48EI} + \frac{PL}{4AG} \quad (\text{deflection equation}) \quad (5)$$

$$\frac{\Delta}{PL} = \frac{1}{EI} \left(\frac{L^2}{48} \right) + \left(\frac{1}{4AG} \right) \quad (\text{rearranged}) \quad (6)$$

Where

Δ = Max deflection at center of specimen

P = Load applied to center of specimen

L = Span

A = Cross sectional area of specimen

I = Second moment of inertia

G = Shear modulus

E = Modulus of elasticity

The first term of the deflection equation is due to bending deformation, and the second due to shear deformation. By re-arranging this expression the second equation was obtained, which isolated EI as the inverse of the slope and correlated AG to the intercept. For each specimen, the load and deflection from the 5ft span and the 10.5ft span was used to create a pair of (x, y) coordinates so that the EI and AG could be back calculated. The EI value obtained was designated E_bI to differentiate it from the apparent EI, or E_aI . X and Y coordinates are shown in Table 13.

$$x = \frac{L^2}{48} \quad (7)$$

$$y = \frac{\Delta}{PL} \quad (8)$$

Table 13: X and Y coordinates for evaluation of $E_b I$

Beam	Span - L (in)	Load - P (lb)	Deflection - Δ (in)	y (x 10^4)	x
4" Width					
E4	126	1820	0.242	11.08	330.8
E4	60	5391	0.117	3.62	75
X4	126	2128	0.449	17.58	330.8
X4	60	5017	0.23	7.64	75
8" Width					
E8	126	4201	0.475	9.42	330.8
E8	60	10001	0.225	3.75	75
X8	126	4198	0.527	10.46	330.8
X8	60	9240	0.196	3.54	75
12" Width					
E12	126	6376	0.49	6.1	330.8
E12	60	9995	0.176	2.93	75
X12	126	6714	0.683	8.07	330.8
X12	60	9985	0.227	3.79	75

The following graphs (Figure 46, Figure 47, and Figure 48) were obtained from the data in Table 13.

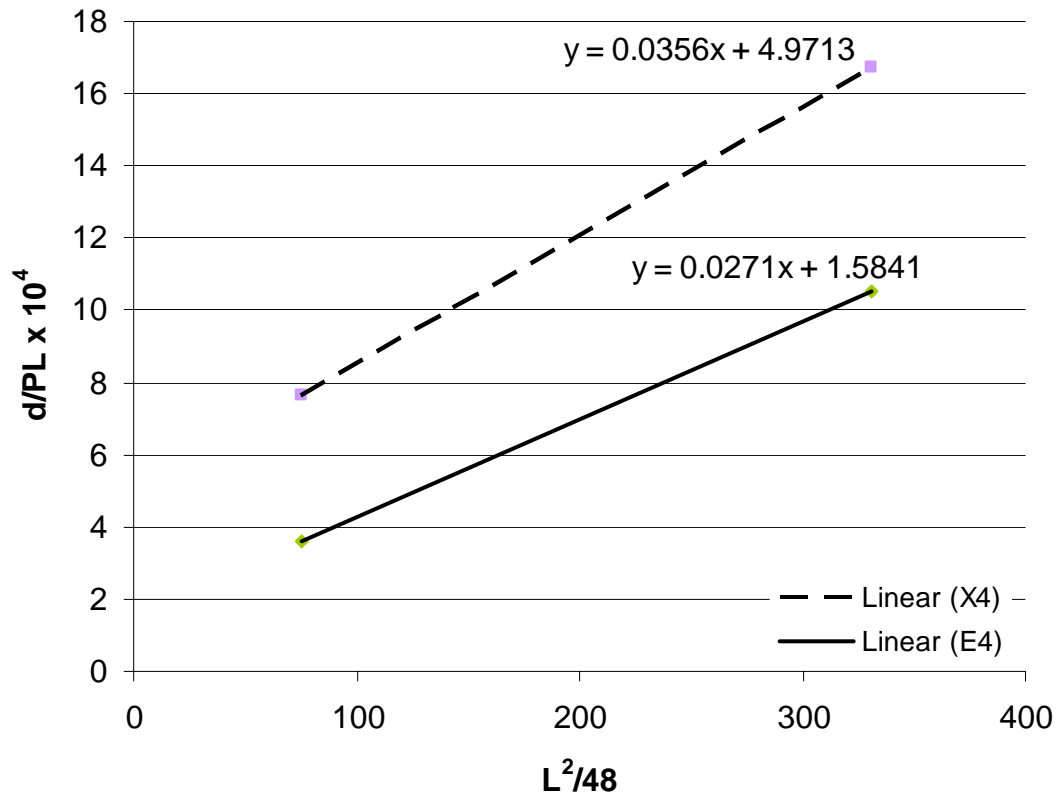


Figure 46: Graph to obtain $E_b I$ and $G_b A$ for 4" width series.

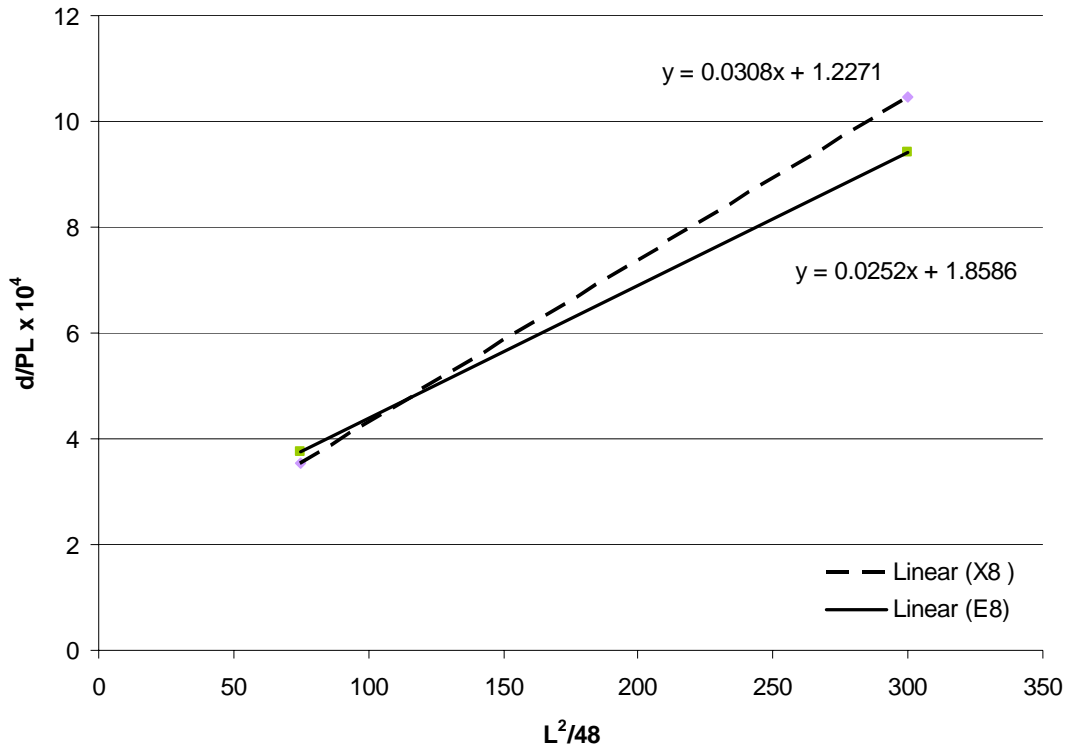


Figure 47: Graph to obtain $E_b I$ and $G_b A$ for 8" width series.

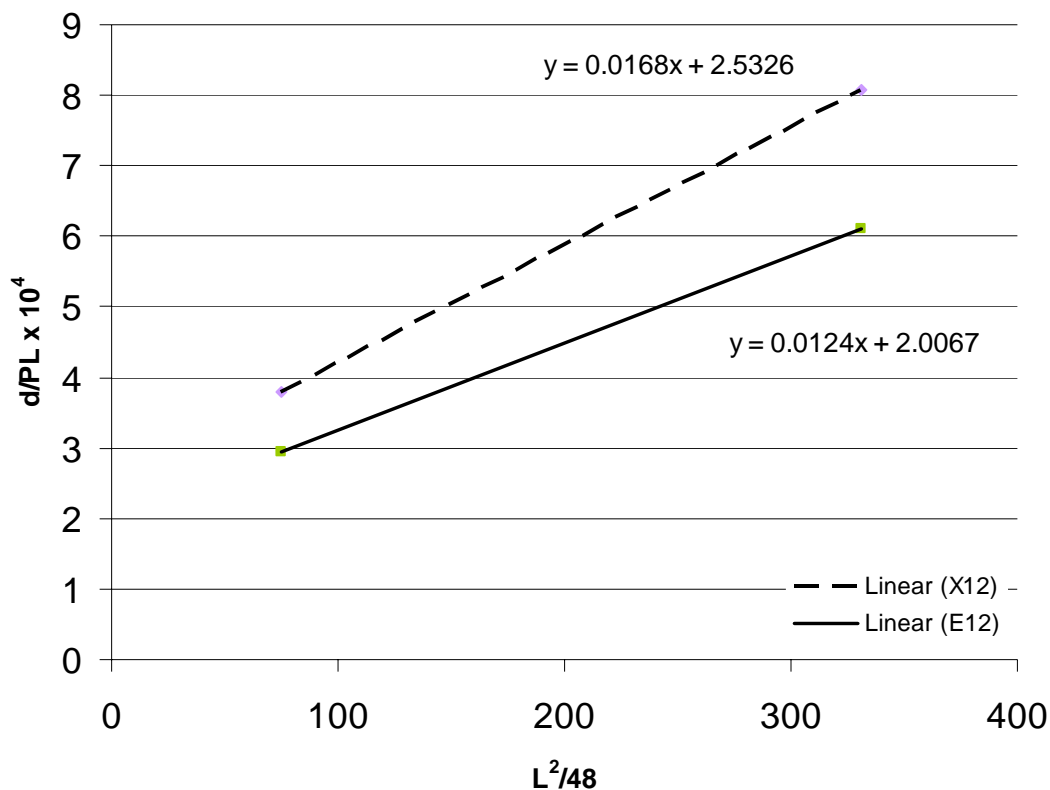


Figure 48: Graph to obtain $E_b I$ and $G_b A$ for 12'' width series.

Finally, the $E_b I$ values were obtained and are shown in Table 14:

Table 14: $E_b I$ Values

Beam	Slope (10^6 1/lb-in ²)	Intercept (10^{-4} 1/lb)	$E_b I$ (10^{11} kip-in ²)	AG_b (ksi)
4" Width				
E4	2.71	1.58	3.69	2500
X4	3.56	4.97	2.81	625
8" Width				
E8	2.52	1.86	3.97	1250
X8	3.08	1.23	3.25	2500
12" Width				
E12	1.20	2.01	8.06	1250
X12	1.70	2.53	5.95	833

Table 15 compares $E_b I$ to $E_a I$:

Table 15: $E_a I$ and $E_b I$ value comparison (units in 10^8 lbs-in^2)

Beam	$E_a I$ 5' span	$E_a I$ 10.5' span	$E_b I$
4" Width			
E4	1.96	3.04	3.69
X4	1.20	2.56	2.81
8" Width			
E8	3.52	5.00	3.97
X8	2.58	4.18	3.25
12" Width			
E12	5.71	8.17	8.06
X12	3.42	5.27	5.95

From Table 15 it is evident that the short 5 ft span does not provide a very accurate EI value; however, the longer 10.5 ft span makes an acceptably close estimation of the EI values. This is expected because shorter spans will experience more shear deformation, while longer spans typically experience deformation closest to pure bending, making the true flexural easier to detect. In addition, it is normally expected that the true value, $E_b I$ would be larger than the apparent value, and the results agree with this.

These results affirm that the testing procedure was successful in creating a basis of comparison for non-composite beams and attempted composite action with MF-FRP strips. It is an accepted fact that working with wood products, as opposed to manufactured materials such as steel and concrete, offers a challenge because of the high likelihood of irregularities in the wood. The elastic modulus from one specimen to the next can be different, and design values given in the NDS are statistical averages. Having established this, it is difficult to obtain stiffness values for beams by using only one specimen of each type. However, the data in Table 15 provide a basis of comparison between fully and partially composite beams over short and long spans. The conclusions drawn from these tests are that long spans are better for determining accurate flexural stiffness and MF-FRP strengthened specimens are able to obtain partial, but not full, composite action.

6. Chapter 6: Phase 1 - Depth Series Tests

For the depth series, beams of 14 inch height were tested on a short (5 feet or 60 inches) span and compared to the beams of 4 inch height from the width series. Note that the MF-FRP specimens are strengthened with the strips in an X-Braced pattern and a V-Braced pattern. It was decided during testing to try a V-shaped bracing pattern, where only the strips that would act in tension were applied. The reasoning behind this was that over such a deep span, the truss-like forces of tension and compression transverse to grain would be more prevalent than bending, and perhaps using the tension strips alone would be sufficient. Table 16 outlines the specimen configurations for Phase 1 Depth Series while Figure 49 and Figure 50 illustrate the MF-FRP specimens from the table.

Table 16: Phase 1 Depth Series Test Specimen Configurations

Depth Series			
Beam Width	Beam Depth	Configuration	Description
4"	14"	Single Beam	A single member
4"	14"	Stacked Beams	One beam on top of the other – no composite action
4"	14"	Epoxied Beams	Simulates fully composite section between two members
4"	14"	FRP V-Braced Beams	FRP fastened to outer surface on either side, achieving some composite action
4"	14"	FRP X-Braced Beams	FRP fastened to outer surface on either side, achieving some composite action



Figure 49: Two members from the depth series stacked and fastened in a V formation with FRP strips and screws. Each beam was 14" deep and the entire system was 28" deep. The FRP strips were 4" wide.



Figure 50: Two members from the depth series stacked and fastened in an X formation with FRP strips and screws. Each beam was 14" deep and the entire system was 28" deep. The FRP strips were 4" wide.

The labeling system for the Depth Series is similar to the Width Series and is outlined in Table 17.

Table 17: Description of labeling convention for test specimens

Label	Description
NB14-#	Not braced, single 14" x 4" beam
NB14-# over NB14-#	Not braced, stacked 14" x 4" beam over a 14" x 4" beam
E14	Epoxied 14" x 4" beam to a 14" x 4" beam
V14	FRP V-braced 14" x 4" beam over a 14" x 4" beam
X14	FRP X-braced 14" x 4" beam over a 14" x 4" beam

6.1. Phase 1: Depth Series Test Setup

The test setup for the depth series was similar to the setup for the width series, but a 100 kip load head was used in order to reach higher applied loads. Figure 51 and Figure 52 show the test setup for the depth series. Recall from the Width Series Test Results it was determined that stiffness values cannot be accurately determined for short span tests. Thus the idea of collecting deflection data became less important and the tests focused on collecting data on transverse compression of the wood members above the supports using LVDTs and strain in the FRP using gauges. The deep beams were only tested on the short (5') span due to constraints in the dimensions of the test setup. Figure 53 shows the compression LVDT and Figure 54 shows the strain gauges on the FRP strips.

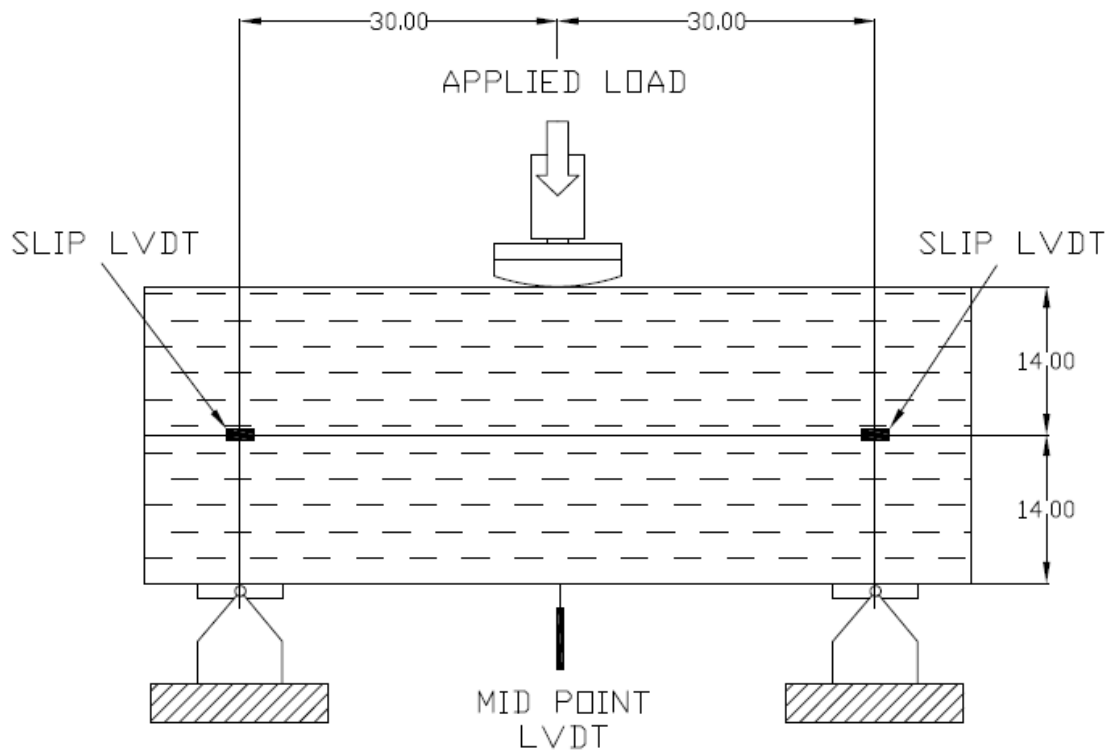


Figure 51: Test setup for Phase 1: Depth Series. Drawing shows two stacked 14" deep members. Dimensions in inches.



Figure 52: Test setup for depth series.



Figure 53: LVDT measuring transverse compression in wood.

6.2. Phase 1: Depth Series Specimen Fabrication

The Depth Series specimens were produced in the same manner as the Width Series MF-FRP specimens, except strain gauges were applied to the FRP strips. The strip that lay closest to the timber had a strain gauge affixed only to its top surface, while the strip that lay on the top had a strain gauge affixed to both the under side and top side, shown in Figure 54.



Figure 54: Strain gauges on depth series beams.

6.3. Phase 1: Depth Series Test Procedure

The test procedure for the depth series is very similar to that of the width series. Though the loads were higher (27 kips for the stacked and 30 kips for the composite sections), the same deflection controlled load application was utilized.

When the first FRP X-Braced combination (X14) was tested, some problems were encountered. The test load on the X14 beams should have gone up to 60 kips as calculated from bending theory. At approx 40 kips the beam experienced significant crushing around the load head, buckling of the compression FRP strips, and slight crushing at the supports. The test was stopped. Steel plates were procured which were 3 inches wide and about 16 inches long to help distribute the loads to prevent crushing. One was placed on each support and under the load head. In addition, it was decided that 60 kips was too high of a load. Upon further examination, the governing load should have been that of shear and not bending. Shear calculations gave a max allowable load of 30 kips. It was decided that future X14 tests would be taken to 30 kips. The first X14 beam was slightly damaged but 3 repetitions at 30 kips were completed. Then, a new X14 beam was fabricated to get 3 repetitions of fresh data. The damaged beam was relabeled as X14-2 so that for ease of presentation the “good” specimen could be called X14. From that point forward the remainder of the depth series was tested to 30 kips. Figure 55 and Figure 56 show before and after images of the crushing problems. Table 18 provides a list of the depth series tests.

Table 18: Record of all tested specimens in the Depth Series

Beam Label	Description (w x h)	Reps	Test Load (lbs)
NB14-2 over NB14-1	4" x 14" / 4" x 14"	3	27000
NB14-2 over NB14-3	4" x 14" / 4" x 14"	3	27000
NB14-4 over NB14-3	4" x 14" / 4" x 14"	3	27000
E14	4" x 14" / 4" x 14" epoxy	3	30000
V14	4" x 14" / 4" x 14"	3	30000
X14	4" x 14" / 4" x 14"	3	30000
X14-2	4" x 14" / 4" x 14"	3	40000



Figure 55: Crushing near the load head of specimen X14.



Figure 56: Steel and wood plates to remedy stress concentrations at both (a) the load head and (b) supports.

6.4. Phase 1: Depth Series Test Results

Load vs. deflection data was plotted for each test specimen, and load vs. slip and load vs. compression data were plotted when available; all are presented in Appendix B. A comparison of curves for each specimen type is shown in

Figure 57.

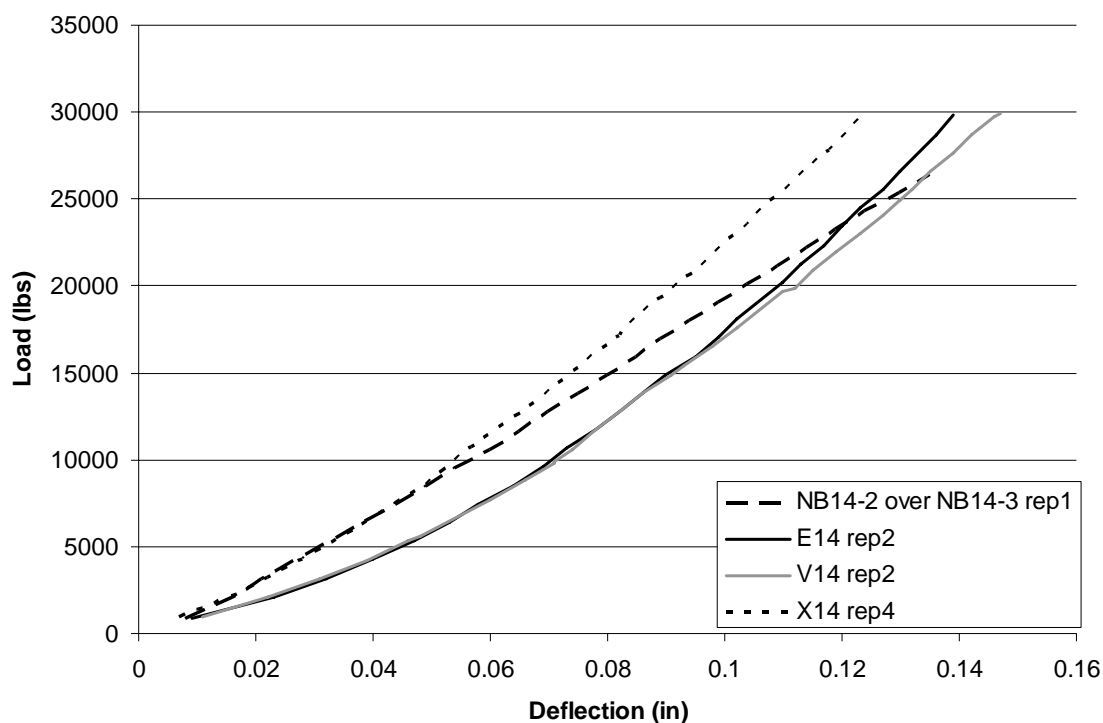


Figure 57: Load vs. Deflection curve for Depth Series.

Strain data from the depth series can also provide useful information. The strain readings from the FRP X-braced strips are shown in Figure 58. There is one curve for the strain gauge on the top surface of the bottom (tension) strip and a curve from each the top surface and bottom surface of the top (compression) strip. A fourth curve is plotted which represents the addition of the tension reading from the top surface and the compression reading of the bottom surface of the buckling strip, giving the resultant axial strain in the FRP.

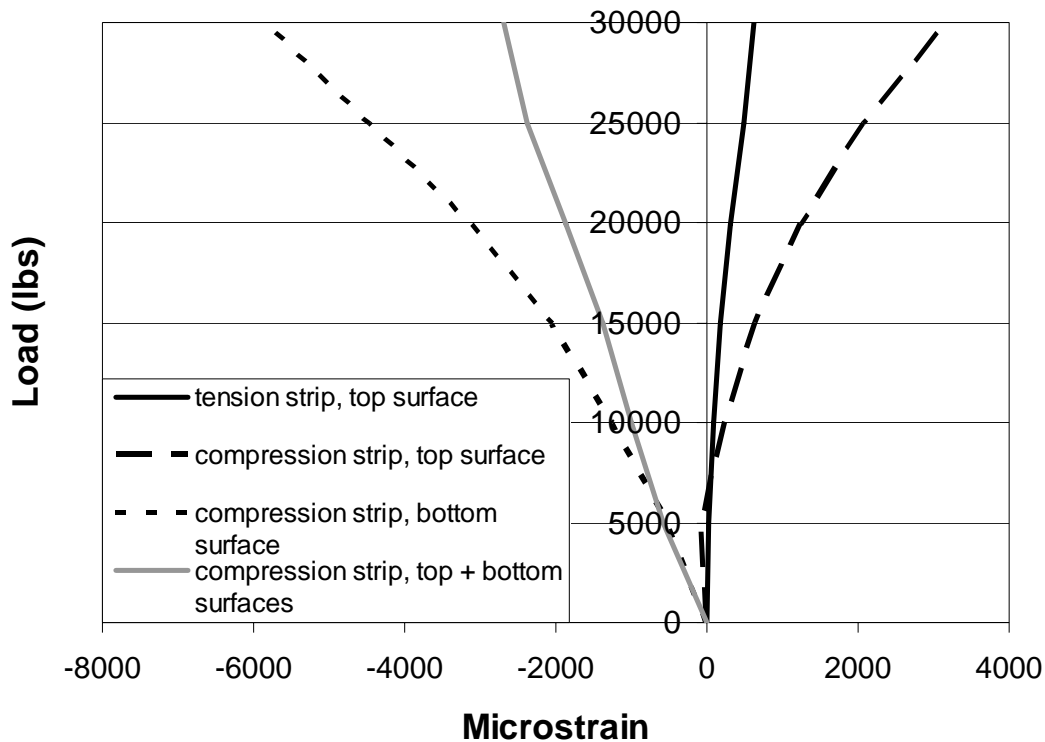


Figure 58: Load vs. strain data from the X14 depth series specimen.

6.5. Phase 1: Depth Series Test Discussion

Note in Figure 57 how the stacked specimen, NB14-2 over NB14-3 has a visibly smaller slope than the other three curves which have some form of composite action. This is expected since two non-composite beams should be much less stiff than two beams attached. In addition, note that the stacked combination appears to be linear for the entire data set. The other three curves start out with a shallower slope and gradually increases until it reaches its final slope and becomes very close to linear. It is possible that the beams in the stacked combination are allowed to slip against one another, and the deflection occurs at a constant rate throughout the test. The other specimens which are attached to one another prevent slip to varying degrees and the deflection is due mostly to contributions from bending. While the specimens may experience some bending initially (hence the less stiff slope), once the FRP

strips engage fully and the beams are at their greatest degree of compositeness, the slope plateaus at a stiffer value.

The best representation of the slope in the load deflection curves for the depth series is the slope obtained from the last few data points. Table 19 shows slope calculations for each specimen using two different sets of points.

Table 19: Slope calculations for curves in Figure 57

NB14-2 over NB14-3				
	load	defl	load	defl
	lb	in	lb	in
Point 1	20100	0.104	23250	0.119
Point 2	26408	0.135	24306	0.124
Slope (lb/in)		203495		211132
E14				
	load	defl	load	defl
Point 1	25549	0.127	26613	0.130
Point 2	29806	0.139	27685	0.133
Slope (lb/in)		354712		357295
V14				
	load	defl	load	defl
Point 1	28721	0.142	26598	0.135
Point 2	29789	0.146	27663	0.139
Slope (lb/in)		267118		266198
X14				
	load	defl	load	defl
Point 1	25380	0.130	28610	0.142
Point 2	29674	0.146	29674	0.146
Slope (lb/in)		268378		265952

Once the slopes were calculated, the apparent modulus, E_a , could be back calculated using flexural deflection equations. As discussed above, this deep beam over a short span was probably not governed by bending theory alone, but rather a combination of bending and shear. That said, the apparent modulus was calculated using bending theory with the knowledge that it may not be the most accurate value, but will show trends in the stiffness of the specimens. Further, the width series found that EI values were less accurate over short

spans due to shear deformation; the preferred method for obtaining accurate EI values is to use the longest span possible; in this case the depth series could only be tested over a short span. Once again, the values calculated will be used to indicate trends and not absolutely accurate material properties. Table 20 shows the E_a values calculated for the depth series.

Table 20: E_a calculations based on data in Figure 57

Beam	Slope	L	$E_a I$	I_{theory}	E_a
	lb/in	in	10^9 lb-in²	in⁴	psi
NB14-2 over NB14-3	207314	60	0.93	914	1019947.54
E14	356004	60	1.60	914	1751474.95
V14	266658	60	1.20	914	1311910.71
X14	267165	60	1.20	914	1314405.53

Recall from the width series tests, the modulus of elasticity, E , for Douglas Fir is in the vicinity of 1.6×10^6 psi. The values of E_a in Table 20 are relatively close to this considering that a short span and flexural deflection equations were used. The important trend to note from the data in Table 20 is the lowest modulus belongs to the stacked combination of beams as expected. The highest modulus corresponds to the epoxied combination, which is also expected because it simulates a fully composite solid piece of timber 4 inches wide \times 28 inches deep. The MF-FRP beams fall somewhere in between these two, which indicates that they achieve some composite action. Possibly the most interesting fact is that the V-braced and X-braced specimens are able to attain very similar load deflection slopes, indicating that the level of composite action obtained by both is also very similar. Because the strips in the V-braced specimen are in tension, it can be concluded that they do the brunt of the work in the X-braced specimen while the compression strips appear to be unnecessary.

The flexural stiffness values from the MF-FRP system were taken as a percentage of the fully composite epoxied system to see how effective the bracing was, and then compared

to the 4 inch depth specimens from Phase 1: Width Series tests. The results were 75% composite action for the 14 inch deep beams and 61% composite action for the 4 inch deep beams. Table 21 shows that having a deeper beam enhances the ability of the FRP strips to obtain composite action. Note that since the Depth Series tests were only done on the short span of 5 feet, they were only compared to the short span of the Width Series; recall that the short spans provided a less accurate stiffness value than long spans, but when short spans are compared against each other they offered reliable trends.

Table 21: FRP X-braced EI values shown as a percentage of EI from same sized epoxied beams

Span	$E_a I$ Epoxied Beam (10^8 lb-in ²)	$E_a I$ - FRP X-Braced (10^8 lb-in ²)	FRP X-Braced Stiffness as % of Epoxied Stiffness
4" Depth			
5' Span	1.96	1.20	61%
14" Depth			
5' Span	16.0	12.0	75%

From the strain values in Figure 58, the stress and axial force in the FRP strips can be calculated. At the maximum transverse load of 30,000 lbs the maximum axial (normal) stress in the tension strip was 5640 psi and the axial forces is 2820 lbs. The axial (normal) stress in the compression strip at the maximum transverse load was 23,500 psi and the axial load was 11,750 lbs. The maximum flexural stress in the post buckled compression strip was 56,000 psi. All the stresses were significantly less than the strength of the strip, 92.9 ksi, (Strongwell 2006). The compression strips, by nature of the span being the equal to the depths of the beams, extended directly from the load head to the support. It is possible that the compression strips saw more stress than the tension strips because they served as a direct load path from the load head to the support.

These results seem to directly contradict the previous findings, which showed that the V-brace had no compression strips yet was as effective as the X-brace. It is likely that the tension strips in the V-brace system and the compression strips in the X-brace system had the same effect on composite action – they both were able to stiffen the stacked beams, and any additional strips were unnecessary. This allows us to draw the conclusion that if it can be determined how many strips are needed and where they can be placed, the most economical solution will be obtained.

7. Chapter 7: Phase 2 Tests

Phase 2 utilized full size Douglas Fir specimens which were donated by WSOR in a similar condition one would find a pile cap; they had been stored outside and were preservative treated. The 12 inch \times 12 inch \times 20 foot creosote treated specimens were trimmed to 14 foot lengths which matched the length of pile caps from a 5 pile bent. These specimens were the closest in size as could be obtained to pile caps in a timber trestle bridge. Specimens were tested as individual members (single pile caps), as stacked members (double pile caps), and stacked with MF-FRP strips. During testing it was found that the variability in the wood material made repeatable results highly unlikely; some specimens had splits or checks in some areas which would close up during loading and affect how the load was distributed. In order to allow results to be compared, it was decided that the different MF-FRP configurations would all need to be tested on the same pair of stacked beams. The four pile caps were named as follows: NB12-1, NB12-2, NB12-3, and NB12-4, which follows a similar pattern to the naming in Phase 1.

7.1. Phase 2: Test Setup

The setup for Phase 2 tests utilized a 300 kip load cell with a steel W shape used as a spreader bar to apply two separate loads, simulating the footprint of loads from the rails. Figure 59 and Figure 60 show the overall setup.

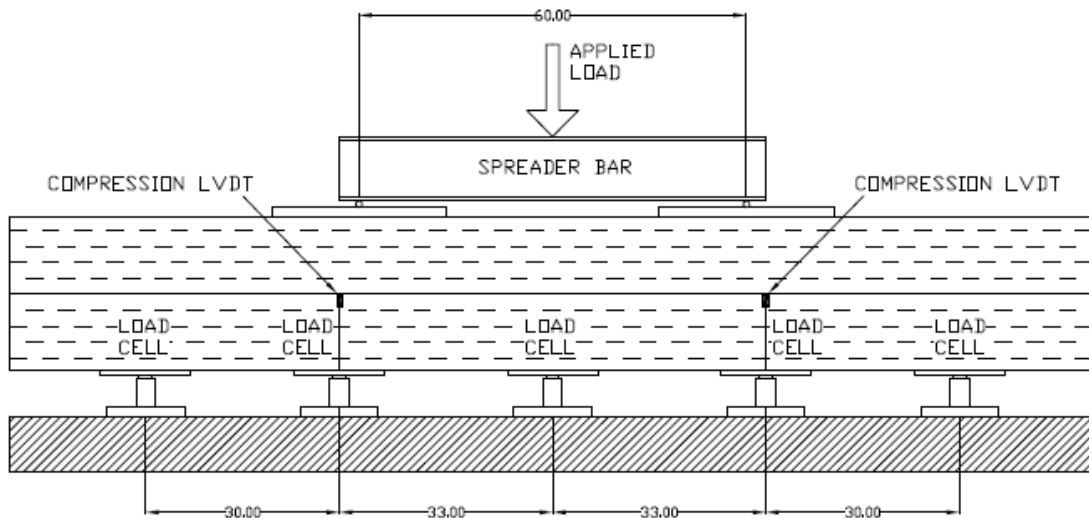


Figure 59: Test setup for Phase 2 tests. Drawing shows two stacked full scale beams. Dimensions in inches.



Figure 60: Phase 2 test setup, with the 3 center supports visible.

The spreader bar distributes the load from a single point to two points which are 60 inches apart, representing the center to center spacing of the rail loads. Beneath the spreader bar steel dowels provide point loads onto steel plate which is the size of three stringers creating a distributed load onto the pile cap. Figure 61 shows a close up detail of the loading plate.

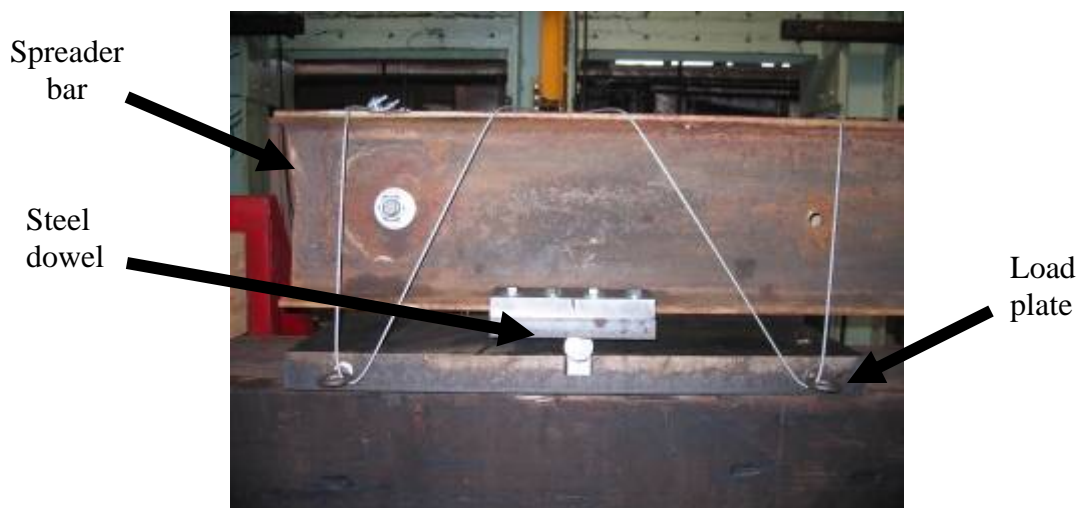


Figure 61: Detail of left loading plate. The I beam is the spreader bar, and the load is channeled through this spreader to a steel dowel point load to a steel plate resting on top of the specimen. The cables which are visible around the spreader bar and plate are for safety reasons.

For the supports, 5 load cells were fitted with 14 inch diameter circular steel plates atop which the specimens would rest. The actual in-situ piles were 14 inch diameter and provide the basis for the test supports. The supports in the test setup are in fact rigid; this is not the case for real piles which consist of a deformable wood material, more like springs. However, in an attempt to limit the variables during testing, the rigid supports were used so that recorded deflections were guaranteed to come from the pile cap itself. Figure 62 shows a detail of a support. Initial tests were done on the prescribed, or design, spacing for the piles. This was 30 inches between outer and intermediate piles, and 33 inches between intermediate and center piles. Once the desired number of tests were completed at that pile spacing, the supports were moved to accommodate the worst spacing found in the field. This was 27 inches between outer and intermediate piles, and 36 inches between intermediate and center piles (Westbrook 2006).



Figure 62: Detail of load cell at support.

7.2. Phase 2: Specimen Fabrication

Phase 2 MF-FRP specimens were fabricated directly in the test setup. Two of the creosote treated 12 inch \times 12 inch timbers were stacked one on top of the other while resting on the supports in the test frame. Full 4 inch wide FRP strips which were pre-drilled with holes were held against the timber surface and screwed in directly to both members. Having strips which were fully covered in a pattern of pre-drilled holes allowed for the strips to be placed in any desired pattern, and screws filled in where necessary. Figure 63 shows MF-FRP strips on the Phase 2 specimens.



Figure 63: MF-FRP specimen fabrication. 12" x 12" stacked beams had 4" strips applied with lag screws directly in the test set up. Note that not all of the pre-drilled holes are being used.

7.3. Phase 2: Test Procedure

Phase 2 tests used similar equipment to Phase 1 tests. The main difference is that a new custom LabView program was used which had 15 channels available for collecting data: 5 channels for the load cells under supports, 5 channels for strain, and 5 channels for LVDTs. There was also a built-in load collecting function. The specimens were pre-loaded with around 200 pounds, again to insure against misplacement of the load head. Initial loading was to 30 kips for single cap piles and 40 kips for double cap piles. Later tests were to 150 kips for the double caps, which was slightly below the service load but was the highest load that the test setup allowed for safely. This time, however, instead of being deflection controlled, the test was load controlled at a ramp of 3,000 pounds per minute for the 30 kip tests, 4,000 pounds per minute for the 40 kip tests, and 12,000 pounds per minute for the 150 kip test, which allowed the chosen loads to be reached in a minimum of ten minutes. Table 22 lists the various specimens and corresponding loads that were tested and Figure 64 shows the ideal (design) spacing and poor spacing as identified in the Westbrook report (2006).

Table 22: Descriptions of specimens tested in Phase 2

Specimen Name	Description	Test Load (lbs)
Prescribed Spacing 33" – 30" – 30" – 33"		
NB12-1	Single pile cap	30,000
NB12-2	Single pile cap	30,000
NB12-3	Single pile cap	30,000
NB12-4	Single pile cap	30,000
NB12-2 over NB12-1	Double pile cap	40,000
NB12-3 over NB12-2	Double pile cap	40,000
NB12-3 over NB12-4	Double pile cap	40,000
Worst Spacing 27" – 36" – 36" – 27"		
NB12-3 over NB12-4	Double pile cap	40,000
NB12-2 over NB12-3	Double pile cap	40,000
NB12-1 over NB12-4	Double pile cap	40,000
NB12-1 over NB12-4 FRP	Double pile cap with MF-FRP strips in various configurations	40,000
NB12-2 over NB12-3 FRP	Double pile cap with MF-FRP strips in various configurations	40,000 and 150,000

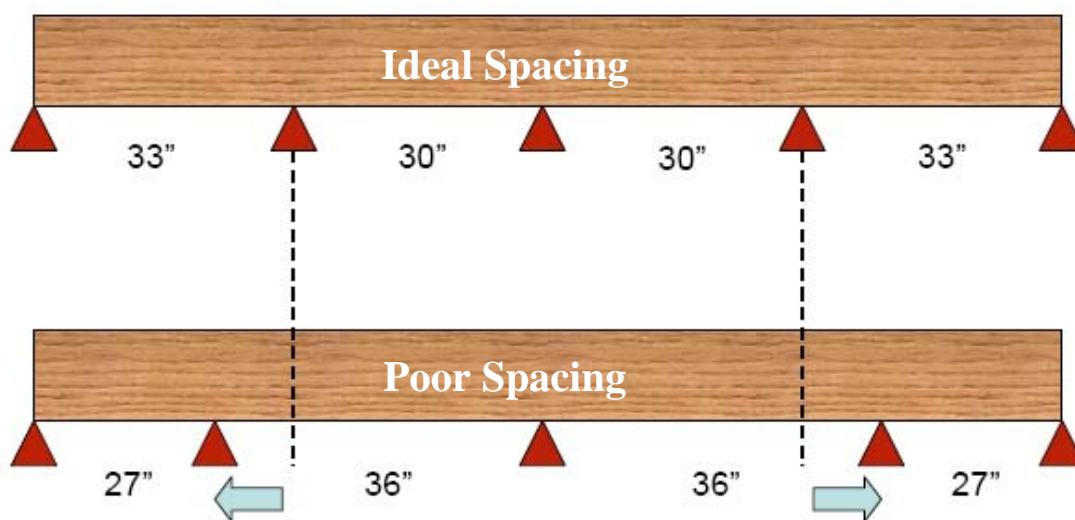


Figure 64: Ideal and Poor spacing as identified by the Westbrook report.

The goal for the full scale MF-FRP strengthened specimens was to try as many different configurations as possible to see what types affected load distribution. In some cases, strictly compression strips were used with the hope of transferring load from the loading area to a

specific support area. In other cases, tension strips were used with the intention of improving composite action to obtain a stiffer section, which would in turn create a more desired load distribution. Lastly, a full X-brace system was used to replicate the X-brace specimens in Phase 1. Figure 65 through Figure 70 show some of the combinations tried. Strain gauges were attached to the X-braced system in much the same fashion as in Phase 1. Two strips lying directly against the wood had strain gauges attached to their top surfaces; one strip which overlapped another had a strain gauge attached to its top surface; and one strip which overlapped another had strain gauges attached to its top and bottom surface. Figure 71 shows attached gauges.



Figure 65: Diagonal compression strips.



Figure 66: Diagonal tension strips.



Figure 67: Vertical compression strips.



Figure 68: Horizontal strips at double cap interface.



Figure 69: Combination of compression and tension strips.



Figure 70: X-brace strips.

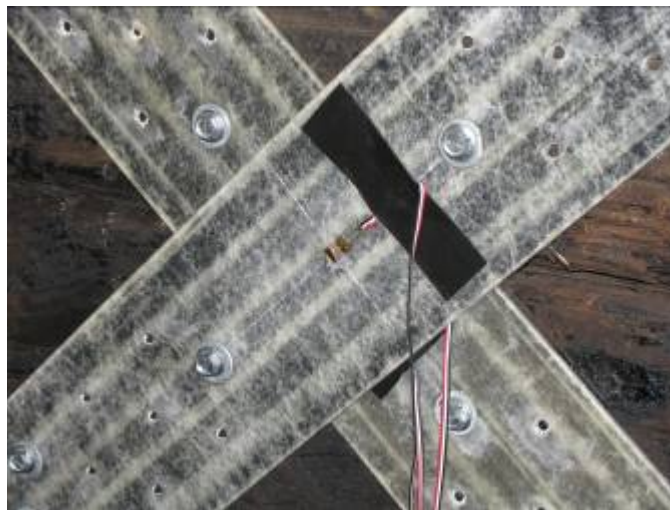


Figure 71: Strain gauges attached to FRP X-braced full scale specimen.

7.4. Phase 2: Test Results

Graphs of the load distributions to each pile were made for the single and double pile caps with prescribed spacing. These results are shown in Figure 72 and Figure 73.

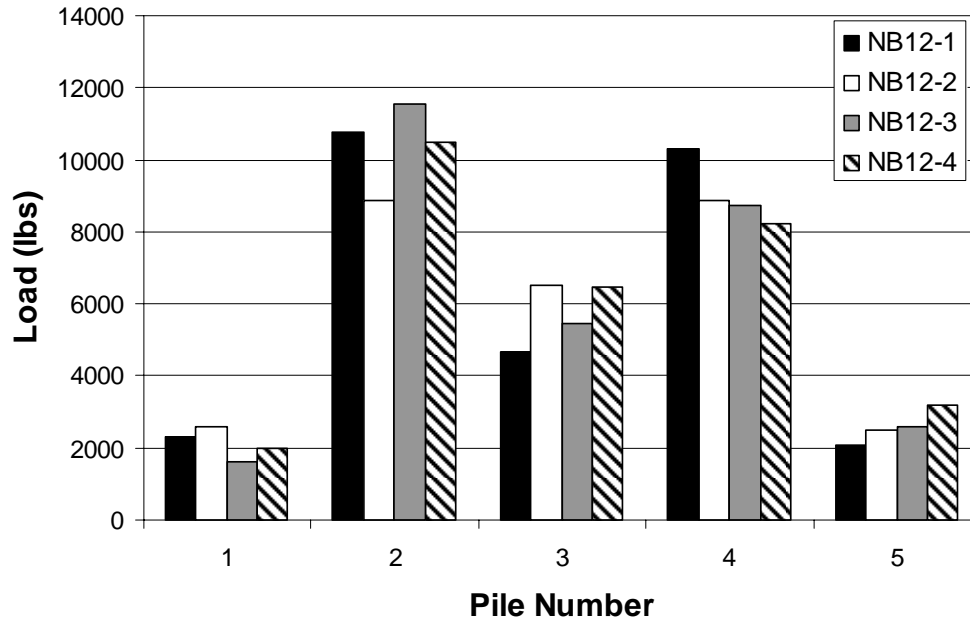


Figure 72: Load distributions for single cap tests with prescribed spacing

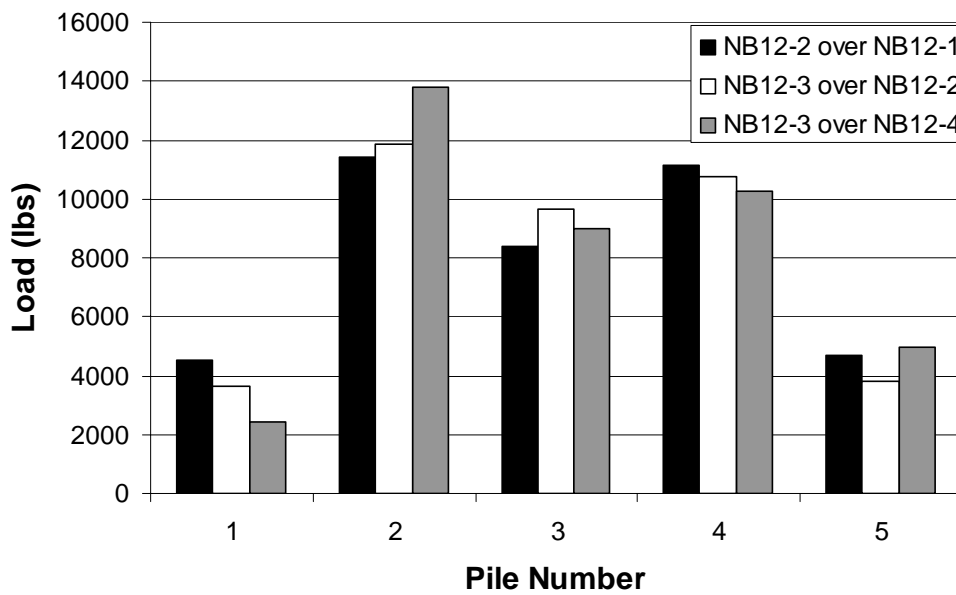


Figure 73: Load distributions for double cap tests with prescribed spacing

The next data set graphed pertained to the double caps with the worst spacing, as shown in Figure 74. Note that when compared to Figure 73 changing the spacing of piles can

drastically affect the load distributions. While the center pile never exceeded 10 kips with the prescribed spacing, it was well above 11 kips in all instances when the worst spacing was used.

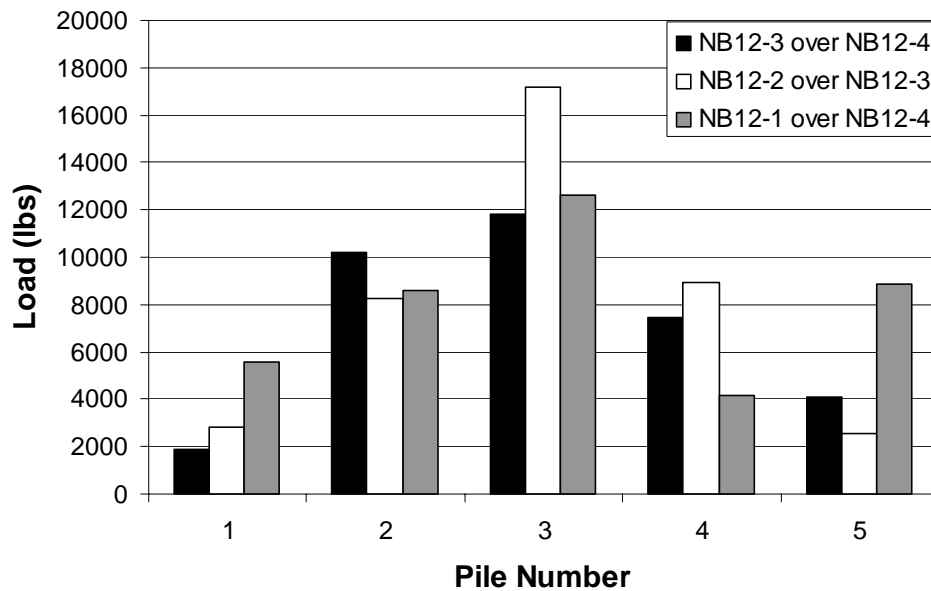


Figure 74: Load distributions for double cap tests with worst spacing

The FRP configurations that were used on NB12-1 over NB12-4 were strictly diagonal compression strips that extended from the load plates towards the outer piles. The results are graphed in Figure 75, however note that the y-axis is percentage of total applied load, and not actual load on each pile. This is for ease of comparison between specimens with different maximum total applied loads.

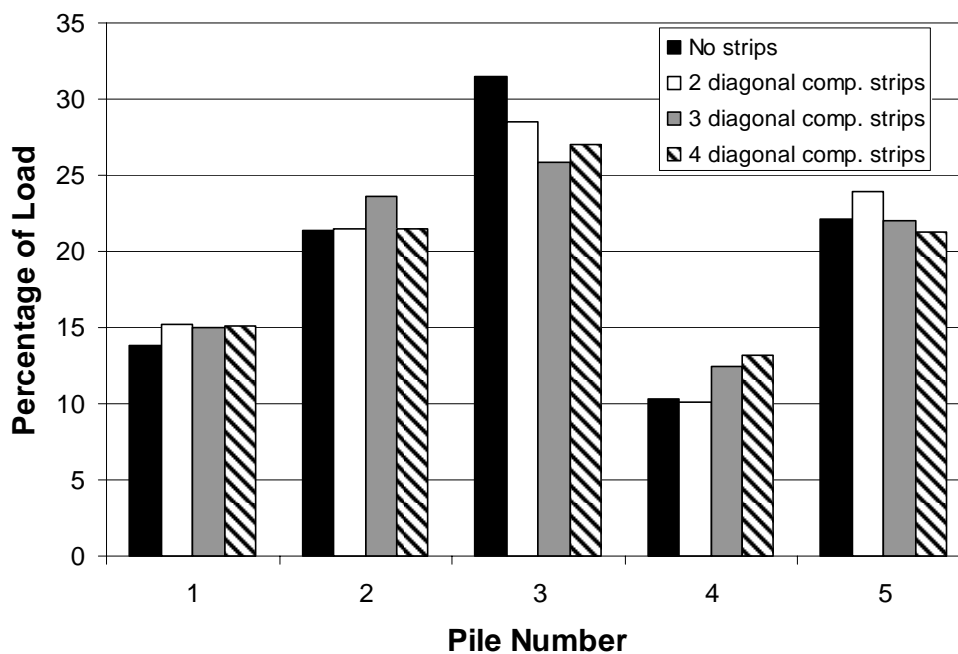


Figure 75: Percentage of load on individual piles for MF-FRP tests on NB12-1 over NB12-4.

From Figure 75 we see that adding FRP diagonal compression strips does have an effect on the load distribution; some of the load is shed from the middle pile and taken up by the intermediate and/or outer piles. Unfortunately, the load shed is only a small percentage (5% at most).

After NB12-1 over NB12-4 was tested several times, the beams were switched out and NB12-2 over NB12-3 were set up. Over 10 different FRP configurations were tested. All of these tests showed similar results, and a few are presented in Figure 76. Again, the improvement trend is small, less than 5% load was shed from the center pile, and in some cases the difference is hardly distinguishable.

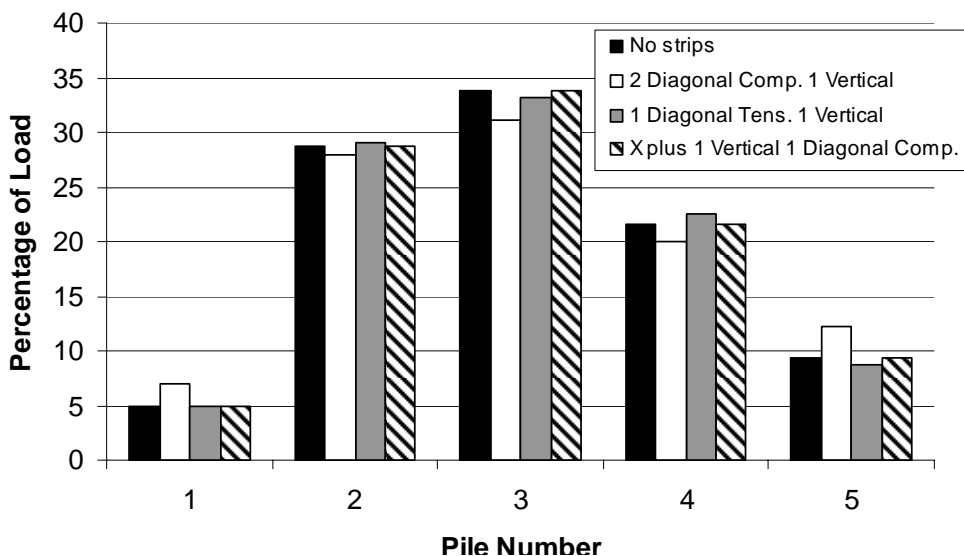


Figure 76: Percentage of load on individual piles for MF-FRP tests on NB12-2 over NB13-3.

Recall that the tests were only being run to loads of 40 kips; the design loads are upwards of 150 kips. The remainder of the tests were conducted with 150 kips of loading, which was the highest load that was safely possible with the test setup.

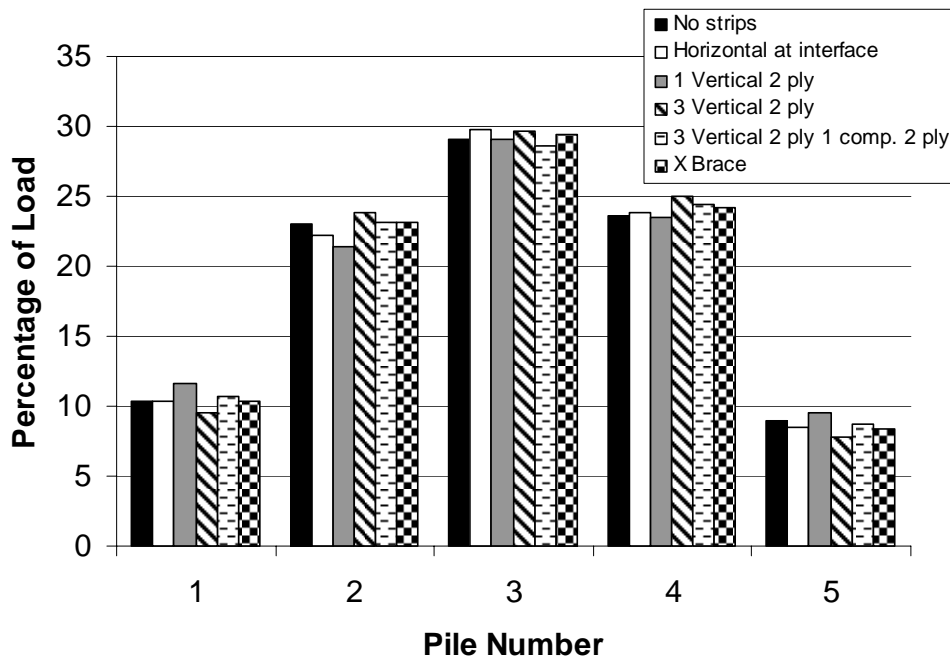


Figure 77: Percentage of load on individual piles for MF-FRP tests on NB12-2 over NB12-3 for 150 kip loads

Figure 77 shows the load distributions for the 150 kip tests on NB12-2 over NB12-3. Five separate MF-FRP strengthened configurations were tried, some even with 2 layers of FRP, denoted as “2 ply.”

Strain data were collected on the X-braced full scale specimen. Strain gauges were placed on the top surface of two tension strips which lie directly against the surface of the wood, and on the top surface of a compression strip crossing over an aforementioned tension strip, and lastly on the top and bottom surface of another compression strip crossing over the other tension strip. Figure 78 shows the strain data from the top surfaces of the two compression strips, Figure 79 shows the strain data from the top surfaces of the two tension strips, and Figure 80 shows the strain data from the top and bottom surfaces of a compression strip, and the curve formed when the two data sets are added.

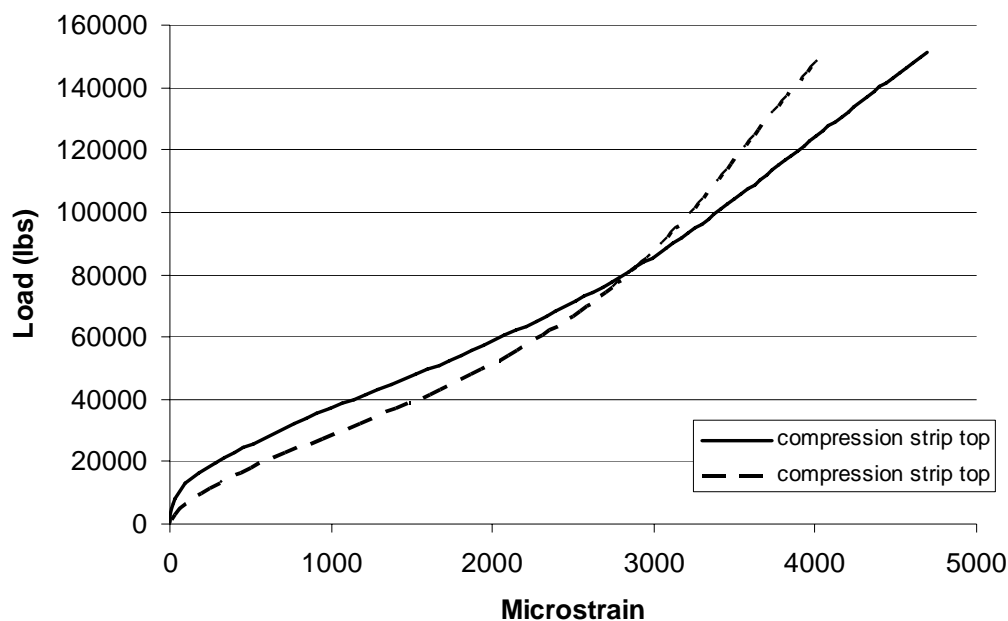


Figure 78: Compression strip top surface strain readings.

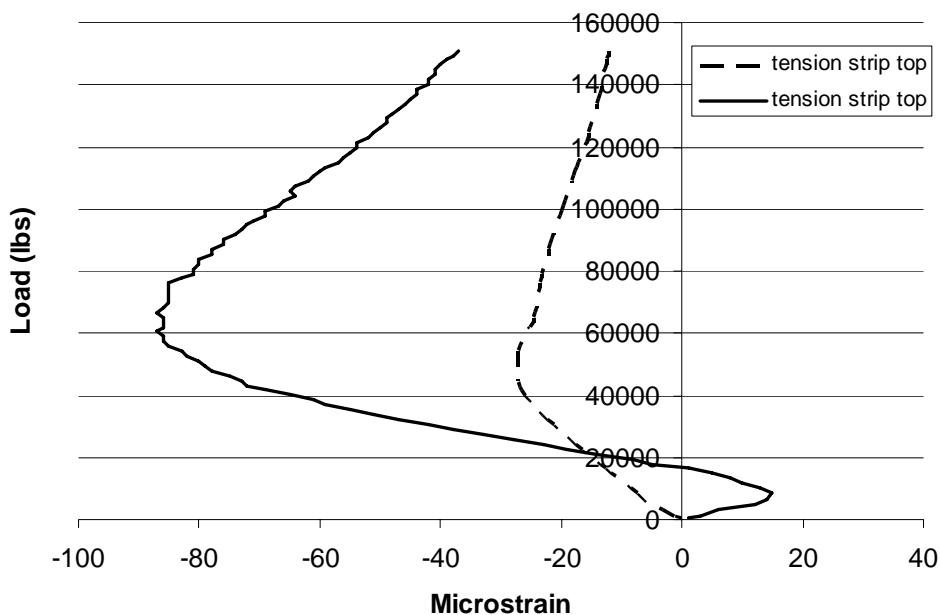


Figure 79: Tension strip top surface strain readings.

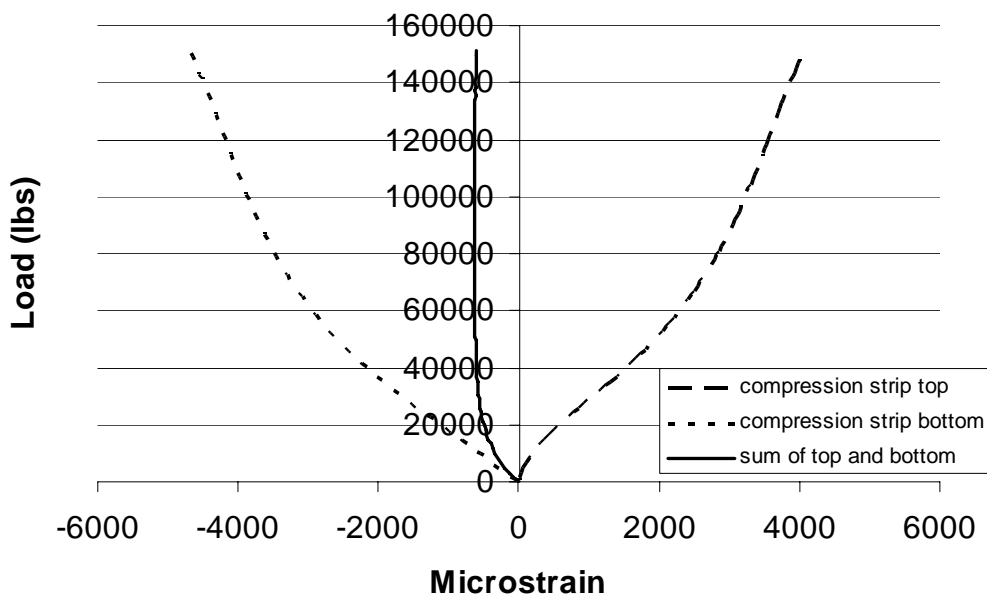


Figure 80: Compression strip top and bottom surface readings, and their sum.

7.5. Phase 2: Test Discussion

It is useful to view the pile loadings as percentages of the total load. The AREMA timber railroad bridge design manual presents equations which determine the percentage of load on

each pile. Table 23 shows the pile loads in percents, and also compares it to the theoretical value that AREMA predicts with its equations, for both a single cap and a double cap. Notable in both the graphed data and tabulated percentages, the variation in load distribution is wide. Some of the specimens yielded a symmetrical distribution while others did not. This was due to the variability in the wood material; material properties themselves may have differed along the length of a member, or physical defects may have affected the results. Regardless, it is important to accept that results will occur over a range, and never be perfectly symmetric or repeatable.

Table 23: Percentage of total load on each pile – prescribed spacing

Specimen Name	Pile 1	Pile 2	Pile 3	Pile 4	Pile 5
AREMA Theoretical¹	8.1	29.7	24.4	29.7	8.1
NB12-1	7.6	35.4	15.3	34.0	6.9
NB12-2	8.6	29.6	21.7	29.5	8.3
NB12-3	5.4	38.3	18.1	28.9	8.6
NB12-4	6.6	34.9	21.5	27.4	10.7
AREMA Theoretical¹	10.1	27.1	25.7	27.1	10.1
NB12-2 over NB12-1	11.9	27.9	21.4	28.8	11.6
NB12-3 over NB12-2	8.6	29.2	25.6	26.9	9.1
NB12-3 over NB12-4	5.5	34.3	22.7	25.8	12.2
<small>¹ AREMA Theoretical values were calculated via the process outlined in Section 2.1.2 and then multiplied by ½ to be comparable to test data.</small>					

For the poor spacing, the data was converted into percentage of load on each pile in Table 24. The theoretical AREMA prediction is in the first row. While there is significant variability in the values, the trend that the center pile takes the highest percentage is consistent. At a high enough applied load, say anything over 150 kips, the center pile would exceed its design capacity of 25 tons (50 kips).

Table 24: Percentage of total load on each pile – worst spacing

Specimen Name	Pile 1	Pile 2	Pile 3	Pile 4	Pile 5
AREMA Theoretical¹	8.3	26.7	30	26.7	8.3
NB12-3 over NB12-4	5.3	28.8	33.5	21.0	11.5
NB12-2 over NB12-3	7.0	20.6	42.8	22.3	6.3
NB12-1 over NB12-4	13.8	21.3	31.4	10.3	22.1
1 AREMA Theoretical values were calculated via the process outlined in Section 2.1.2 and then multiplied by ½ to be comparable to test data.					

The results of the 150 kip tests in Figure 77 show even less difference from test to test than the lower loads. It is possible that the loading became so large that the strips reached a limit of load that they were carrying, either because the screws could transfer no more or because the strips became too buckled, and as loading was continued any beneficial effects of the FRP was lost.

The MF-FRP method was successful in Phase 1 creating composite action between stacked members. It was puzzling that the same methodology, applied to much larger beams, was not showing the same effectiveness. Even though the span was deep beams over multiple continuous short spans, making a fully composite section should have significantly improved the results.

Looking at the mechanics of the system more closely it is possible to see why the effectiveness of the MF-FRP system is not apparent. In Phase 1, the beams were not deep and their span was long. Even though the FRP that was fastened to these specimens was cut down in size to 1.75 inches to accommodate the smaller beam sections, the percentage of FRP to wood is much higher. The long span allowed for many X patterns to fit, and in addition to that, there was much less surface area of wood exposed on the sides of the beams. The full sized specimens, using 4 inch width strips, still had large areas of wood exposed between the X pattern, and overall only a few X's would fit the entire length. The large

amount of FRP coupled with the very small amount of shear deformation in Phase 1 specimens allowed the MF-FRP system to attain over 60% of composite action. Conversely, with the large areas of plain, un-strengthened wood between FRP strips, a lot of shear deformation occurred in the majority of the beam. This means that load would still have been transferred in a similar fashion as it was before the MF-FRP system was introduced.

Recall that previous studies, for example, Akbiyik et al 2007, successfully used MF-FRP plates to strengthen damaged beams in shear. Fundamentally, as their beams wanted to deform in shear, the rigid plate on the outside prevented this from happening, and it also helped to transfer shear forces over checks and splits in the damaged wood. The same concept of transferring shear forces across the beam interface was being applied to stacked pile caps in this report, however, leaving so much un-strengthened wood between strips still allowed for shear deformation. Each strip was not related to the next strip in a “rigid” sense, meaning that one strip was rigid relative to itself only, not relative to other strips. As the pile caps experienced shear deformation under loading, one strip could move in relation to another. In essence, the cross section of the beam was only stiffened where the strips were, and not along its whole length. A good analogy from a more familiar subject would be to look at a reinforced concrete beam. When it cracks, a cracked moment of inertia exists, but only where the section is cracked. In doing a deflection analysis, it would be inappropriate to use the cracked moment of inertia for the whole beam, because the majority of the beam remains in tact with the original gross moment of inertia. To solve this problem, an effective moment of inertia is found which accounts for the cracked moment of inertia in a small portion of the beam and gross moment of inertia in the majority of the beam. The same concept applies to this research; it would be inappropriate to assume a composite moment of

inertia across the whole beam, when only portions of it are strengthened. The large distance between FRP strips still allows slip and deformation like a normal beam. Therefore, in order to achieve a high degree of composite action so that the improvements which were predicted could be seen, FRP would have to be configured in a way that stiffens the cross section along the whole length of the beam. A latticed configuration which overlaps multiple strips would probably show significant improvements. At this point, however, it is questionable whether it is most time and cost efficient to fasten many strips, or just use an FRP plate.

This problem is one unique to the wood material. Because the wood is highly compressible and deformable, stiffening the cross section in several discrete places leaves the non-stiffened sections as they were before. This issue is not present when using steel or concrete; these are relatively stiff materials compared to wood. Because the material is quite rigid, stiffening the cross section at just one point would have a much greater effect over the whole beam. This is the reason that the Bernoulli beam theory is applicable for good approximations in beam behavior for stiff materials like steel – plane sections can be assumed to remain plane. In wood, however, the Bernoulli theory applies less because shear deformation is so high that we cannot rely on the cross section remaining plane, even when part of the beam is stiffened.

7.6. Phase 2: Dynamic Test Setup and Procedure

Dynamic tests were done on exactly the same setup as the full sized Phase 2 tests. Only the X-braced MF-FRP pattern was used. Data acquisition and instrumentation was all the same as the full sized Phase 2 tests.

Cyclic loading was set at 0.75 cycles per second, and the load varied between approximately 8 kips and 45 kips during each cycle. A total of 1,000,000 cycles were completed with 8 static tests to 150 kips at intervals of roughly 150,000 cycles. The intervals were not all equal since the cyclic loading was conducted 24 hours a day, and the interval tests were run at times during the day, picked as close as possible to 150,000 cycle increments. The 150 kip static tests were conducted at the following intervals: 150,000; 215,000; 365,000; 466,666; 580,000; 750,000; 875,000; and 1,000,000 cycles.

7.7. Phase 2: Dynamic Test Results

Total applied load vs. individual pile load data is graphed for each test and presented in Appendix B. Total applied load vs. FRP strain is also graphed for each test and presented in Appendix B. Figure 81 shows how the load on the center pile changed as the number of completed test cycles increased to 1,000,000 cycles.

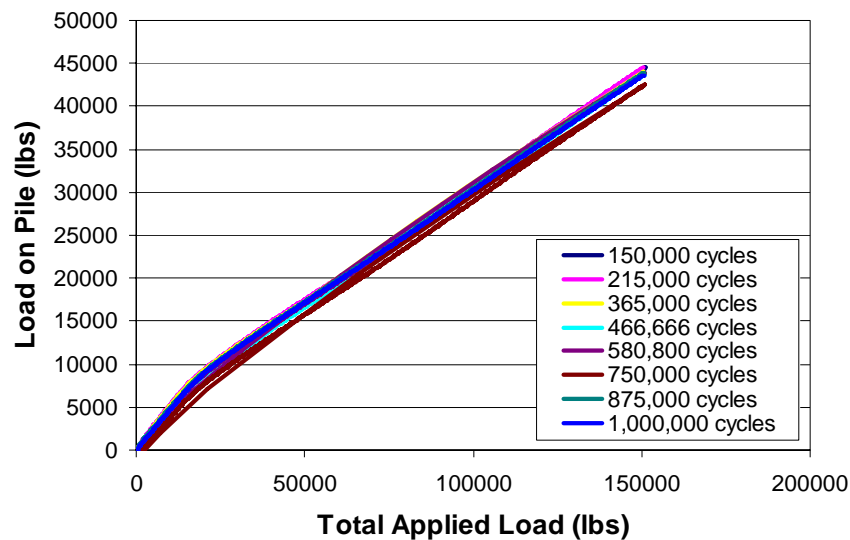


Figure 81: Load on center pile for 150 kip static tests at increments during 1,000,000 load cycles.

Figure 82 shows how the strain on the underside (compression side) of an FRP strip changed as the number of completed test cycles increased to 1,000,000 cycles.

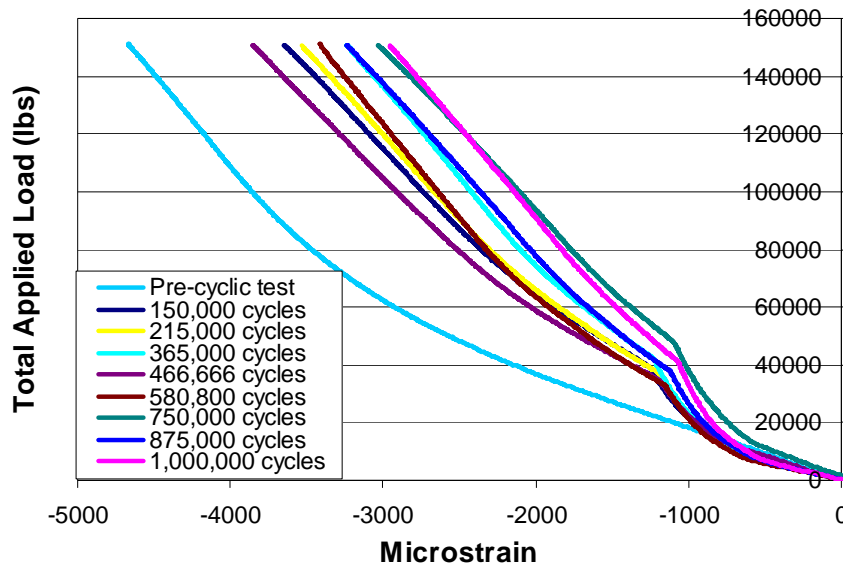


Figure 82: Compression strain in FRP strip for 150 kip static tests at increments during 1,000,000 load cycles.

No FRP strip failures occurred, and no loss of bearing was visible around any of the screws except for one, which came loose as a result of the FRP buckling near to it. No other screws near the buckled FRP came loose so it is assumed that the loose screw did not have proper purchase, which is a problem with the wood/screw interface and not typical of the system.

7.8. Phase 2: Dynamic Test Discussion

Figure 81 shows that the load distributions did not change significantly in the full sized pile caps, even after being tested to 1,000,000 cycles. The cause of this is similar to the reasoning in section 7.5 which explained that only discrete sections of the beam were stiffened, and in between those sections, regular deformation occurred, causing hardly any change in load distribution. Since the stiffened beam was acting like an un-stiffened beam in the sense that the load distribution was not affected, there was very little damage that cyclic

loading could do. If the MF-FRP system was not improving load distribution, then degrading the MF-FRP system would not affect the load distribution.

Figure 82 shows that the strain in the FRP strips was altered as more cycles of loading were completed. The first data set is from the 150 kip static tests of Phase 2 before cyclic testing was started. The relationship of strain is proportional to the total applied load. The rest of the curves on the graph represent tests at increments during cyclic loading. These curves have a distinct discontinuity in slope around the 40 kip region. Recall that the cyclic loading covered a range of approximately 8 kips to 45 kips. The curves between these load values show a strain lower than that of the strain at equal load values before cyclic loading. Once the load passes 45 kips, the curves behave as if cyclic loading never occurred and follow a slope similar to that of the pre-cyclic tests. This indicates that during the 8 to 45 kip range, the system was experiencing movement. There are several places the system could “loosen up” and cause the FRP to experience less strain; for example, as the screws were bearing against the wood and compressed it, they eventually would have small deflections. Any movement like this would cause the FRP to be less taut under loading. When this happened, it took more load to attain the same strain level.

This loss of strain is important because it indicates that the MF-FRP system can degrade over time. The cyclic loading only was conducted to 40 kips, and loads of railcars are actually much higher. While there was no failure in the strips, this system loosening will cause a loss of effectiveness in the composite behavior of the system over time.

8. Chapter 8: Conclusion

The results of this study conclude that (1) MF-FRP strips did not significantly improve load distributions to piles, but showed potential to do so by creating a stiffer composite pile cap, (2) MF-FRP strips increase the flexural stiffness of timber beams in bending with large span to depth ratios, (3) composite action between two timber members can be achieved with mechanically fastened FRP strips, and (4) while composite action may be achieved between two members, this is not enough to significantly improve the load distribution of double cap beams on timber trestle bridges which have severe overloading of piles. Where composite action is most likely to come into use on a trestle bridge is after one or more piles settles and is no longer in contact with the pile cap. This will cause the pile cap to span a longer distance and have a greater span to depth ratio than before. Once it spans a greater distance and experiences more bending than shear, the increased flexural stiffness created by the MF-FRP strips will improve the behavior of the pile cap.

Phase 1 tests concluded that (1) the width of the beams had some effect on the composite nature of the MF-FRP system. For 4 inch, 8 inch, and 12 inch widths the percent of composite action obtained with MF-FRP strips on a 10.5' span was 84, 83, and 64% respectively. 4 and 8 inch widths behaved similarly while the 12 inch width was still effective, but to a lesser degree. (2) The span length affected how accurate the stiffness could be represented. The 10.5 foot span was much more effective in showing the improved composite behavior because it acted in flexure with minimal shear effects.

Phase 2 tests concluded that (1) the MF-FRP technique can benefit a stacked pile cap, but either the number of strips should be greatly increased or an FRP plate be used instead. (2) Loads were not re-distributed with the MF-FRP technique used, but as mentioned before, a

more robust stiffening system, like an FRP plate, would be more effective. (3) the beams generally acted in accordance with design equations and charts presented by AREMA; the single and stacked members gave results very similar to those predicted by the 5 pile load distribution equations. This is useful because the equations are a good model for the actual pile cap behavior, and the equations predict that a fully composite section can improve the load distribution. This means that once a fully composite section can be achieved for the whole length of the pile cap, the results will improve as we predicted.

It was found that using strips to channel load away from one pile and towards another is not the most efficient method for solving the problem of poor load distribution. The AREMA equations show that creating a composite member of two pile caps can improve the load distribution. FRP strips or plates should be utilized to form a single composite pile cap from a double capped bent rather than using them to shift loads. It is recommended that future studies move their focus from the pile cap beam towards adjusting the individual pile stiffness levels (by retrofitting with spring-type assemblies) to redistribute a significant portion of the center pile loads to the outer piles.

References

Akbiyik, A., Lamanna, A.J., and Hale, W.M. (2007), "Feasibility Investigation of the Shear Repair of Timber Stringers with Horizontal Splits," *Construction and Building Materials*, Vol. 21, pp. 991-1000.

American Railway Engineering and Maintenance-of-Way Association (AREMA). (2007), *Manual for Railway Engineering Chapter 7*, AREMA, Lanham, MD.

American Railway Engineering Association (AREA). (1996), *Manual for Railway Engineering Chapter 7*, AREA, Chicago, IL.

American Railway Engineering Association (AREA). (1953), *Manual for Railway Engineering*, AREA, Chicago, IL.

American Society for Testing and Materials (2006), *Standard Practice for Evaluating Material Property Characteristic Values for Polymeric Composites for Civil Engineering Structural Applications*, ASTM D 3039/D 3039M – 00, ASTM International, West Conshohocken, PA.

American Society for Testing and Materials (2005), *Standard Test Methods of Static Tests of Lumber in Structural Sizes* ASTM D198 - 05a, ASTM International, West Conshohocken, PA.

American Society for Testing and Materials (2006), *Standard Test Method for Tensile Properties of Polymer Matrix Composite Materials*, ASTM D 3039/D 3039M – 00, ASTM International, West Conshohocken, PA.

American Wood Council (2005), *National Design Specification (NDS) for Wood Construction 2005 Edition*, ANSI/AF&PA NDS-2005, American Forest and Paper Association, Washington, DC.

Bank, Lawrence C.. (1989), "Flexural and Shear Moduli of Full-Section Fiber Reinforced Polymer (FRP) Pultruded Beams," *Journal of Testing and Evaluation*, Vol. 17, No. 1, pp 40-45.

Bank, L.C., and Arora, D.. (2007), "Analysis and Design of RC Beams with Mechanically Fastened FRP (MF-FRP) Strips," *Composite Structures*, Vol. 79, No. 2, pp. 180-191.

Corradi, Marco, and Borri, Antonio (2006), "Fir and chestnut timber beams reinforced with GFRP pultruded elements," *Composites Part B: Engineering*, Vol. 38, pp 172-181.

Dempsey, D.D., and Scott, D.W. (2006), "Wood Members Strengthened with Mechanically Fastened FRP Strips," *Journal of Composites for Construction*, Vol. 10, No. 5, pp 392-398.

Duwadi, Sheila R. and Ritter, Michael A.. (1997) “Timber Bridges in the United States,” *Public Roads* Winter 1997, Vol 60, No. 3, pp 32-40.

Halpin, Kevin (2008). Personal Communication – E-mail. May 6, 2008. Green Bay, WI.

Lamanna, A.J., Bank, L.C., and Scott, D.W. (2001), “Flexural Strengthening of RC Beams using Fasteners and FRP Strips,” *ACI Structures Journal*, Vol. 98, No. 3, pp. 368-376.

Lopez-Anido, Roberto, Michael, Antonis P., and Sandford, Thomas C., (2004) “Fiber Reinforced Polymer Composite – Wood Pile Interface Characterization by Push-Out Tests,” *Journal of Composites for Construction*, American Society of Civil Engineers, Vol. 8, No. 4, pp 360-368.

Martin, Jeremy A., and Lamanna, Anthony J., (2008) “Performance of Mechanically Fastened FRP Strengthened Concrete Beams in Flexure,” *Journal of Composites for Construction*, American Society of Civil Engineers, Vol. 12, No. 3, pp 257 – 265.

Radford, D.W., Van Goethem, D., Gutkowski, R.M., Peterson, M.L.,(2002) “Composite Repair of Timber Structures,” *Construction and Building Materials* 16, pp 417-425.

Strongwell. (2008), *Brochure – SAFSTRIP® Fiber Reinforced Strengthening Strip*. www.strongwell.com.

Tascioglu, Cihat, Goodell, Barry, and Lopez-Anido, Roberto, (2003), *Composites Science and Technology*, Vol. 63, pp 979-991.

Triantafillou, Thanasis C., (1997), “Shear Reinforcement of Wood Using FRP Materials,” *Journal of Materials in Civil Engineering*, May 1997, pp 65-69.

United States Department of Agriculture (USDA), Smith, Robert L., Bush, Robert J., (1995), “A Strategic Evaluation of Factors Affecting the Adoption of Timber Bridges,” Timber Bridge Information Resource Center (TBIRC), United States Department of Agriculture Forest Service.

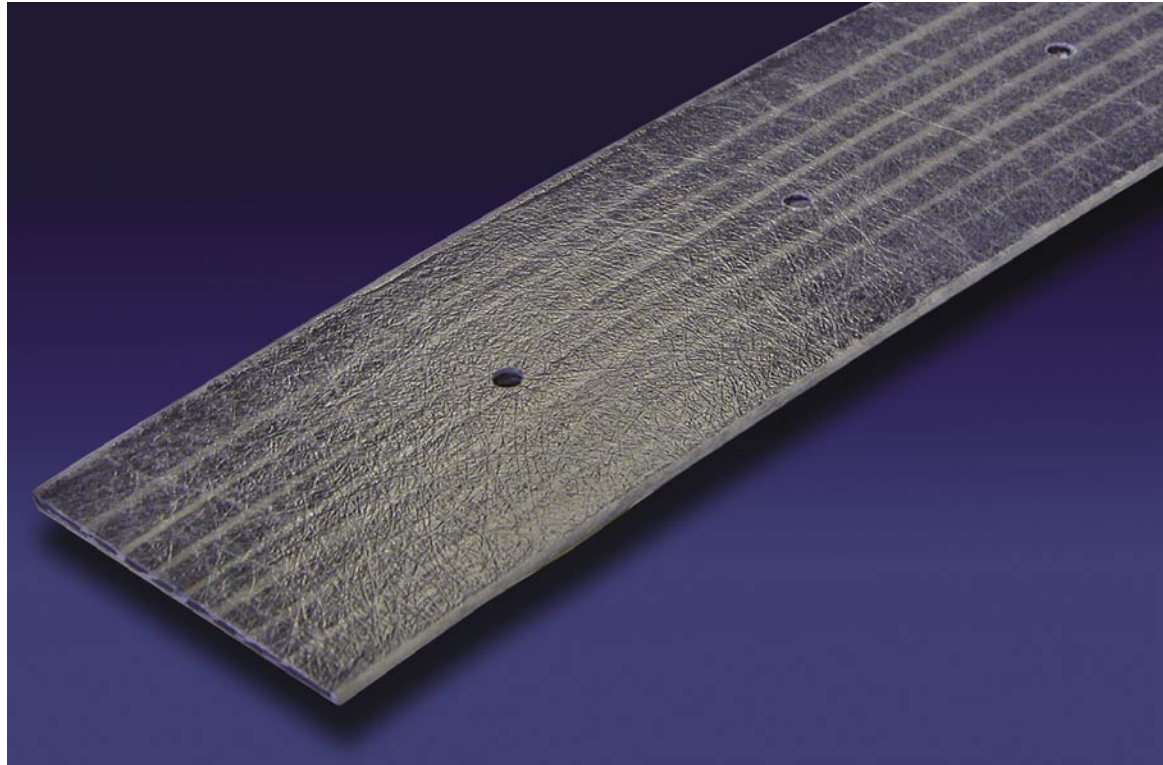
Westbrook Associated Engineers Inc. and E80 Plus Constructors LLC. (2006), *Final Study Report: Impact of Railcar Weight Change on Wisconsin Bridges*, Wisconsin.

Wisconsin & Southern Railroad Co.: Projects. (2008) [online] Available <http://www.wsorroad.com/projects/projects07.html> June 17, 2008.

Appendix A

SAFSTRIP®

FIBER REINFORCED STRENGTHENING STRIP



SAFSTRIP® is a pultruded composite strip that improves the strength of an existing structural member when mechanically fastened to the structure. SAFSTRIP® has high bearing and longitudinal properties and is designed to strengthen the flexural capacity on the tension face of concrete girders, slabs and decks. Installation on bridges can occur without any interruption of service.

SAFSTRIP® is supplied in rolls and may be pre-drilled with holes at the required fastener spacing to receive fasteners. SAFSTRIP® measures 4" wide x 1/8" thick and is shipped in rolls up to 100 ft. long. SAFSTRIP® is designed to be easily field cut by the customer into shorter lengths using standard carpenter tools.



SAFSTRIP® provides these features:

- Easy to install, no skilled labor necessary
- Minimal surface preparation is needed for installation
- Structure is usable immediately after installation
- Cost effective system for increasing load capacity of bridges
- Will not split or delaminate when drilled

FIBER REINFORCED STRENGTHENING STRIP



Workers installed SAFSTRIP® on this bridge in Edgerton, Wisconsin, using the MF-FRP system. The load rating for the bridge increased from HS-17 to HS-25 as a result.



The posted load for this bridge that spans the Meramec River in Missouri was increased from 10 tons to 18 tons by installing SAFSTRIP® using the MF-FRP system.



The abutment and deck of this bridge in Phelps County, Missouri, was strengthened using SAFSTRIP®.

Materials of Construction

SAFSTRIP® is composed of carbon tows sandwiched between layers of fiberglass mats and rovings. The materials are bonded together by a highly corrosion resistant vinyl ester resin. Carbon fibers increase the stiffness of the strip while glass mat provides the proper bearing strength. These combined properties allow SAFSTRIP® to be mechanically attached to a structural member. A synthetic surfacing veil is also incorporated into the composite to improve resistance to corrosion and UV degradation.

What is MF-FRP?

SAFSTRIP® is designed to be installed using an attachment method known as mechanically-fastened fiber reinforced polymer (MF-FRP). Using this method, SAFSTRIP® is attached to an existing concrete girder, slab or deck using closely spaced powder actuated fastening pins or steel expansion anchors. The pins are applied by using a powder actuated fastener gun or other portable fastener gun. Expansion anchors are installed with a pneumatic powered torque wrench. If desired, rubber or neoprene washers may be used between the fasteners and the strip prior to inserting the fastener through the strip.

MF-FRP is an alternative to externally bonded fiber reinforced polymer (EB-FRP). As opposed to the MF-FRP system, in which the load is transferred to the composite strip through a fastener, the EB-FRP system uses an adhesive.

Research and Development

Research and development for SAFSTRIP® was funded by the U.S. Army Engineer Research and Development Center (ERDC). Laboratory research was conducted at the University of Wisconsin Structures and Materials Testing Laboratory and at ERDC's test laboratories. Bridge demonstration projects were conducted in Wisconsin and Missouri.

Engineering Design

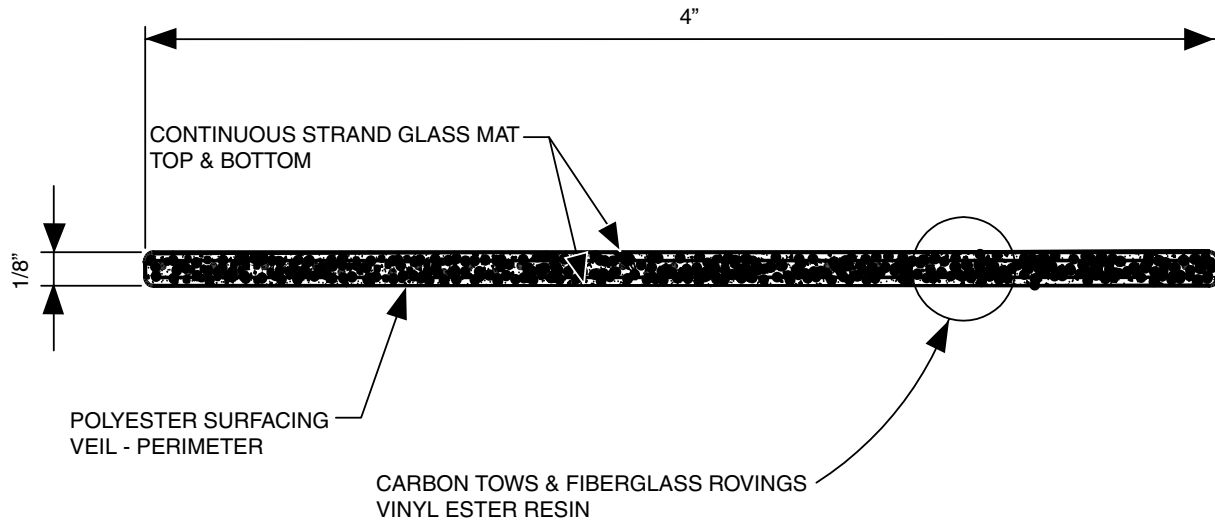
The repair of concrete structures using SAFSTRIP® is dependent upon the concrete's condition. The local engineer must determine the strength of the existing concrete. It must then be determined how much SAFSTRIP® is required and the spacing of fasteners. Design assistance can be obtained by technical data on the following web sites:

<http://campus.umn.edu/utc/research/r098/reports/vol2/Y-0298.pdf>
<http://campus.umn.edu/utc/research/r135/reports/1330005.pdf>

Additionally, the U.S. Army Corps of Engineers technical reports, *Rapid Strengthening of Full-Size Concrete Beams with Powder-Actuated Fastening Systems and Fiber Reinforced Polymer (FRP) Composite Materials*, can be found at:

<http://gsl.erd.c.usace.army.mil/1pubs.html>
(Reports: ERDC/GSL TR-02-4, 02-12 and 04-12)

MECHANICAL PROPERTIES



Property	Average Value ¹		Design Value ²		ASTM Test Method
	US Units (psi)	SI Units (MPa)	US Units (psi)	SI Units (MPa)	
Tensile Strength*	123,613	852	92,902	640	D-638
Tensile Modulus** ³	9.02 x 10 ⁶	62,190	9.02 x 10 ⁶	62,190	D-638
Clamped Bearing Strength*	50,955	351	40,540	279	D-5961
Unclamped Bearing Strength**	31,044	214	26,046	180	D-5961
Open Hole Strength*	94,641	652	78,846	543	D-5766

* 20 Sample coupons per test series

** 17 Sample coupons per test series

¹ Average value of test series

² Average value minus three standard deviations

³ Modulus design values are not reduced in accordance with ACI 440.2R-02



As a result of a SAFSTRIP® retrofit, the existing 12-ton load posting for this bridge in Phelps County, Missouri, was removed.



This bridge, located in St. James, Missouri, was load posted at the time of strengthening. After mechanically attaching SAFSTRIP® with concrete wedge bolts and anchors, the bridge load limit was raised to 20 tons.



Severe deterioration prevented the application of a bonded strengthening system to this bridge in Pulaski County, Missouri, but MF-FRP applied SAFSTRIP® was able to repair the bridge.

COMPARE!**MF-FRP INSTALLATION****VS.****EB-FRP INSTALLATION**

FASTENING SYSTEM	Mechanical - concrete wedge bolts and anchors or powder actuated fasteners.	Adhesive - usually epoxy.
SURFACE PREPARATION	Minimal.	Requires the time consuming process of sandblasting, cleaning and application of epoxy putty that must be ground down for a smooth surface.
WEATHER CONDITIONS FOR APPLICATION	No restrictions. Can be installed even during inclement weather.	Application surface must be moisture-free. Cannot be properly installed in extreme temperatures.
INSTALLATION TIME	Minimal - generally a few hours.	Extensive due to the surface preparation, mixing of adhesives and care required to properly apply the adhesive.
LABOR COSTS	Unskilled labor using standard carpenter tools for cutting and installing strips reduces labor costs.	Skilled labor required to properly prepare the surface and mix the adhesives, which results in higher labor costs.
BOND STRENGTH	Not highly affected by poor condition of the existing outer/superficial concrete substrate.	Dependent on the quality of the concrete substrate.
AVAILABILITY OF STRUCTURE	Available for immediate use upon application.	May require up to seven days to achieve full adhesive strength.
DURABILITY	Tests show excellent retention strength for anchor bolts. Very good fatigue strength.	Research suggests high strain gradient is found in adhesive layer where strips terminate or in proximity of substrate discontinuity (such as cracks). Debonding can be problematic.

THE CHOICE! SAFSTRIP® MF-FRP APPLIED STRENGTHENING STRIP**STRONGWELL***ISO-9001:2000 Certified Manufacturing Plants***BRISTOL DIVISION**

400 Commonwealth Ave., P. O. Box 580, Bristol, VA 24203-0580
 (276) 645-8000 FAX (276) 645-8132

CHATFIELD DIVISION*

1610 Highway 52 South, Chatfield, MN 55923-9799
 (507) 867-3479 FAX (507) 867-4031

**SAFSTRIP® manufacturing location*

www.strongwell.com

INT2M0108
 © Strongwell



Hex Drive



T-Star



Grade 5 hardened steel, synthetic coating

coating colors:

- high corrosion resistant
- zinc

Diameter	Shear Strength in lbs*	Diameter	Shear Strength in lbs*	Diameter	Shear Strength in lbs*
1/4 x 2"	750	5/16 x 3"	830	1/2 x 5"	1.650
1/4 x 2"	750	5/16 x 3-1/2"	850	1/2 x 6"	1.750
1/4 x 2-1/2"	750	5/16 x 4"	1.100	1/2 x 8"	1.890
1/4 x 3"	750			1/2 x 10"	1.950
1/4 x 3"	750	3/8 x 5"	1.200	1/2 x 12"	1.950
1/4 x 3-1/2"	770	3/8 x 6"	1.260		
1/4 x 4"	800	3/8 x 8"	1.350		
1/4 x 4-1/2"	800				
1/4 x 5"	820				
1/4 x 6"	840				

*SPAX® Lags have a patented thread design and **do not require pre-drilling**. The green coating is used for outside applications. The zinc coating is used for inside applications. 25 % of shear load is recommended as a safe work load.

Epoxy Curing Agents and Modifiers

Ancamide® 2050 Curing Agent

DESCRIPTION

Ancamide 2050 curing agent is a special polyamide adduct designed for use with liquid epoxy resins in two-part, ambient-cure coatings.

ADVANTAGES

- Good cure at 50 °F
- Good corrosion resistance
- High aqueous acid and Skydrol^(A) resistance
- Zero induction time at ambient temperature
- Moderate viscosity
- Good flexibility
- High-gloss finish
- Noncritical loading (70–100 phr)

APPLICATIONS

- High-solids marine and maintenance coatings
- High-solids lining coatings
- High-solids primers and coatings for concrete
- Sealants and putties

STORAGE LIFE

At least 24 months from the date of manufacture in the original sealed container at ambient temperature. Store away from excessive heat and humidity in tightly closed containers.

HANDLING PRECAUTIONS

Refer to the Material Safety Data Sheet for Ancamide 2050 curing agent.

TYPICAL CURE SCHEDULE

7 days at ambient temperature.

(A) Monsanto Company

TYPICAL PROPERTIES

Appearance	Clear, Amber Liquid
Color ¹ (Gardner)	7
Viscosity ² @ 77 °F (cP)	4,000
Specific Gravity ³ @ 77 °F	1.02
Amine Value ⁴ (mg KOH/g)	225
Flash Point ⁵ (closed cup) (°F)	>200
Equivalent Wt/{H}	150
Recommended Use Level (phr, EEW=190)	70

TYPICAL HANDLING PROPERTIES*

	70 phr	100 phr
Mixed Viscosity ² @ 77 °F (cP)	6,400	5,000
Gel Time ⁶ (150g mix @ 77 °F) (min)	100	80
Thin Film Set Time ⁷ @ 77 °F (hr)	7.0	6.0
Peak Exotherm ⁸ (100g mix @ 77 °F) (min)	95	104
Peak Exotherm Time ⁸ (min)	136	133

TYPICAL PERFORMANCE*

(7 days @ 77 °F)		
Glass Transition Temperature ⁹ (°F)	108	—
Heat Deflection Temperature ¹⁰ (°F)	108	90

* Ancamide 2050 curing agent formulated with standard Bisphenol-A based (DGEBA, EEW=190) epoxy resin.

Footnotes:

- (1) ASTM D 1544-80
- (2) ASTM D-445-83, Brookfield, RVT, Spindle 4
- (3) ASTM D 1475-85
- (4) Perchloric Acid Titration
- (5) Seta Flash Closed Cup
- (6) Techne GT-4 Gelation Timer
- (7) BK Drying Recorder
- (8) ASTM D 2471-71
- (9) ASTM D 3418-82
- (10) ASTM D 648 @ 264 psi

Air Products and Chemicals, Inc., 7201 Hamilton Boulevard, Allentown, PA 18195-1501

Tel: (800) 345-3148, (610) 481-6799, Fax: (610) 481-4381, <http://www.airproducts.com/epoxyadditives>

The information contained herein is offered without charge for use by technically qualified personnel at their discretion and risk. All statements, technical information and recommendations contained herein are based on tests and data which we believe to be reliable, but the accuracy or completeness thereof is not guaranteed and no warranty of any kind is made with respect thereto.

SUPPLEMENTARY DATA

Formulations

Exhibits 1 and 2 show formulations for an aluminized epoxy mastic and an anticorrosive primer based on Ancamide 2050 curing agent.

Handling Properties

Table 1 compares the handling properties of Ancamide 2050 curing agent and a conventional polyamide such as Ancamide 350A curing agent. The low viscosity of the Ancamide 2050 curing agent allows formulators to develop high-solids coatings with lower VOC. Ancamide 2050 curing agent has excellent resistance to blush and exudation, so an induction time is not necessary at ambient temperature. Pot life for Ancamide 2050 curing agent is less than that of Ancamide 350A curing agent, but is still sufficient. The aluminized mastic and anticorrosive primer formulations in Exhibits 1 and 2 have pot lives of 5 hours and 8 hours, respectively.

The comparative dry times at ambient and low temperature for Ancamide 2050 and Ancamide 350A curing agents are also shown in Table 1. At ambient temperature, Ancamide 2050 curing agent has a tack-free time of 6-7 hours, depending on use level (100 vs 70 phr) compared with 11 hours for Ancamide 350A curing agent. At 50 °F, the tack-free time of Ancamide 2050 is 19-24 hours vs 36 hours for Ancamide 350A curing agent.

Table 1

Handling Properties	Ancamide 2050	Ancamide 350A
Viscosity (cP)	4,000	11,000
Mixed Viscosity (cP)	5,000-6,400	18,600
Pot Life (min)	80-100	200
Tack Free (hr @ 72 °F)	6-7	11
Tack Free (hr @ 50 °F)	19-24	36
Use Level (phr)	70-100	60

Curing agents were mixed with liquid epoxy (EEW=190) at use levels indicated. The full formulations in Exhibits 1 and 2 have dry to touch times of 3.5-4 hours and dry through times of 9-10 hours at ambient temperature.

Film Properties

Table 2 shows comparisons of flexibility, gloss, VOC and film appearance for Ancamide 2050 and Ancamide 350A curing agents. Formulators can use Ancamide 2050 curing agent to achieve superior flexibility by taking advantage of its noncritical loading, and by increasing its use level to 100 phr.

Table 2

Film Properties	Ancamide 2050	Ancamide 350A
Direct Impact (in/lb)		
500 EEW resin (a)	44	52
400 EEW resin (a)	38	33
300 EEW resin (a)	20	20
200 EEW resin (a)	20	12
Reverse Impact (in/lb) (b)	12/110	<20
1/8 in Mandrel bend (b)	Pass	Pass
Gloss (60°) (c)	100	90
VOC (lb/gal) (d)	1.7	1.8
Film Appearance (e)		
1 day, 77 °F, 50% RH	Clear, tack-free	
1 day, 50 °F, 90% RH	Haze, tacky	
1 day, 40 °F, 80% RH	Clear, very tacky	
7 days, 50 °F, 90% RH	Haze, tack-free	
7 days, 40 °F, 80% RH	Clear, tacky	

- (a) Pigmented formulations with usage of 70 phr for Ancamide 2050 and 60 phr for Ancamide 350A.
- (b) With liquid epoxy (EEW=190), with Ancamide 2050 being used at 70 phr and 100 phr, respectively. Ancamide 350A is used at stoichiometry. Film thickness 10 mils DFT. Measured per ASTM 2794.
- (c) Pigmented formulations based on solid epoxy resin (EEW=325) were mixed with each curing agent, applied to cold rolled steel panels (5) (5 mil DFT) and cured 7 days at 72 °F before testing.
- (d) In pigmented liquid epoxy resin (EEW=190) at stoichiometry.
- (e) Unpigmented formulations with liquid epoxy resin (EEW=190).

Ancamide 2050 at 70 phr has comparable flexibility to Ancamide 350A. When Ancamide 2050 curing agent's use rate increases to 100 phr, reverse impact in a liquid epoxy formulation increases from 12 in-lbs to 110 in-lbs. Gloss is superior to Ancamide 350A, and Ancamide 2050 can achieve lower VOC in similar formulations compared with Ancamide 350A curing agent. Films utilizing Ancamide 2050 curing agent also have very good appearance over a range of temperature and humidity conditions.

Corrosion Resistance

The aluminized epoxy mastic and anticorrosive primer formulations shown in Exhibits 1 and 2 were evaluated for salt spray resistance and humidity resistance after 1000 hours of exposure. Both formulations performed very well as detailed in Tables 3 and 4.

Table 3
Salt Spray Resistance - Ancamide 2050

	General Corrosion	Scribe Corrosion	Field Blistering	Blister Size
Aluminum Mastic	10	5.5-6.0	9	6
Red Primer	10	8.0-8.5	9-10	8.5

5% salt spray, cabinet temperature 95 °F — ASTM B-117, film thickness 2.5 mils.
Rating: 10 = Best; 0 = Worst

Table 4
Humidity Exposure - Ancamide 2050

	General Corrosion	Blistering Degree	Blister Size	Blanching
Aluminum Mastic	10	10	10	None
Red Primer	10	10	10	None

Continuous 100% Humidity Exposure — ASTM D-2247, cabinet temperature 122 °F, film thickness 2.5 mils. Rating: 1=Best, 0=Worst

Adhesion

The Ancamide 2050-based primer and aluminum mastic formulations were evaluated for adhesion to heavy, hot rolled steel per ASTM D-4541, Pull-Off adhesion. Panels were blasted to an SSPC-SP5 white metal quality with a mil profile of 3.0 mils. Greater than 400 psi was required to cause failure, and all failures occurred in the adhesive. No cohesive failure in the coating nor adhesive failure at any interface was observed. Both formulations showed good results.

Chemical Resistance

Table 5 contains chemical resistance data for Ancamide 2050 curing agent. Evaluations of Ancamide 2050 at 70 phr and 100 phr with standard liquid bisphenol A epoxy resin (EEW=190) in immersion conditions were made. Improved results are seen at the 70 phr use level compared with the higher loading.

Overall, Ancamide 2050 curing agent shows good resistance after 28 days to 10% acetic acid, Skydrol, 70% sulfuric acid and deionized water. Performance is not as good for solvents and alcohols. In a comparison with several representative reagents, Ancamide 2050 out-performed Ancamide 350A curing agent.

Table 5

Reagent	Immersion Time (Days)	Ancamide 2050 (70 phr)	Ancamide 2050 (100 phr)	Ancamide 350A (60 phr)
Deionized Water	1	0.32	0.39	
	3	0.51	0.74	
	7	0.69	0.98	
	28	1.49	2.09	
70% Sulfuric Acid	1	0.20	0.47	0.29
	3	0.29	0.62	0.71
	7	0.30	0.64	1.63
	28	0.47	0.51	10.30
10% Acetic Acid	1	0.93	2.50	7.57
	3	1.55	4.21	13.88
	7	2.20	6.43	20.72
	28	4.47	14.23	36.78
Skydrol LD-4	1	0.05	0.02	
	3	0.13	0.05	
	7	0.14	0.01	
	28	0.57	0.43	
Ethanol	1	2.06	2.81	3.26
	3	3.58	4.81	4.73
	7	5.10	7.23	6.09
	28	11.80	10.67	10.40
Xylene	1	3.53	5.09	
	3	6.40	9.03	
	7	9.50	D	
	28	D	-	
Butyl Cellosolve	1	1.90	2.77	
	3	3.50	4.87	
	7	5.27	7.40	
	28	12.13	D	
Toluene	1	7.67	11.15	13.66
	3	12.12	D	26.32
	7	D	-	D
	28	-	-	-
1,1,1 Trichloroethane	1	5.43	8.43	
	3	9.81	14.90	
	7	14.97	23.60	
	28	D	D	

* Chemical resistance data is expressed as % weight change, and testing was completed in accordance with ASTM D 543-84.

** Formulated with liquid epoxy resin (EEW=190) and cured 7 days at ambient temperature before immersion.

Exhibit 1
Ancamide 2050 Curing Agent Aluminum Mastic
Preliminary Formulation

Part A

	lb	gal
Liquid DGEBA Epoxy	300.7	31.00
Cabosil TS 720 (Cabot)	5	0.33
<i>Mix well, then add at high speed:</i>		
Lansford L243 (Silberline)	125.4	10.17
<i>Mix well, then add at low speed:</i>		
Aromatic 100 (Exxon)	48.5	6.67
Beetle 216-8 (Cyanamid)	20.0	2.30
Totals	499.6	50.47

Part B

Ancamide 2050 (Air Products)	241.6	28.55
MPA-1078 (Rheox)	8.0	1.08
10 AS Wollastokup (NYCO)	220.0	9.09
<i>Grind to 5 Hegman, reduce speed and add:</i>		
Aromatic 100 (Exxon)	60.6	8.34
Diacetone Alcohol (Union Carbide)	23.5	3.00
Cabosil TS 720 (Cabot)	6.5	0.42
Totals	560.2	50.48

Properties	
Volume solids (%)	73.9
PVC (%)	18.1
CPVC (%)	42.2
PVC/CPVC	.429
Wt/gal - part A	9.90
Wt/gal - part B	11.10
Wt/gal	10.50
VOC (lb/gal)	1.9
Mixing ratio (by volume)	1:1
Pot Life (hr)	5
Dry to Touch (hr)	4
Dry Through (hr)	10

Exhibit 2
 Ancamide 2050 Curing Agent Anticorrosive Primer
 Preliminary Formulation

Part A

	lb	gal
Liquid DGEBA Epoxy	233.7	24.093
MPA-1078 (Rheox)	4.0	0.541
<i>Mix well, then add at high speed:</i>		
TiPure R-900 (DuPont)	25.0	0.751
10 Wollastokup AS (NYCO)	370.0	15.289
<i>Disperse to 5 Hegman.</i>		
<i>Reduce speed and add:</i>		
Xylene (Ashland)	85.9	11.848
Totals	718.6	52.522

Part B

Ancamide 2050 (Air Products)	195.8	23.310
MPA-1078 (Rheox)	4.0	0.541
Beetle 216-8 (Cyanamid)	15.0	1.724
<i>Mix well at high speed, then add:</i>		
Red Iron Oxide J-3100 (Mineral Pigments)	60.0	1.441
Beaverwhite 325 (Cyprus)	96.7	4.204
Phosplus J-0866 (Mineral Pigments)	141.4	5.065
<i>Disperse to 5 Hegman and 125 °F.</i>		
<i>Reduce speed and add:</i>		
Diacetone Alcohol (Union Carbide)	31.3	3.997
Super High Flash Naptha (Ashland)	89.0	12.242
Totals	633.2	52.527

Properties

Volume solids (%)	71.8
PVC (%)	35.5
CPVC (%)	54.8
PVC/CPVC	0.647
Wt/gal - part A	13.68
Wt/gal - part B	12.06
Wt/gal	12.87
VOC (lb/gal)	2.07
Mixing ratio (by volume)	1:1
Pot life (hr)	8
Dry to touch (hr)	3.5
Dry through (hr)	9

Epic Resins

R3500

600 Industrial Blvd.
Palmyra, WI 53156
Phone: (262) 495-3400
Fax: (262) 495-3410
Email: customerservice@epicresins.com

Revised 3/12/2007

Product Datasheet

Description

EPIC R3500 is an unfilled, completely reactive, general purpose epoxy resin that finds use in adhesive and casting or potting applications.

Versions

[R3500/H5044](#) [R3500/H5016](#) [R3500/X98B2886](#) [R3500/H5057](#) [R3500/H5070](#) [R3500/H5064](#)
[R3500/H5079](#) [R3500/H5081](#) [R3500/S7045B](#) [R3500/H5015](#) [R3500/X01A3374B](#) [R3500/H5096](#)
[R3500/H5002](#) [R3500/H5032](#) [R3500/X01A3373B](#) [R3500/H5097](#) [R3500/X06B4071](#) [R3500/H5044-01](#)
[R3500/X06H4141](#)

Typical Properties

Product Identification: Potting Compound

Product Identification: Adhesive

Product Identification: Casting

Product Resin: Epoxy

Color, Part A: Amber

Shelf Life 25C, Part A: 12 Months

Viscosity

Viscosity, Part A (ASTM D2393): 11,000 - 16,000 cps @ 25C, 20 rpm

Viscosity, Part A (ASTM D2393): 500 - 1,000 cps @ 50C, 20 rpm

Weight per Gallon

Weight/Gallon A (ASTM D1875): 9.50 - 9.68 lb/gal

Processing Information

Processing Information: Mix ratios and pot life of material will vary greatly depending on the type of hardener used. Recommended cure schedules are as follows: 24 hours @ 25C or 2 hours @ 65C; or for a higher elevated temperature cure, allow to gel @80C to 100C plus post cure several hours @ 125C.

Mixing Instructions

Epoxy Mixing Instructions: When mixing two component epoxy resins, the ideal method is to mix by weight using a balance or digital scale. The mixing container should be placed on the scale and set to read zero, the appropriate amount of resin should be weighed followed by the appropriate amount of hardener. The material should then be stirred, ideally with a metal spatula, ensuring that the material is thoroughly mixed to a homogenous state by scraping the sides, bottom and the area where the sides meet the bottom of the container. Failure to do so can result in uncured sections of material or altered properties of the cured material. When mixing epoxy resins it is important to keep in mind that the larger the quantity of material mixed, the shorter the pot life (working time) will be.

Handling and Storage

Please refer to the Material Safety Data Sheet when determining the proper precautions to be used when storing or handling Epic R3500. Most epoxy resins and hardeners are skin and eye irritants. Some epoxy hardeners may actually be corrosive to the skin and eyes. Other health problems may be aggravated by exposure to these materials. Epic Resins recommends that engineering controls be used to minimize employee exposure to this or any other industrial chemical.

LIMITATION OF WARRANTY: Epic warrants its Product to be free of defects in materials and workmanship and to conform with all product specifications. Epic's liability is limited to replacement product only. Epic shall not be liable to Customer or any other party for any incidental, consequential or special damages, or any lost profits which may be incurred by Customer or any other party. THIS WARRANTY IS IN LIEU OF ALL OTHER WARRANTIES, EXPRESSED OR IMPLIED, INCLUDING, BUT NOT LIMITED TO WARRANTIES OF MERCHANTABILITY AND FITNESS FOR ANY PARTICULAR PURPOSE. NO EMPLOYEE, AGENT OR REPRESENTATIVE OF EPIC IS AUTHORIZED TO CHANGE THIS WARRANTY IN ANY WAY.

Product Information

▶ **AEROSIL® R 202** Hydrophobic Fumed Silica

AEROSIL® R 202 is a fumed silica aftertreated with a polydimethylsiloxane.

Applications and Properties

Applications

- Adhesives and sealants
- Epoxy-, vinylester resins and gelcoats
- Cable gels

Properties

- Thickening and thixotropy of complex polar liquids based on epoxy, polyurethane or vinylester resins.
- Thickening and thixotropy of cable gels for fiber optic cables.
- Anti-settling agent for heavy fillers.

Physico-chemical Data

<i>Properties</i>	<i>Unit</i>	<i>Typical Value</i>
Specific Surface Area (BET)	m ² /g	100 ± 20
Carbon content	wt. %	3.5 – 5.0
Average Primary Particle Size	nm	14
Tapped Density* (<i>approx. value</i>) acc. to DIN EN ISO 787/11, Aug. 1983	g/l	approx. 60
Moisture * <i>2 hours at 105 °C</i>	wt. %	≤ 0.5
Ignition loss , 2 hours at 1000 °C, based on material dried for 2 hours at 105 °C	wt. %	4.0 – 6.0
pH <i>in 4% dispersion</i>		4.0 – 6.0
SiO₂-content <i>based on ignited material</i>	wt. %	≥ 99.8

* *ex plant*

The data represents typical values and not production parameters.

Safety and Handling

With each (sample-) delivery of our products we will send a Material Safety Data Sheet. Of course you can also ask at any time for a MSDS or any other information regarding product safety.

Packing and Storage

AEROSIL® R 202 is supplied in multiple layer 10 kg bags. We recommend to store the product in closed containers under dry conditions and to protect the material from volatile substances. AEROSIL® R 202 should be used within 2 years after production.

Registration

	CAS-No.	EINECS	TSCA (USA) AICS (Australia), CEPA (Canada) PICCS (Philippines)	MITI (Japan)	ECL (Korea)	NEPA (China)
AEROSIL® R 202	67 762-90-7	Exempted	Registered	1-548 / 7-476	KE-31207	List III

► For further information please contact:

Commercial Contact

Degussa AG

Business Line Aerosil
Weissfrauenstrasse 9
D-60287 Frankfurt am Main,
Germany
Phone: +49 69/218-2532
Fax: +49 69/218-2533
E-Mail: aerosil@degussa.com
<http://www.aerosil.com>

NAFTA

Degussa Corporation

Business Line Aerosil
379 Interpace Parkway,
P. O. Box 677
Parsippany, NJ 07054-0677
Phone: +1 (800) AEROSIL
Phone: +1 (973) 541-8510
Fax: +1 (973) 541-8501

Asia (without Japan)

Aerosil Asia Marketing Office

c/o NIPPON AEROSIL CO., LTD.
P.O. Box 7015
Shinjuku Monolith 13F
3-1, Nishi-Shinjuku 2-chome
Shinjuku-ku, Tokyo
163-0913 Japan
Phone: +81-3-3342-1786
Fax: +81-3-3342-1761

Japan

NIPPON AEROSIL CO., LTD.

Sales & Marketing Division
P.O. Box 7015
Shinjuku Monolith 13F
3-1, Nishi-Shinjuku 2-chome
Shinjuku-ku, Tokyo
163-0913 Japan
Phone: +81-3-3342-1763
Fax: +81-3-3342-1772

Technical Contact

Degussa AG

Technical Service Aerosil
Rodenbacher Chaussee 4
P.O. Box 1345
D-63403 Hanau-Wolfgang,
Germany
Phone: +49 6181/59-3936
Fax: +49 6181/59-4489

NAFTA

Degussa Corporation

Technical Service Aerosil
2 Turner Place
Piscataway, NJ 08855-0365
Phone: +1 (888) SILICAS
Phone: +1 (732) 981-5000
Fax: +1 (732) 981-5275

Asia (without Japan)

Degussa AG

Technical Service Aerosil
Rodenbacher Chaussee 4
P.O. Box 1345
D-63403 Hanau-Wolfgang,
Germany
Phone: +49 6181/59-3936
Fax: +49 6181/59-4489

Japan

NIPPON AEROSIL CO., LTD.

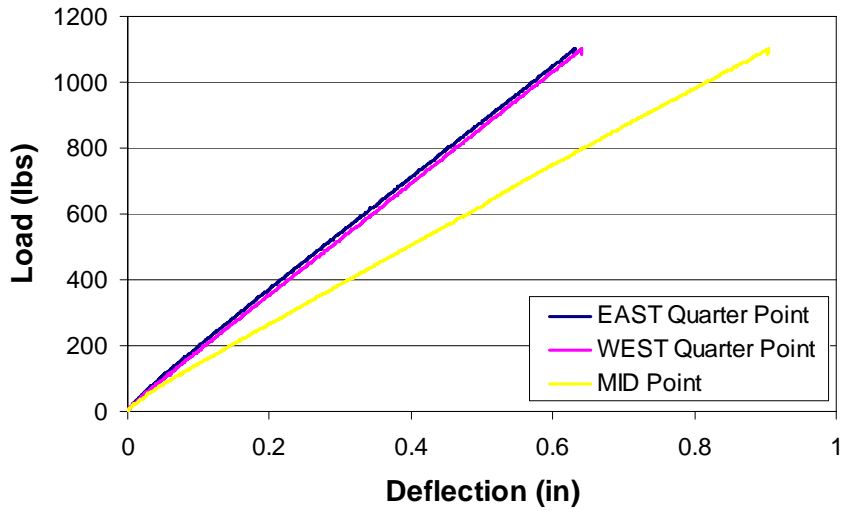
Applied Technology Service
3 Mita-cho
Yokkaichi, Mie
510-0841 Japan
Phone: +81-593-45-5270
Fax: +81-593-46-4657

Or your local Degussa Representative

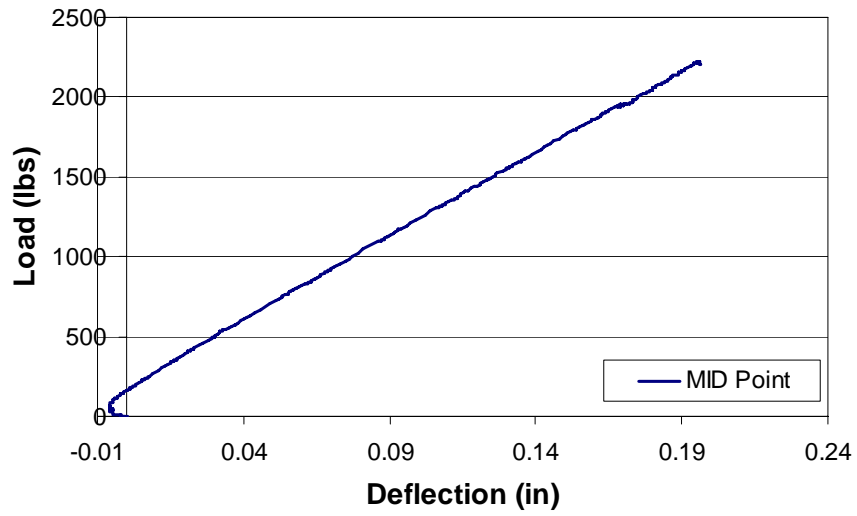
Our information in this document is based on our best knowledge. We disclaim any warranty and liability whatsoever as to accuracy and completeness of such information as well as to the potential infringement of any proprietary rights. We reserve the right to effect technical alterations. Any user of our products shall bear the full risk connected to their use including but not limited to their properties and fitness for any purpose.

Appendix B

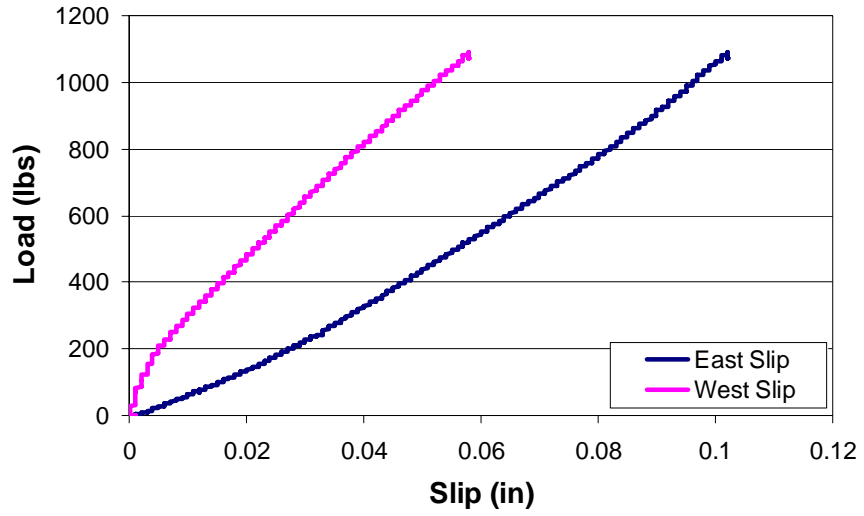
Phase 1: Width Series
4 inch width



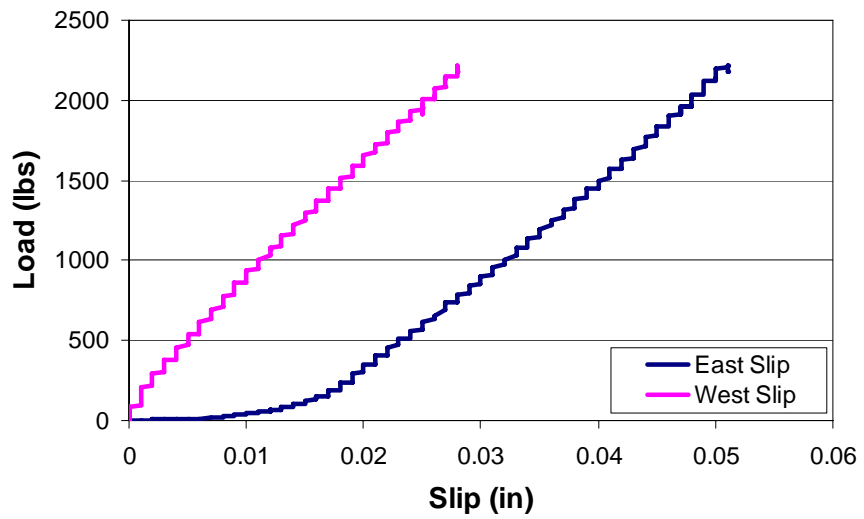
Load vs. Deflection for NB4-3 over NB4-4 10'-6" Span



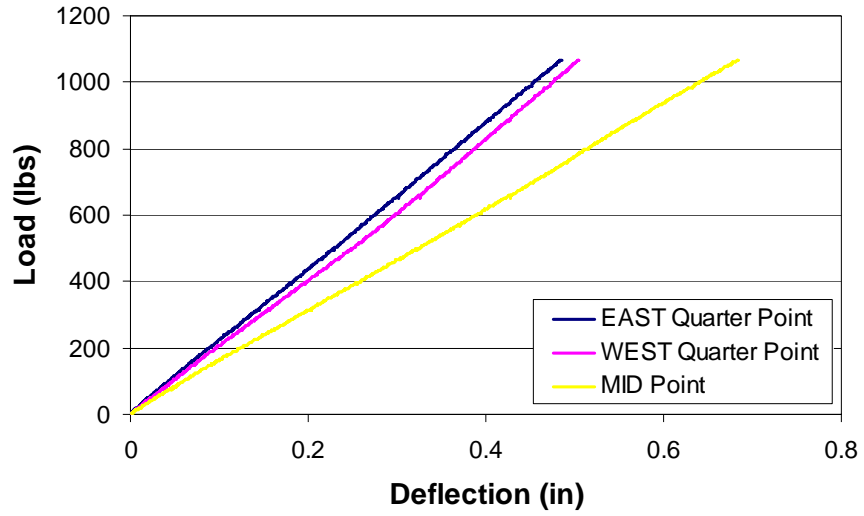
Load vs. Deflection for NB4-3 over NB4-4 5' Span



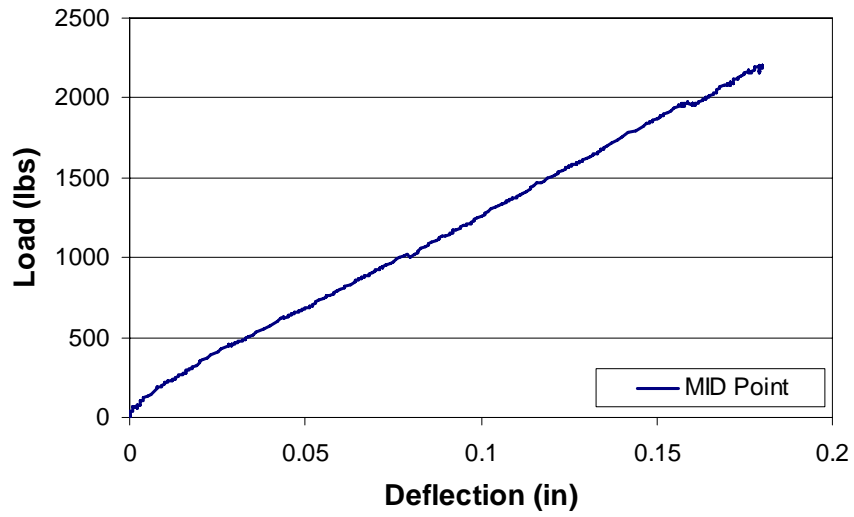
Load vs. Slip for NB4-3 over NB4-4 10'-6" Span



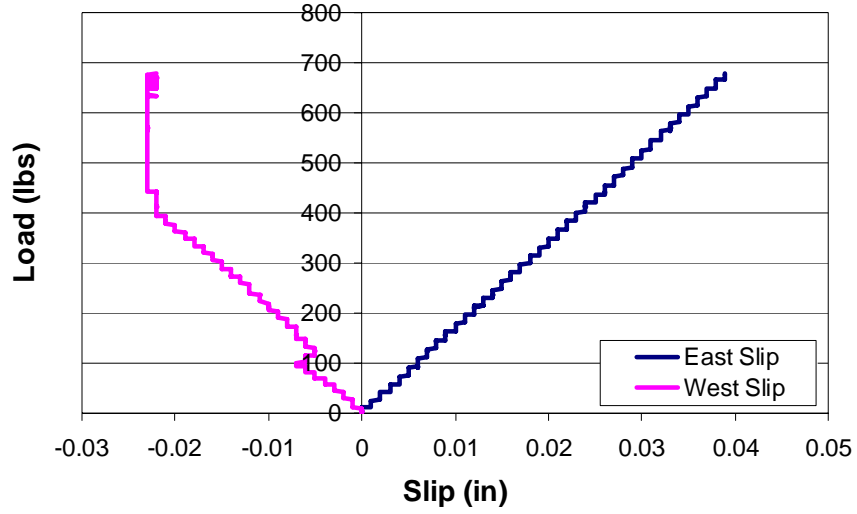
Load vs. Slip for NB4-3 over NB4-4 5' Span



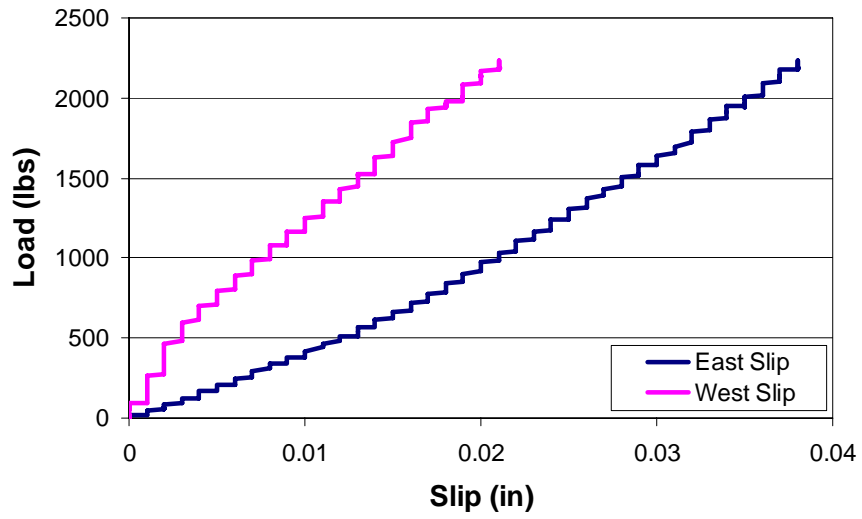
Load vs. Deflection for NB4-4 over NB4-2 10'-6" Span



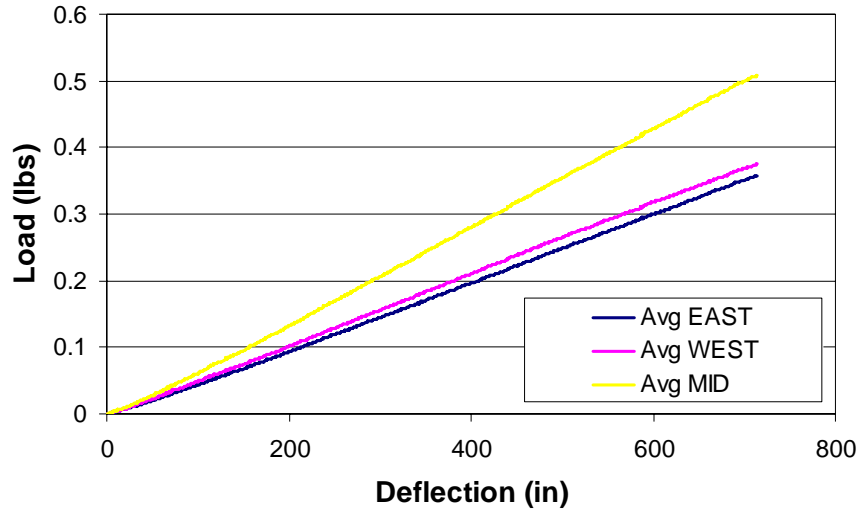
Load vs. Deflection for NB4-4 over NB4-2 5' Span



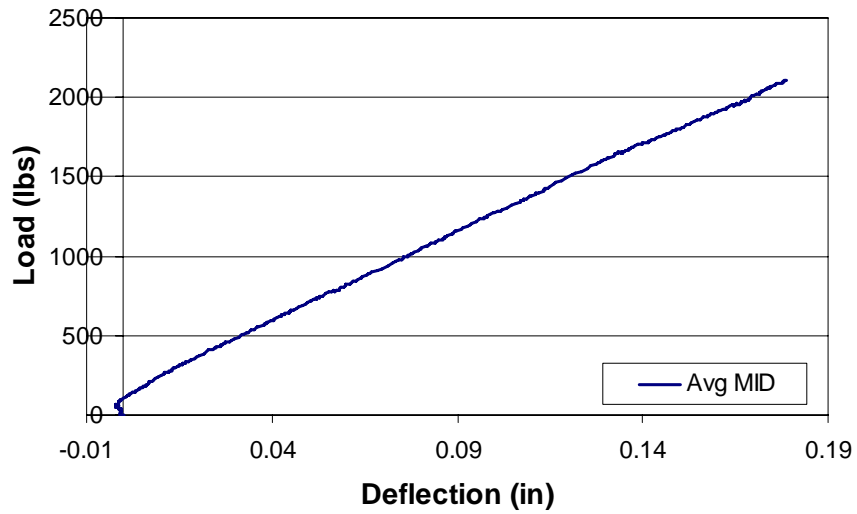
Load vs. Slip for NB4-4 over NB4-2 10'-6" Span



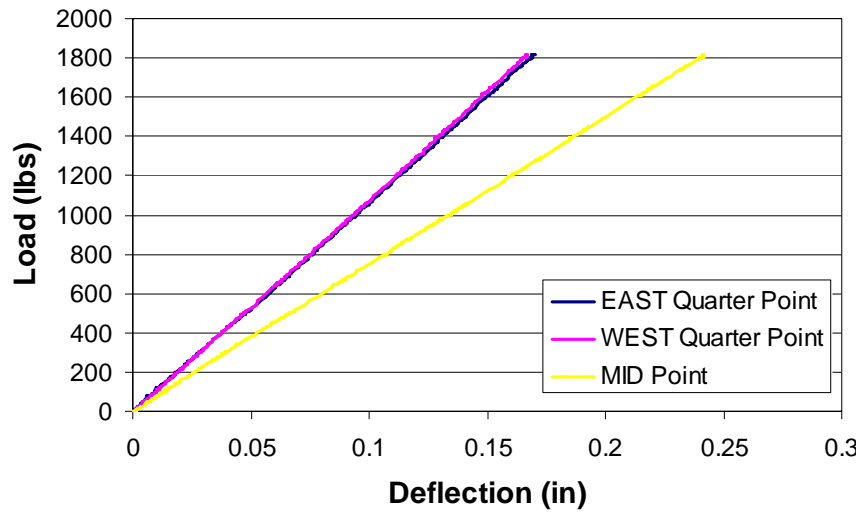
Load vs. Slip for NB4-4 over NB4-2 10'-6" Span



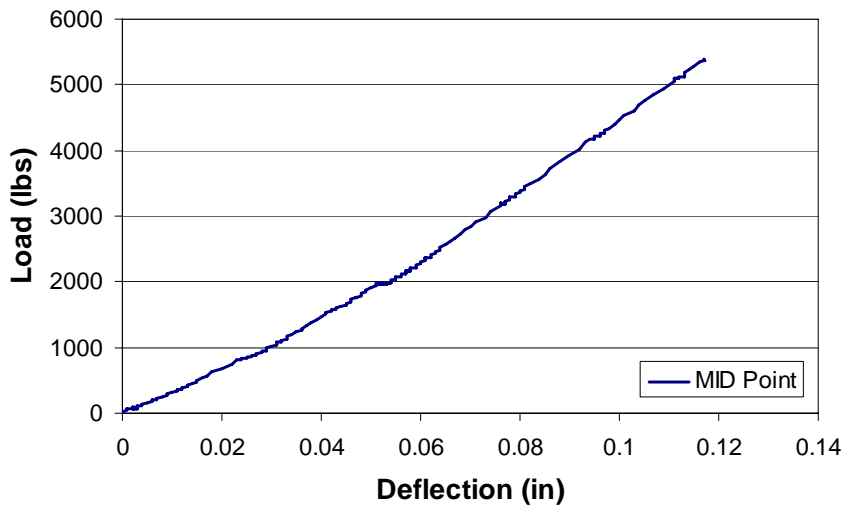
Load vs. Deflection for Average of 4 inch Stacked Beams 10'-6" Span



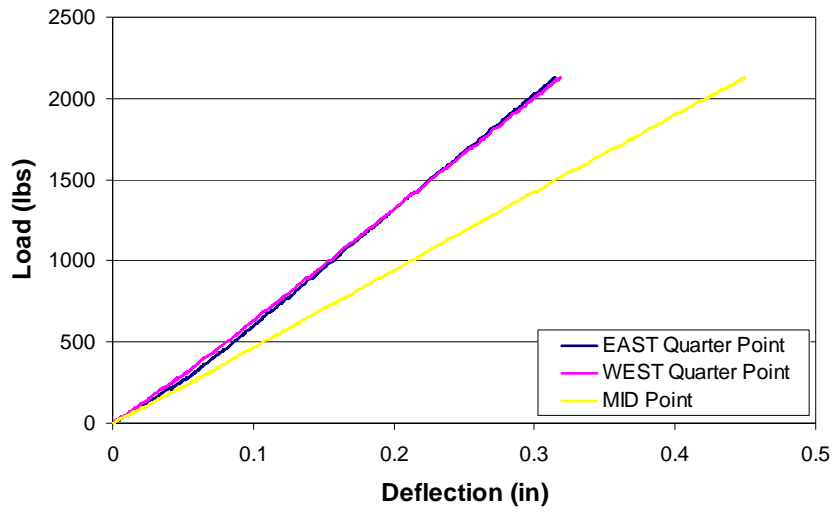
Load vs. Deflection for Average of 4 inch Stacked Beams 5' Span



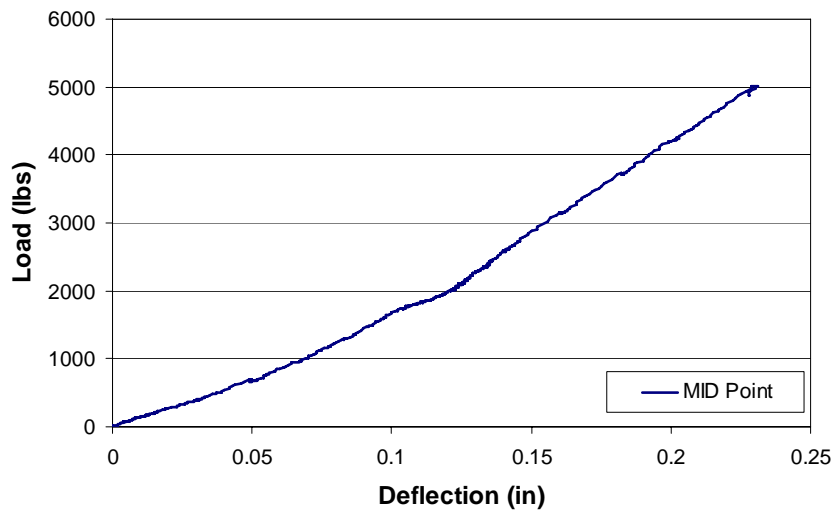
Load vs. Deflection for E4 10'-6" Span



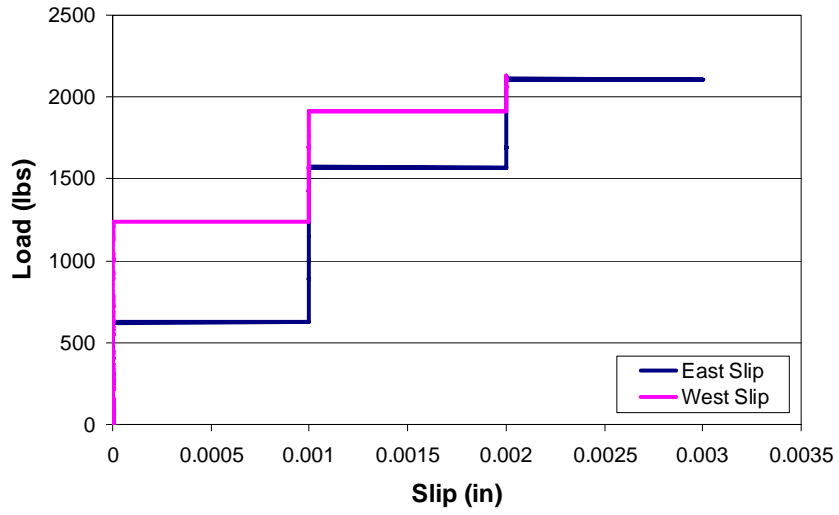
Load vs. Deflection for E4 5' Span



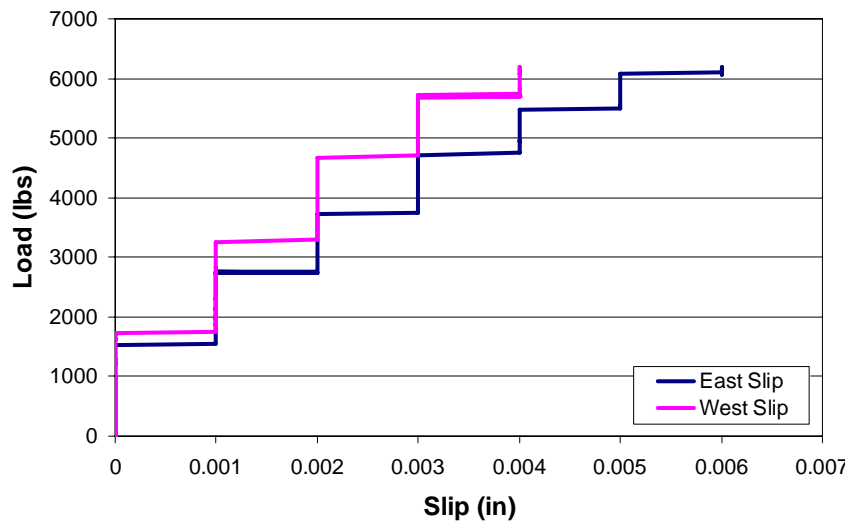
Load vs. Deflection for X4 10'-6" Span



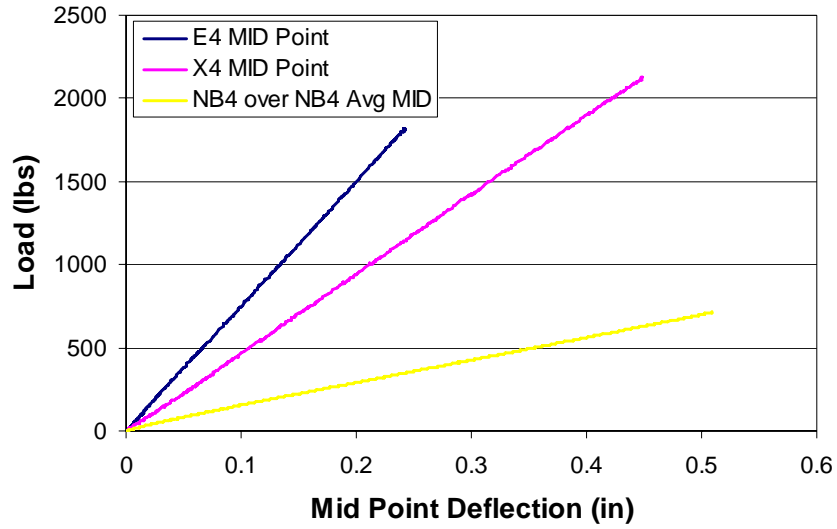
Load vs. Deflection for X4 5' Span



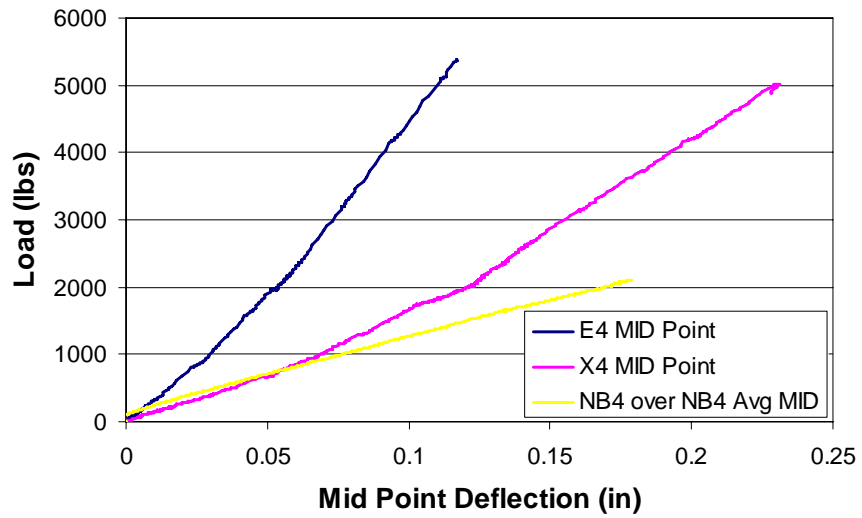
Load vs. Slip for X4 10^{-6} " Span



Load vs. Slip for X4 5' Span

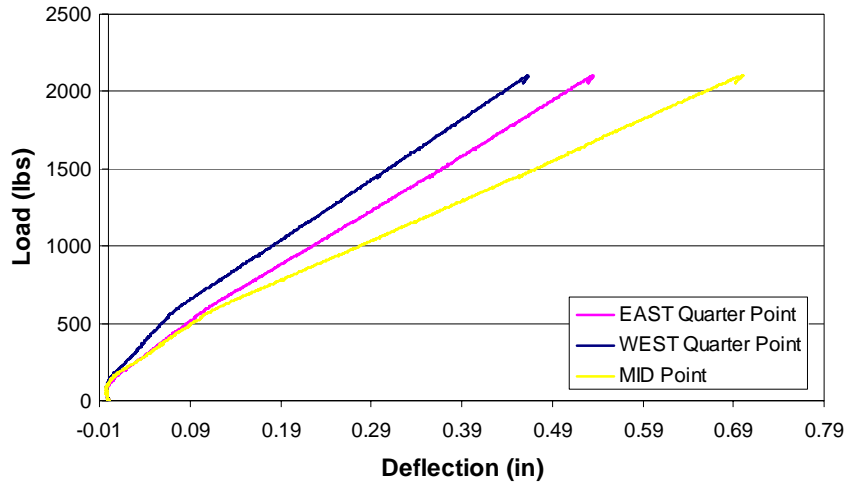


Load vs. Deflection Comparison Across 4 inch Width Series 10'-6" Span

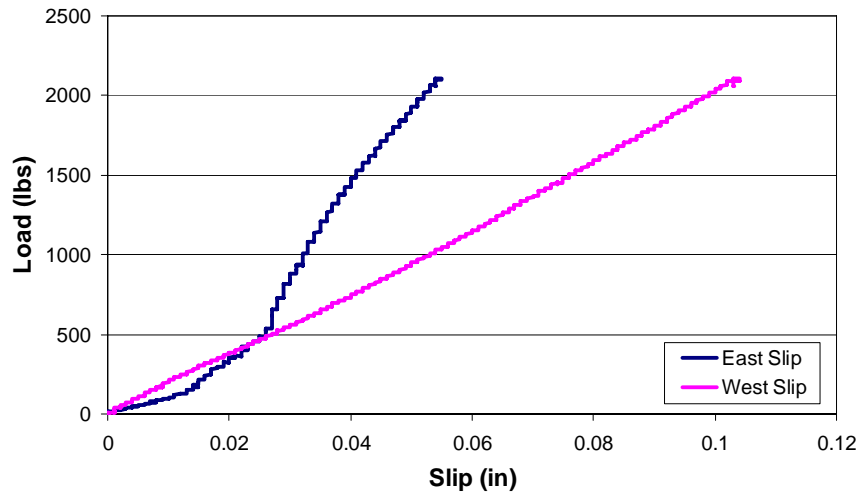


Load vs. Deflection Comparison Across 4 inch Width Series 5' Span

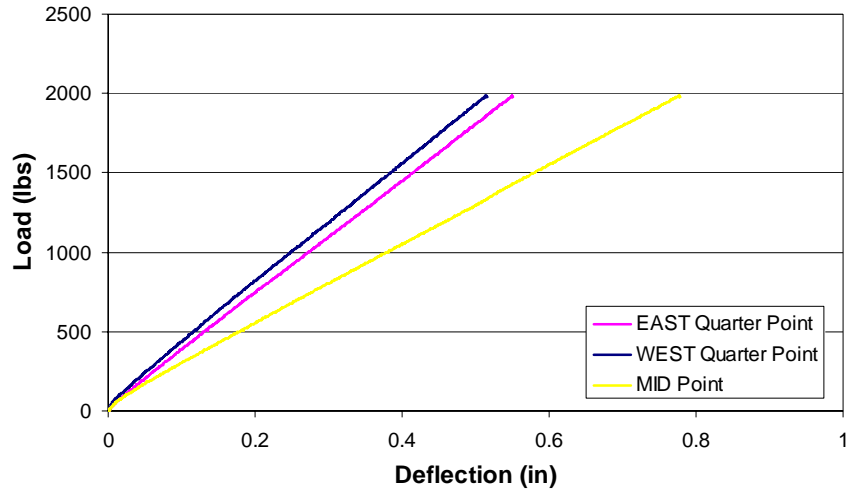
**Phase 1: Width Series
8 inch with**



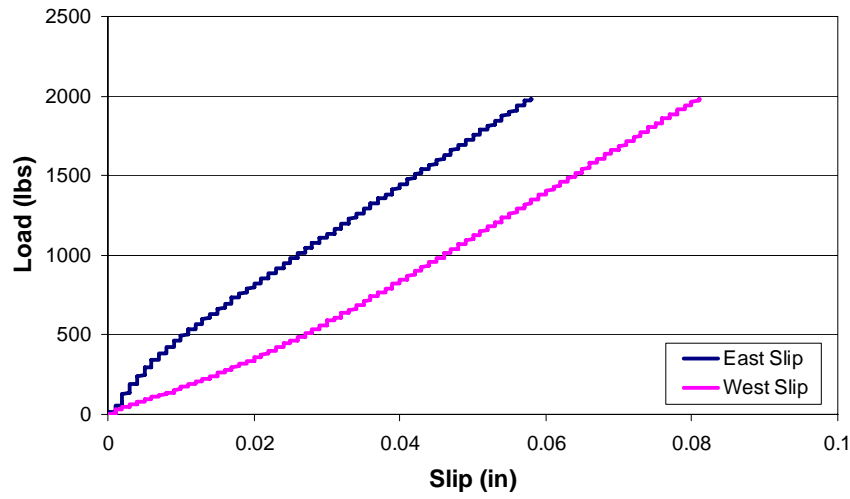
Load vs. Deflection for NB8-2 over NB8-3 10⁻⁶” Span



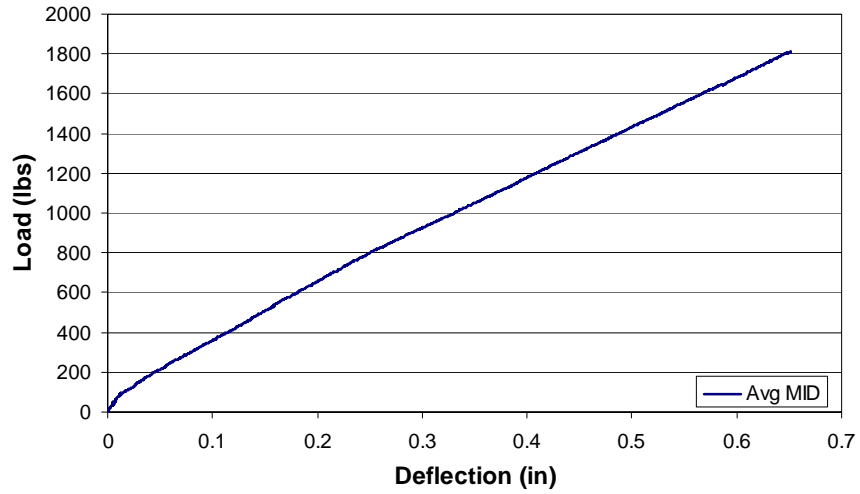
Load vs. Slip for NB8-2 over NB8-3 10⁻⁶” Span



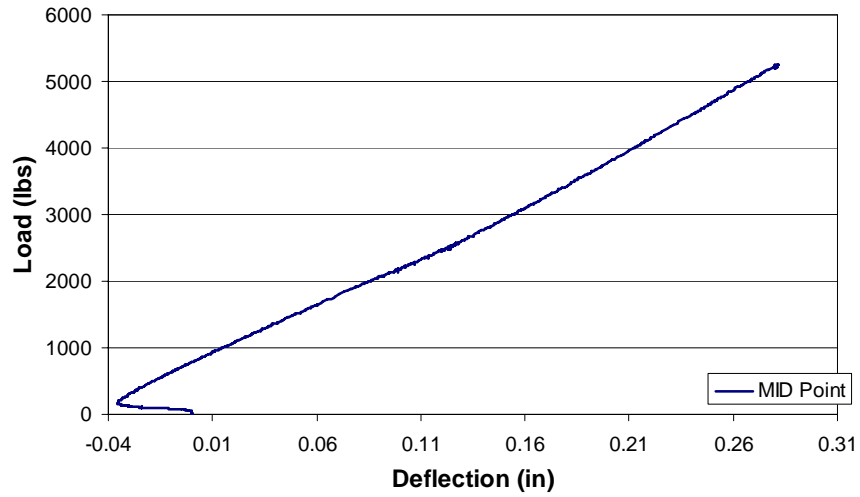
Load vs. Deflection for NB8-2 over NB8-1 10'-6" Span



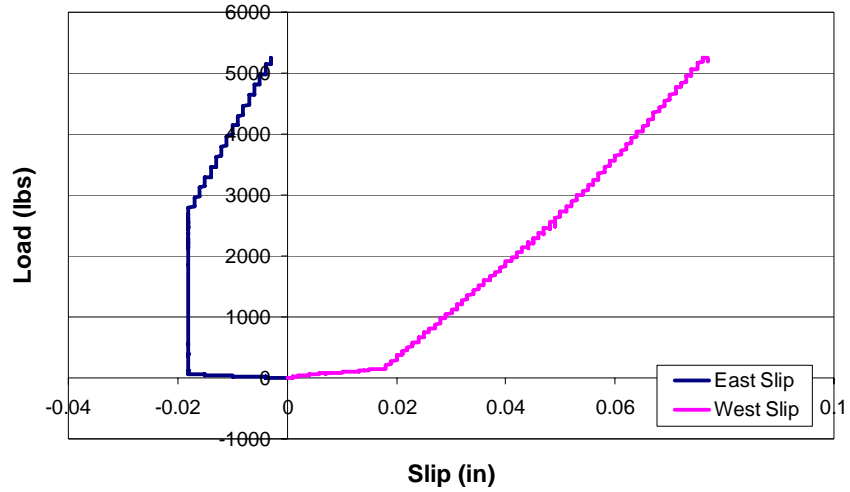
Load vs. Slip for NB8-2 over NB8-1 10'-6" Span



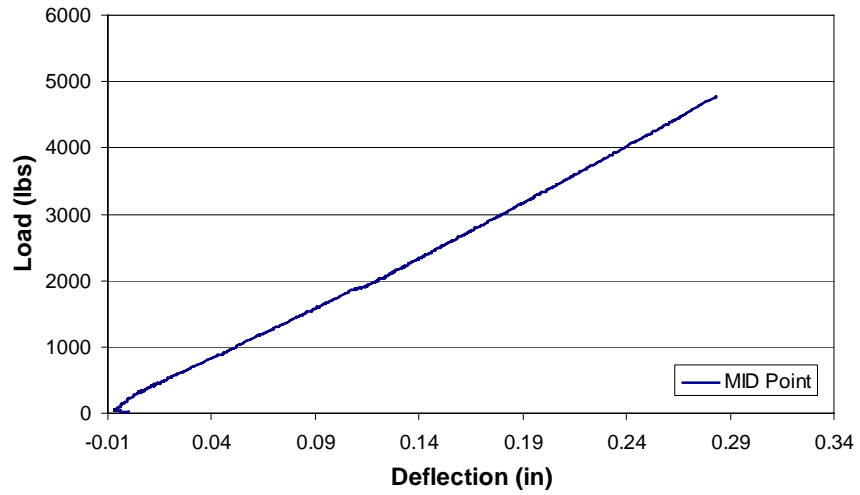
Load vs. Deflection for 8" Width Stacked Beams Average 10⁻⁶-6" Span



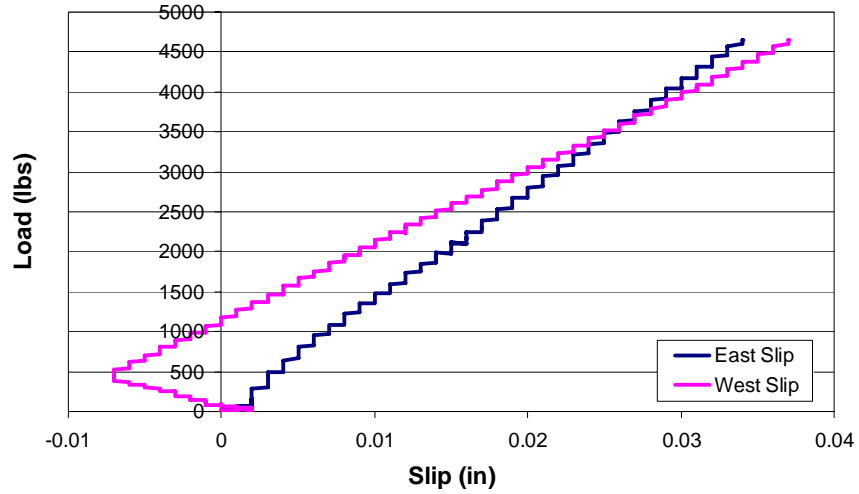
Load vs. Deflection for NB8-2 over NB8-4 5' Span



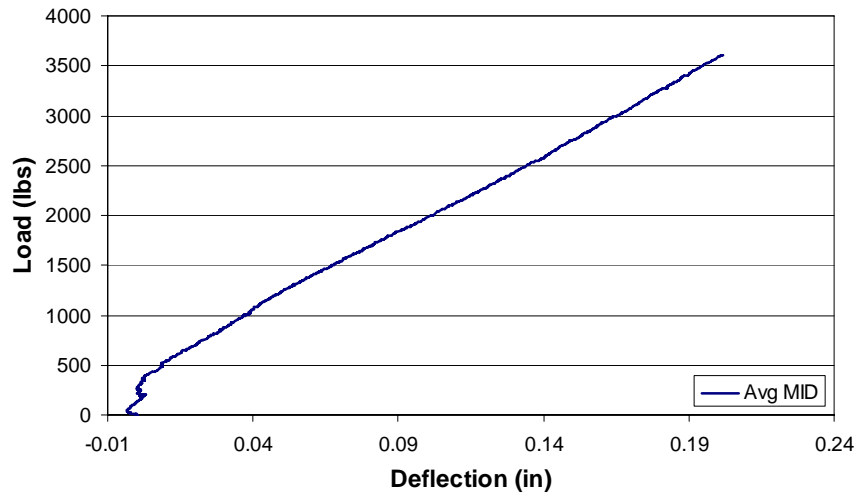
Load vs. Slip for NB8-2 over NB8-4 5' Span



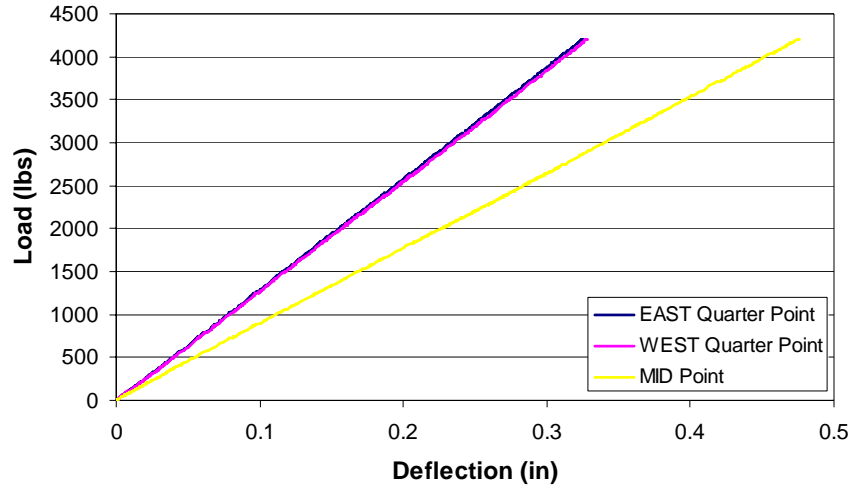
Load vs. Deflection for NB8-3 over NB8-4 5' Span



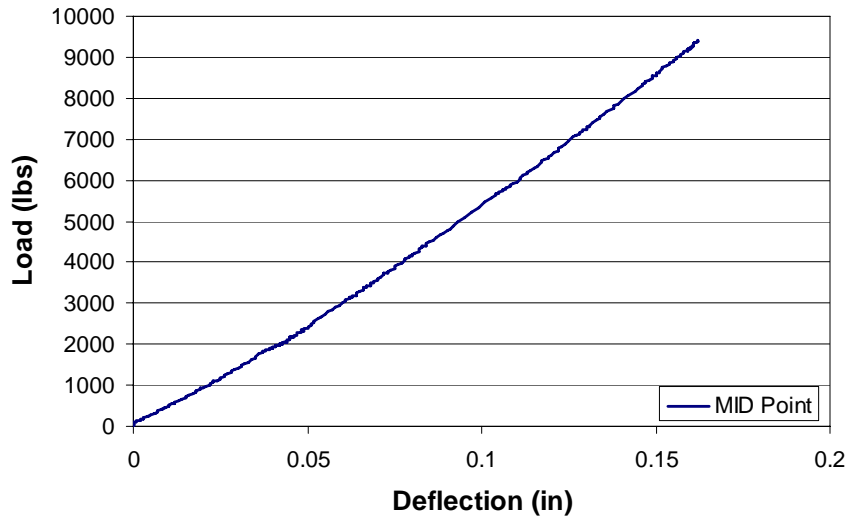
Load vs. Slip for NB8-3 over NB8-4 5' Span



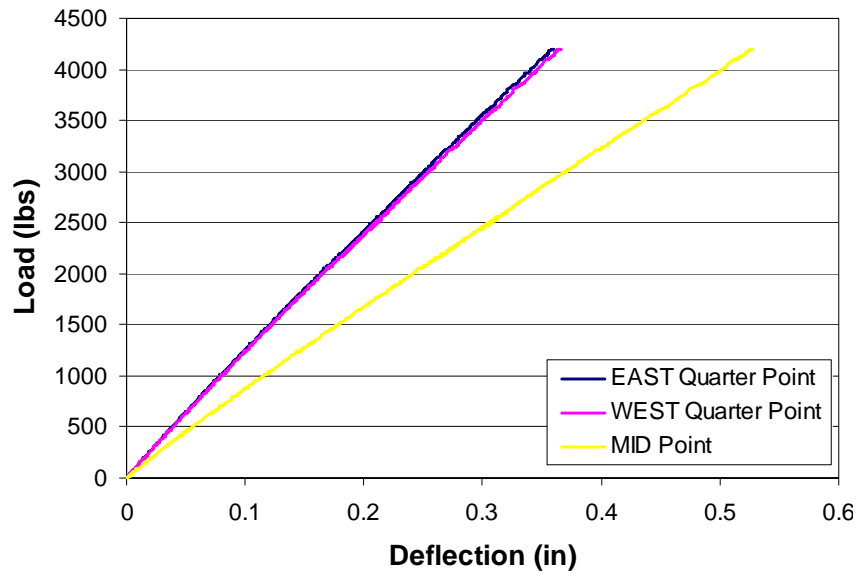
Load vs. Deflection for 8" Width Stacked Beams Average 5' Span



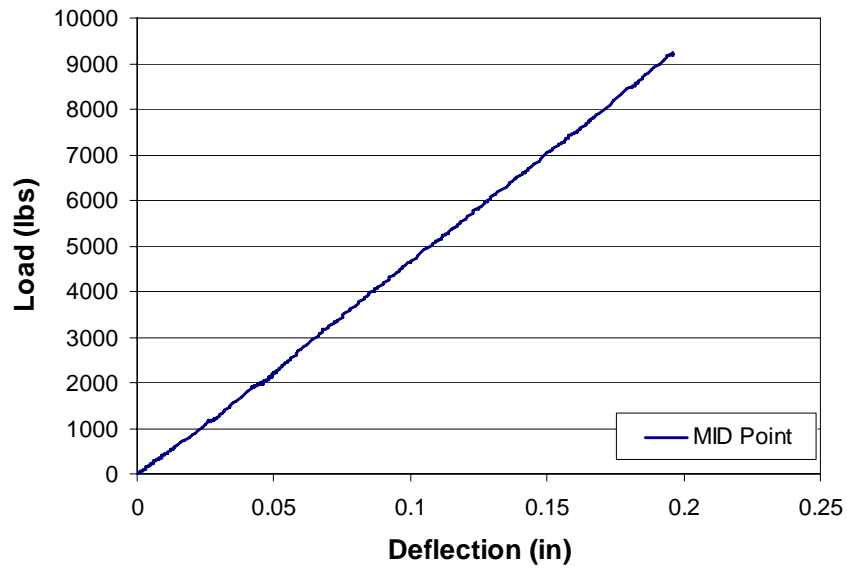
Load vs. Deflection for E8 10'-6" Span



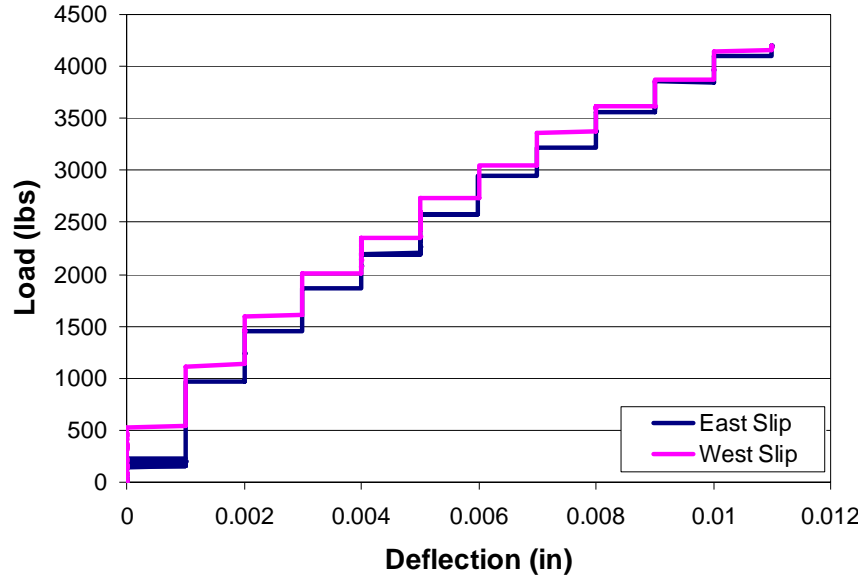
Load vs. Deflection for E8 5' Span



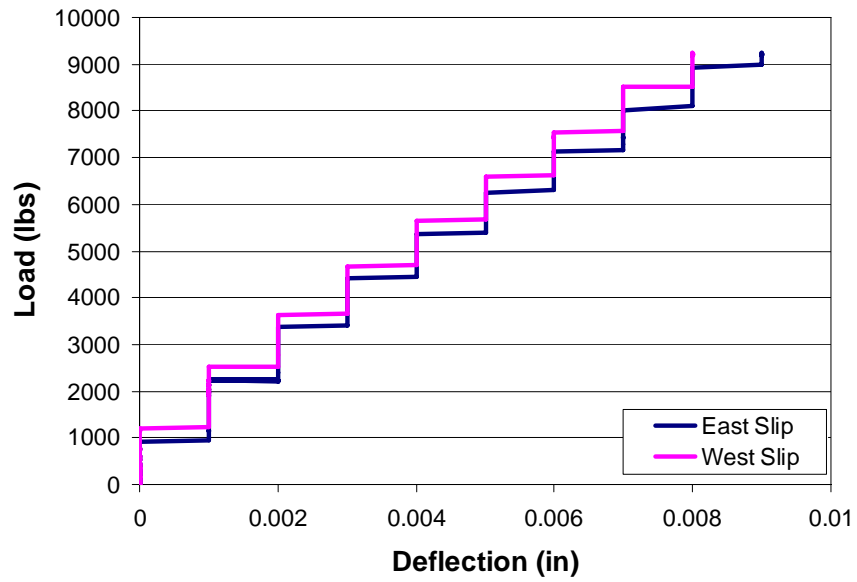
Load vs. Deflection for X8 10'-6" Span



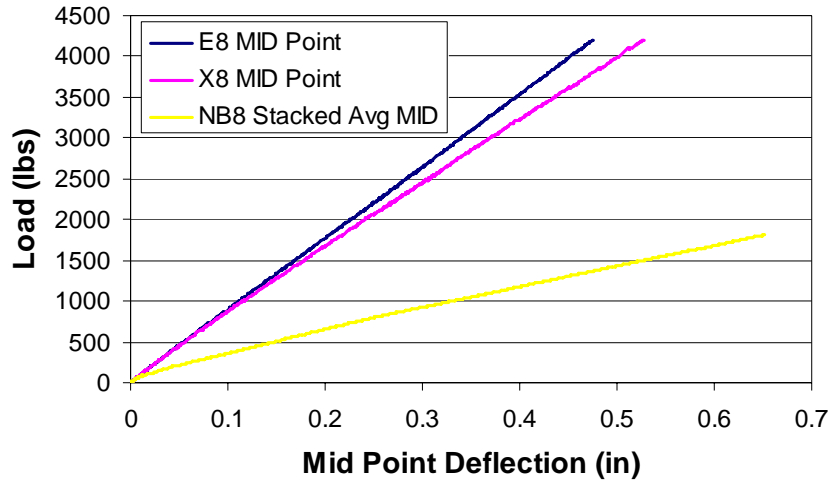
Load vs. Deflection for X8 5' Span



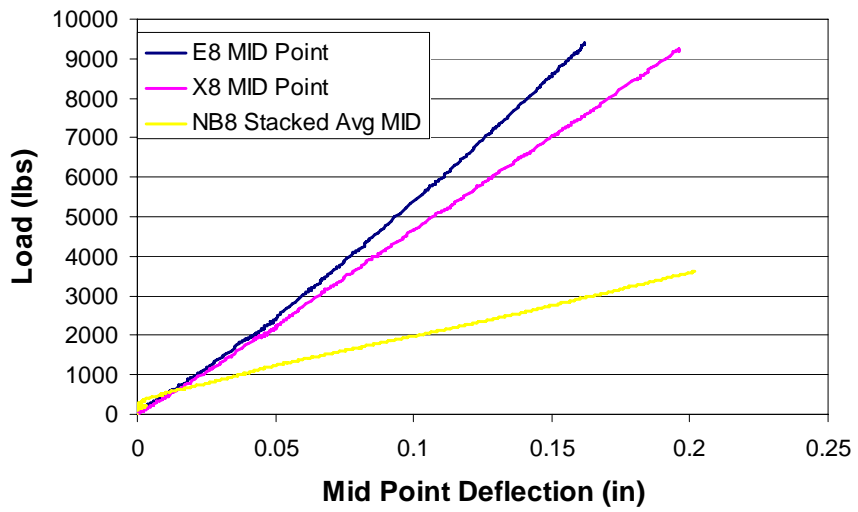
Load vs. Slip for X8 10'-6" Span



Load vs. Slip for X8 5' Span

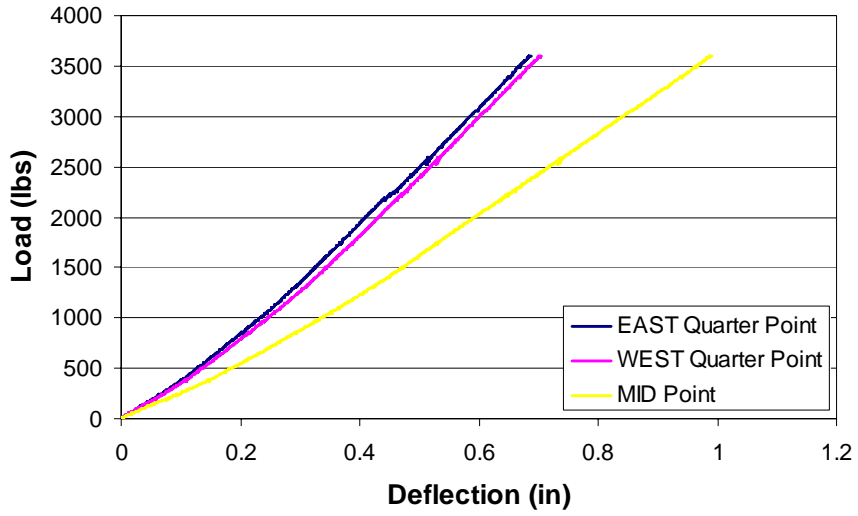


Load vs. Deflection Comparison Across 8 inch Width Series 10'-6" Span

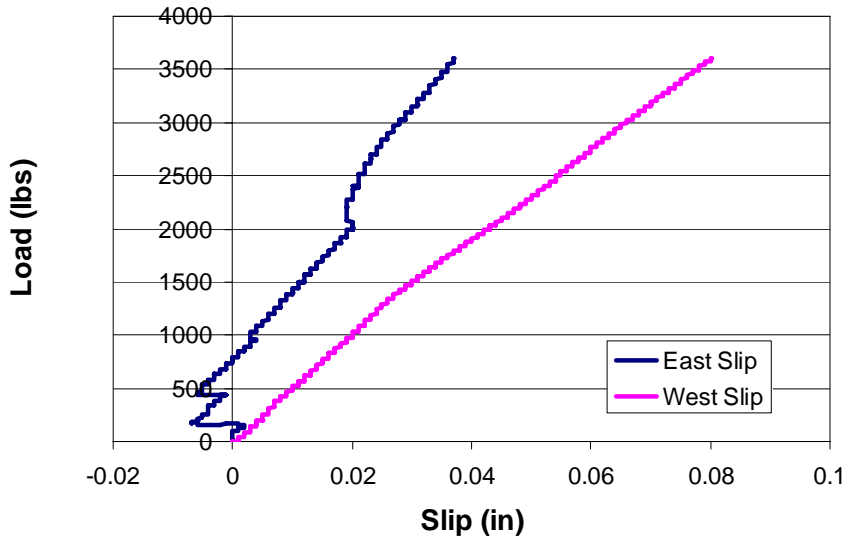


Load vs. Deflection Comparison Across 8 inch Width Series 5' Span

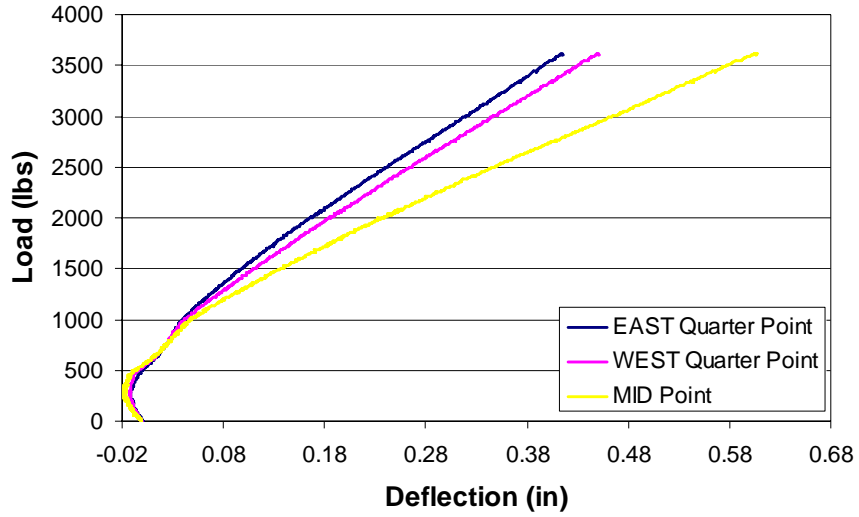
**Phase 1: Width Series
12 inch width**



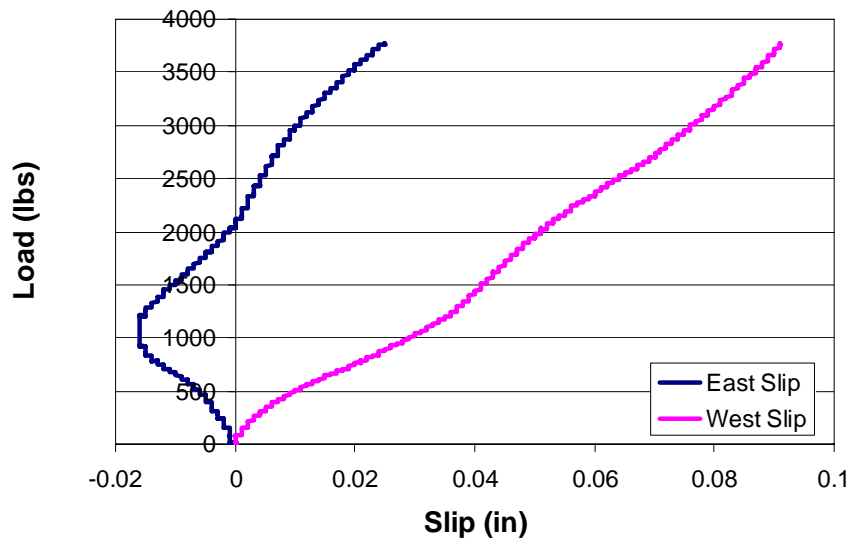
Load vs. Deflection for NB12-1 over NB12-3 10'-6" Span



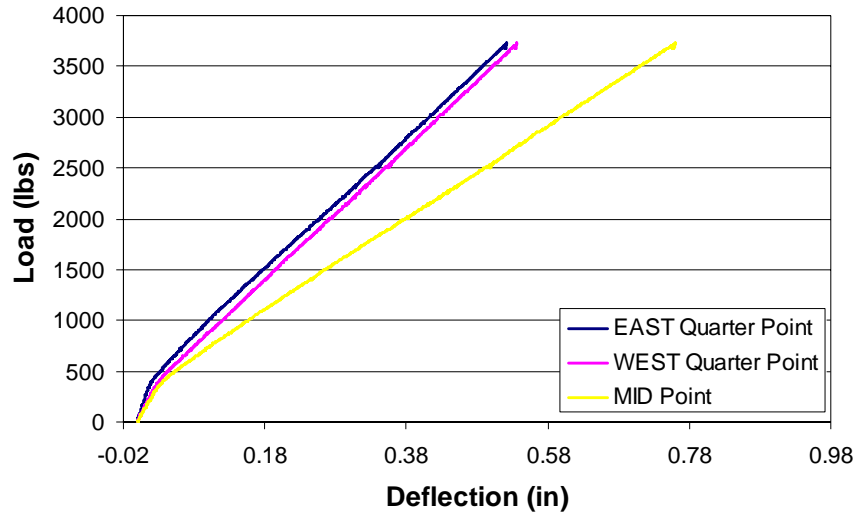
Load vs. Slip for NB12-1 over NB12-3 10'-6" Span



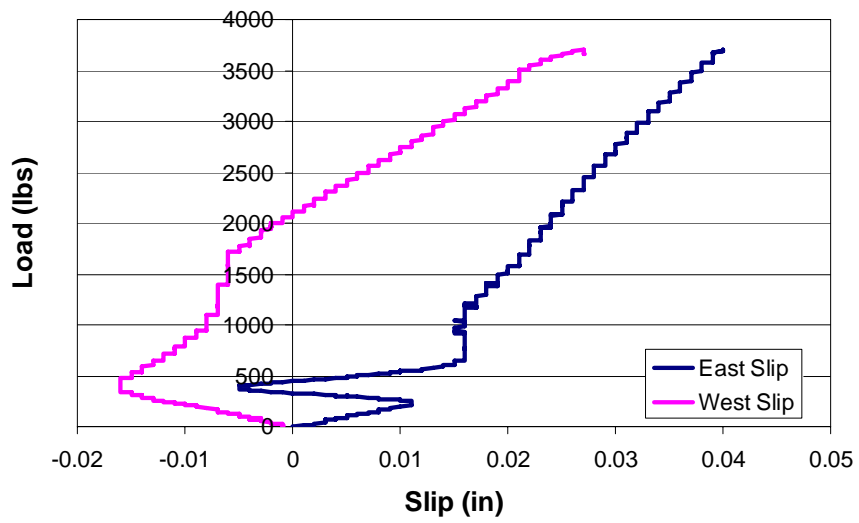
Load vs. Deflection for NB12-2 over NB12-1 10'-6" Span



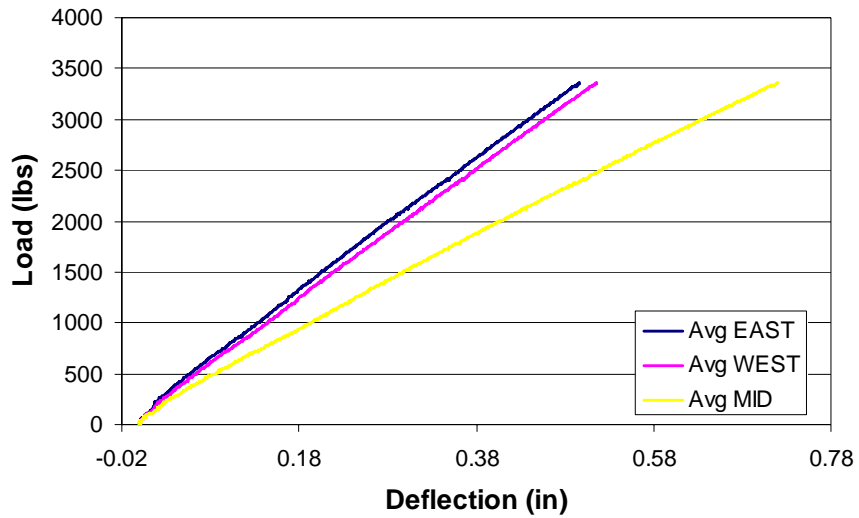
Load vs. Slip for NB12-2 over NB12-1 10'-6" Span



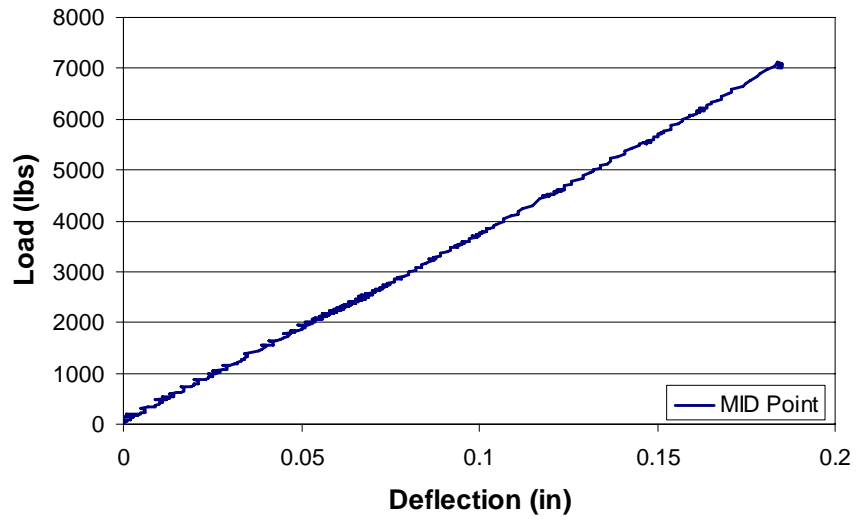
Load vs. Deflection for NB12-2 over NB12-3 10'-6" Span



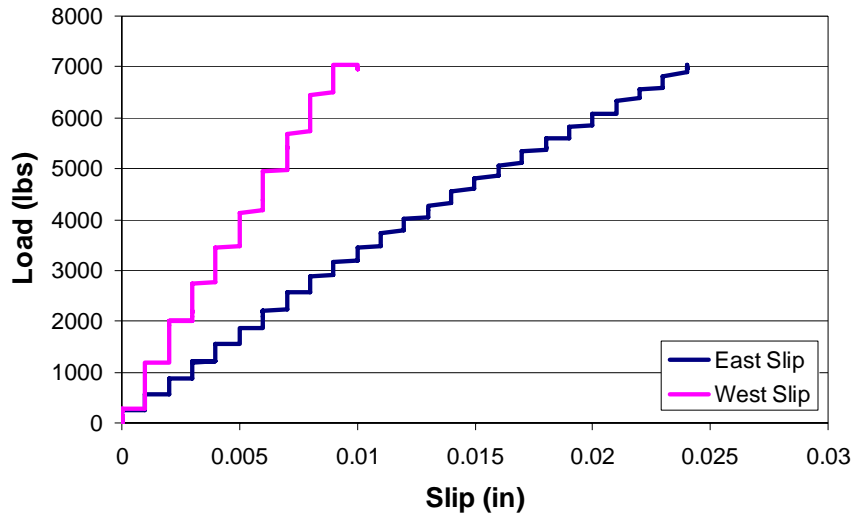
Load vs. Slip for NB12-2 over NB12-3 10'-6" Span



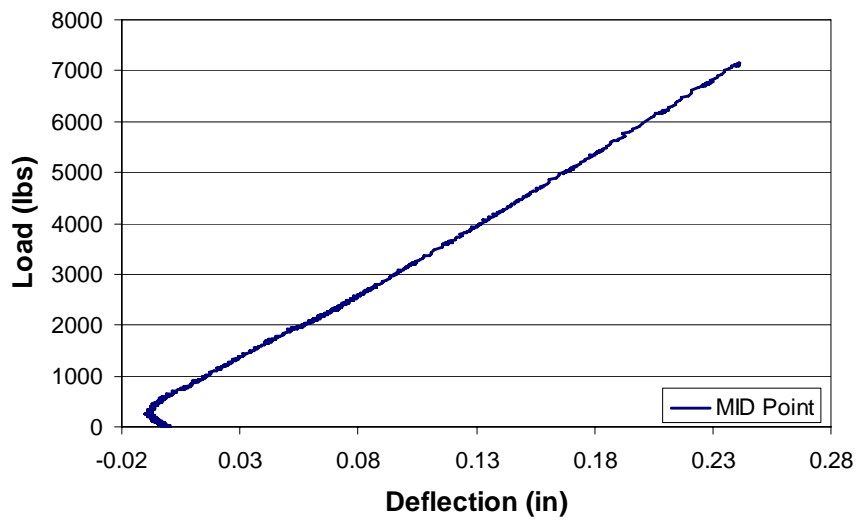
Load vs. Deflection for 12 inch Stacked Beams Average 10'-6" Span



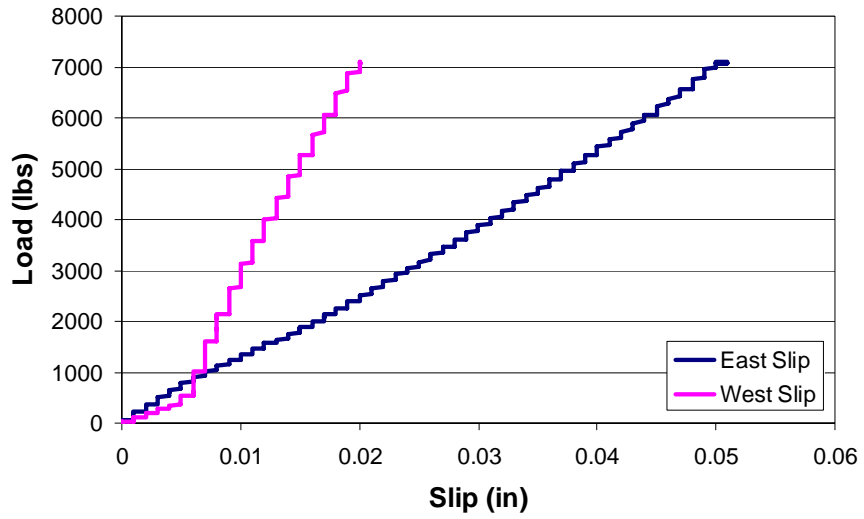
Load vs. Deflection for NB12-5 over NB12-4 5' Span



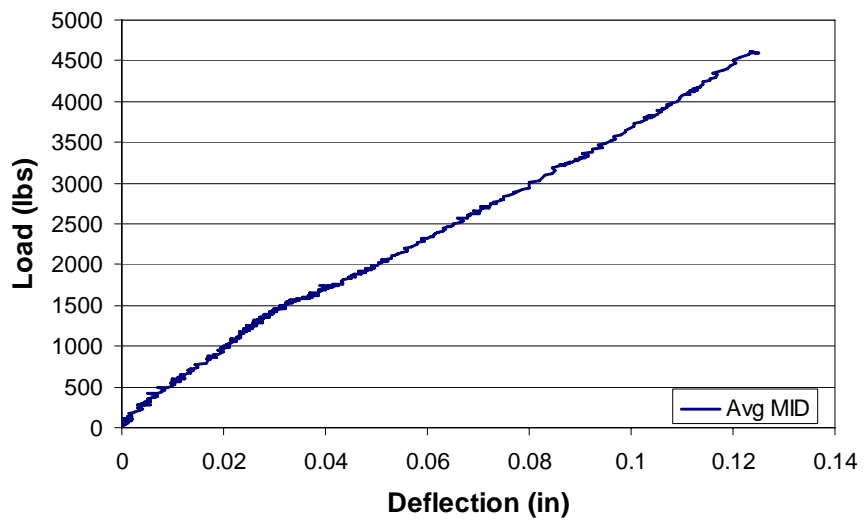
Load vs. Slip for NB12-5 over NB12-4 5' Span



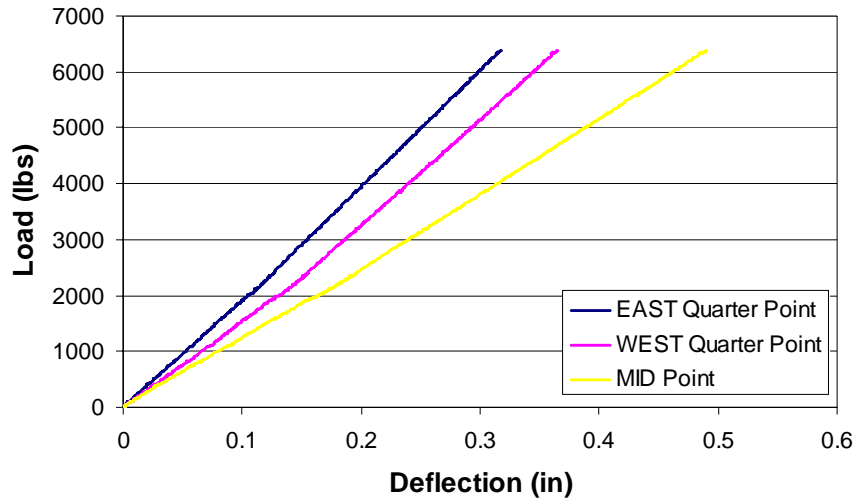
Load vs. Deflection for NB12-5 over NB12-6 5' Span



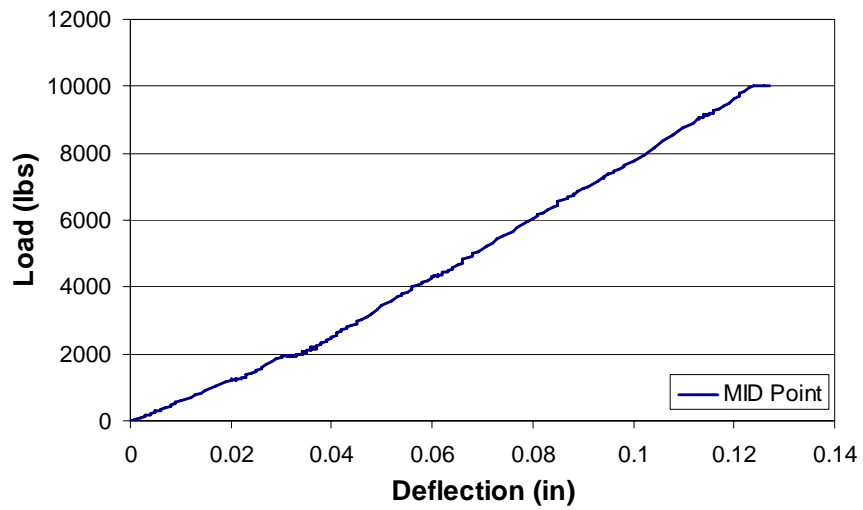
Load vs. Slip for NB12-5 over NB12-6 5' Span



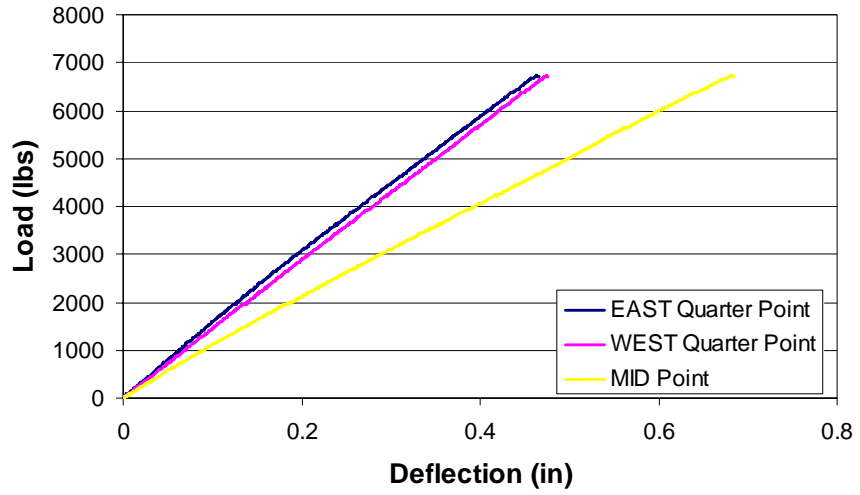
Load vs. Deflection for 12 inch Stacked Beams Average 5' Span



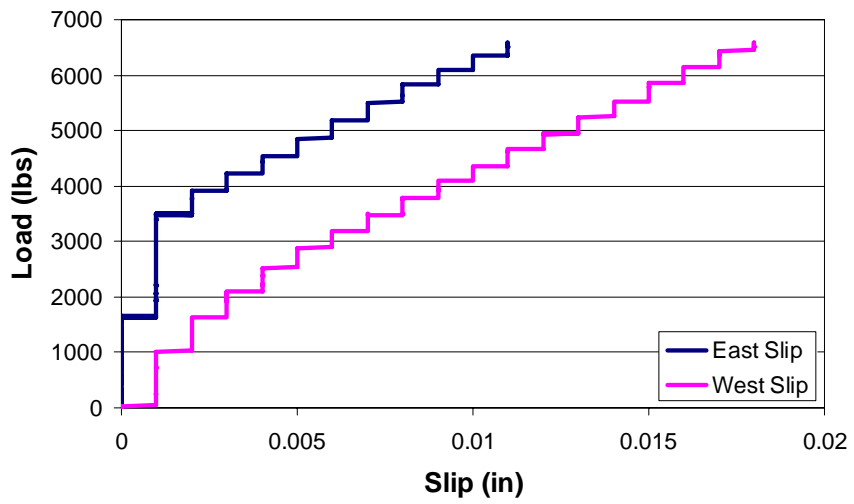
Load vs. Deflection for E12 10'-6" Span



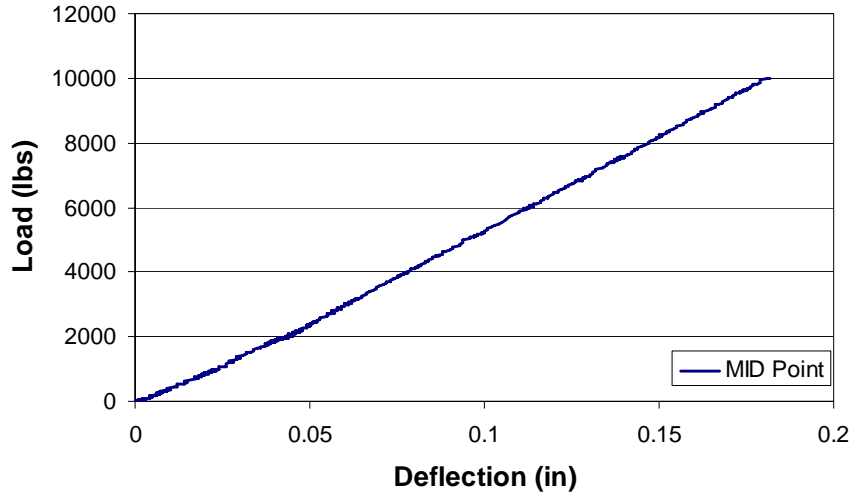
Load vs. Deflection for E12 5' Span



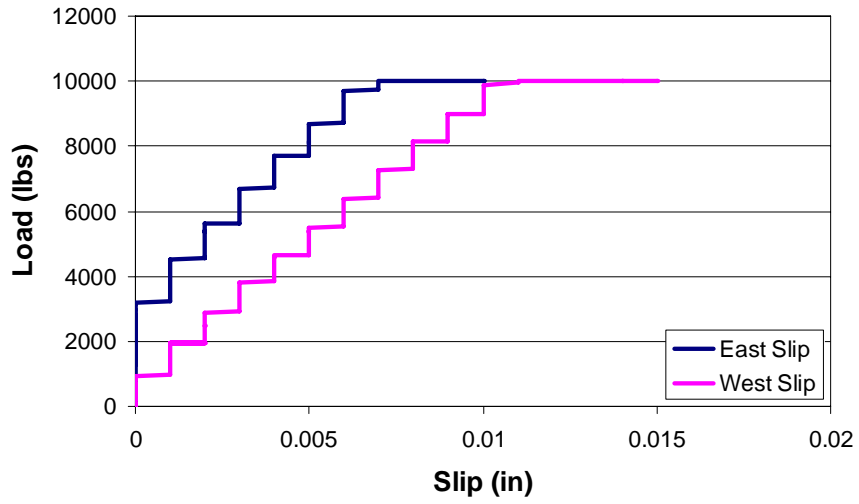
Load vs. Deflection for X12 10'-6" Span



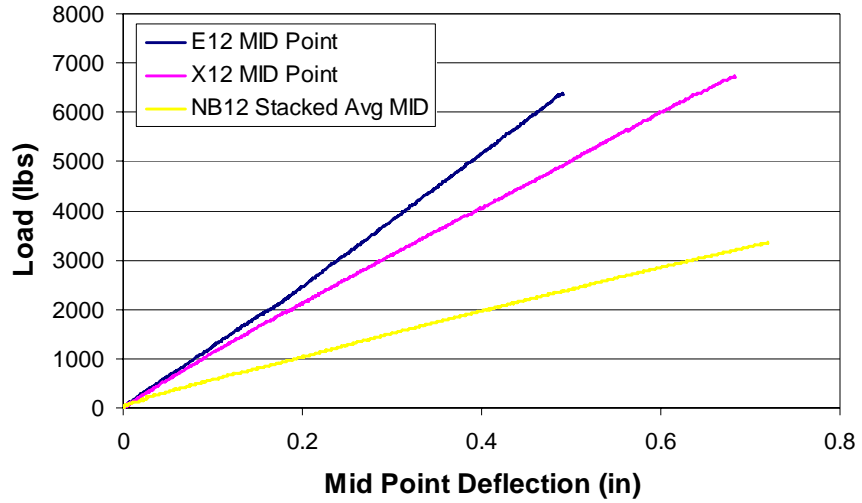
Load vs. Slip for X12 10'-6" Span



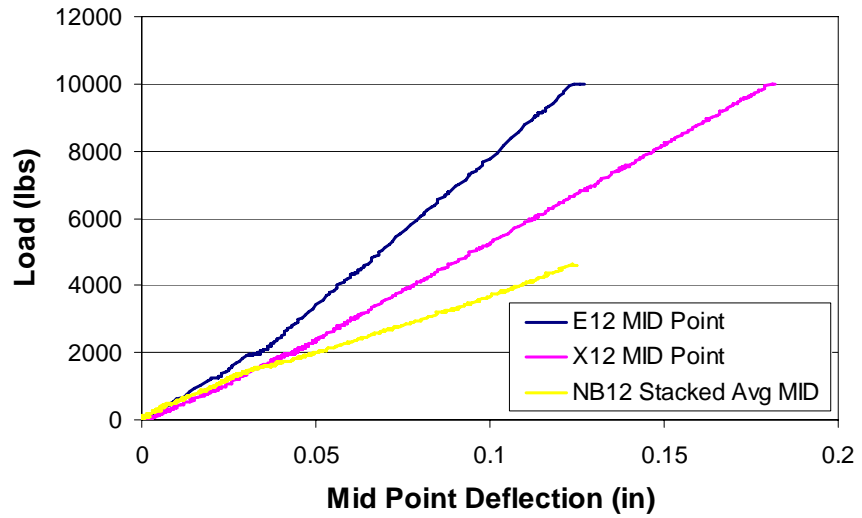
Load vs. Deflection for X12 5' Span



Load vs. Slip for X12 5' Span

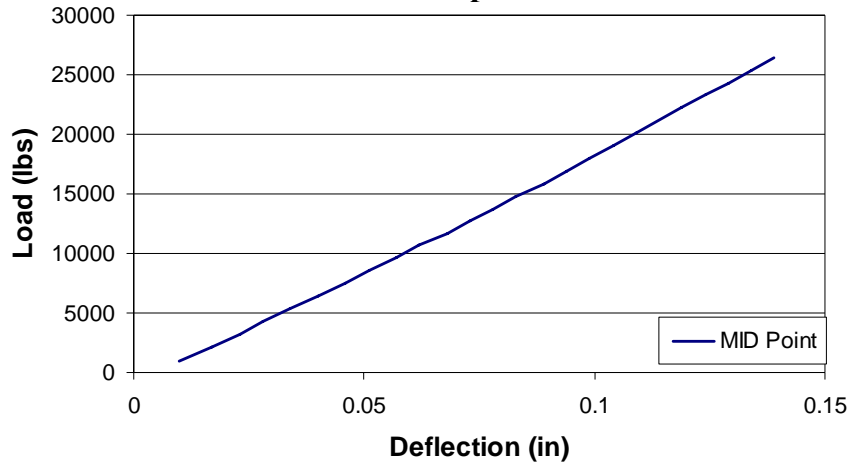


Load vs. Deflection Comparison Across 12 inch Width Series 10'-6" Span

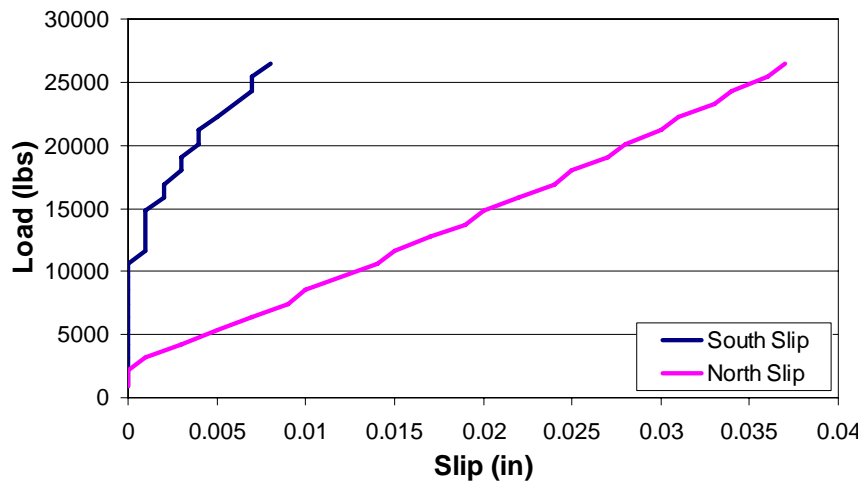


Load vs. Deflection Comparison Across 12 inch Width Series 5' Span

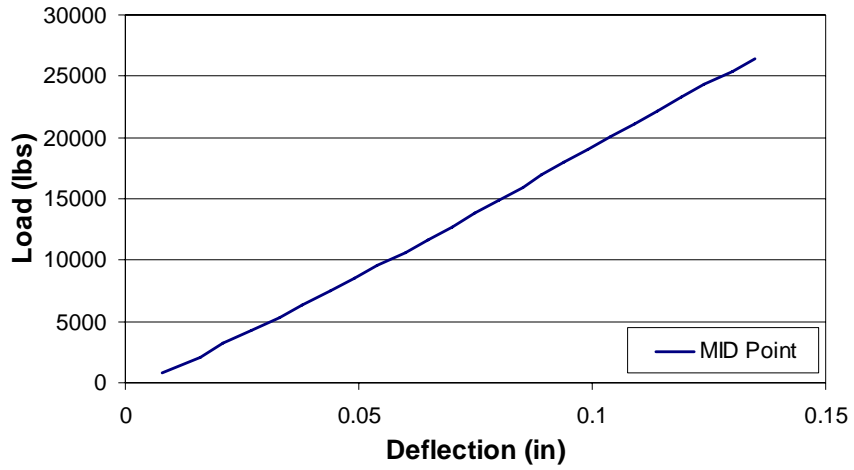
Phase 1: Depth Series 14 inch depth



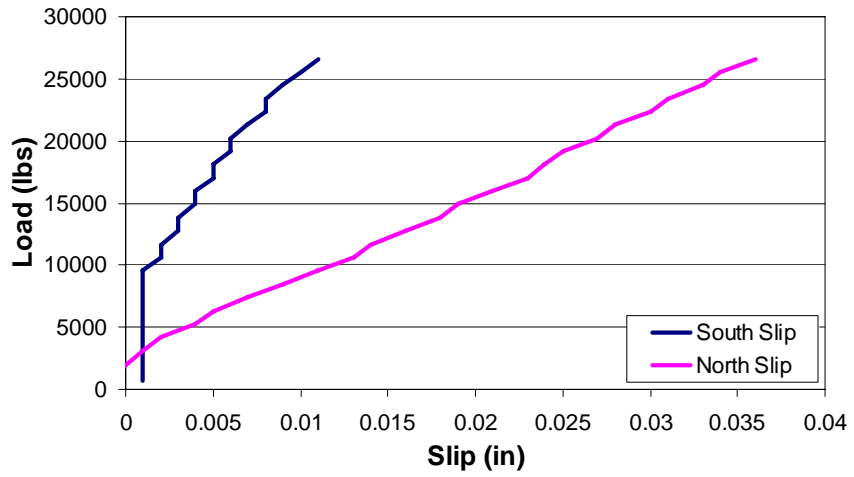
Load vs. Deflection for NB14-4 over NB14-3 5' Span



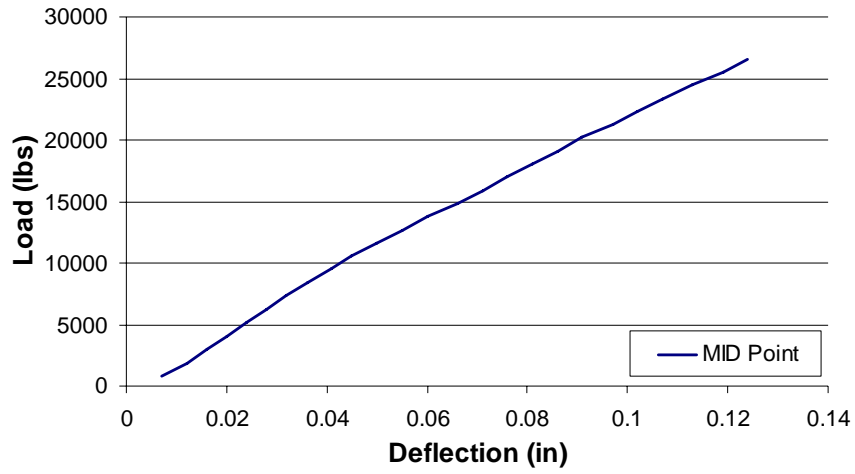
Load vs. Slip for NB14-4 over NB14-3 5' Span



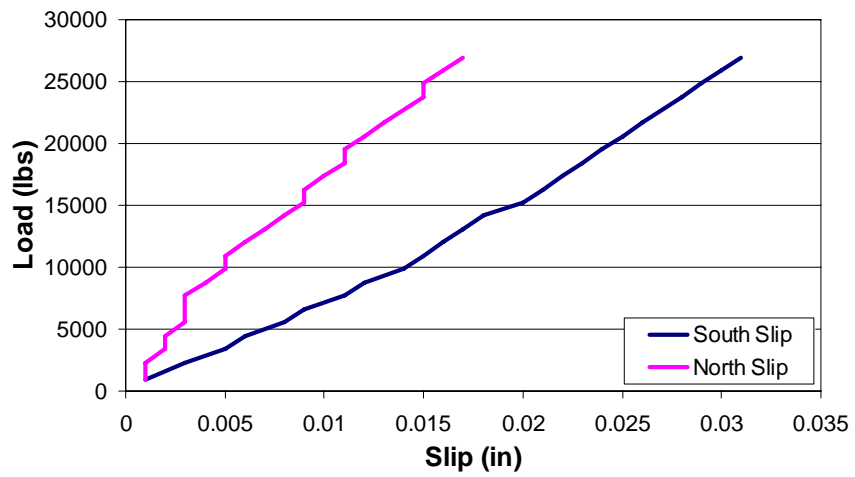
Load vs. Deflection for NB14-2 over NB14-3 5' Span



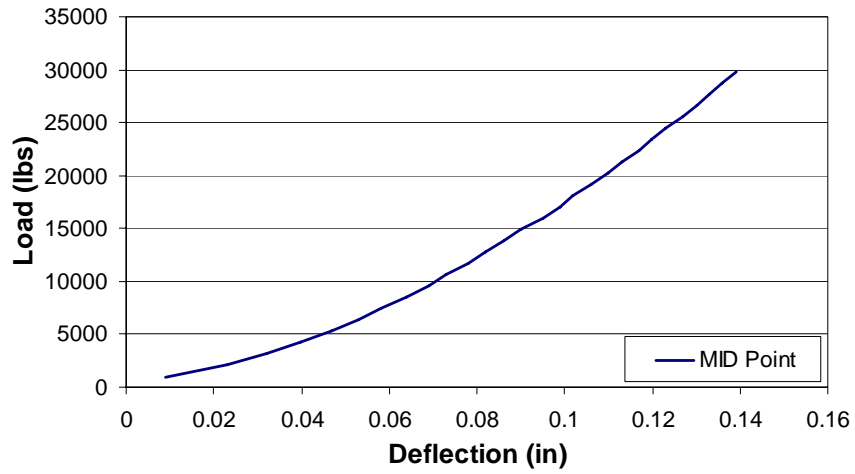
Load vs. Slip Deflection for NB14-2 over NB14-3 5' Span



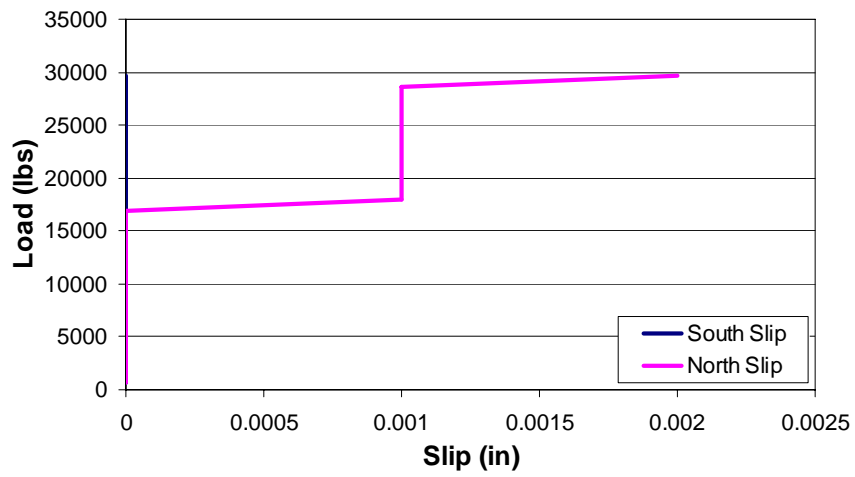
Load vs. Deflection for NB14-2 over NB14-1 5' Span



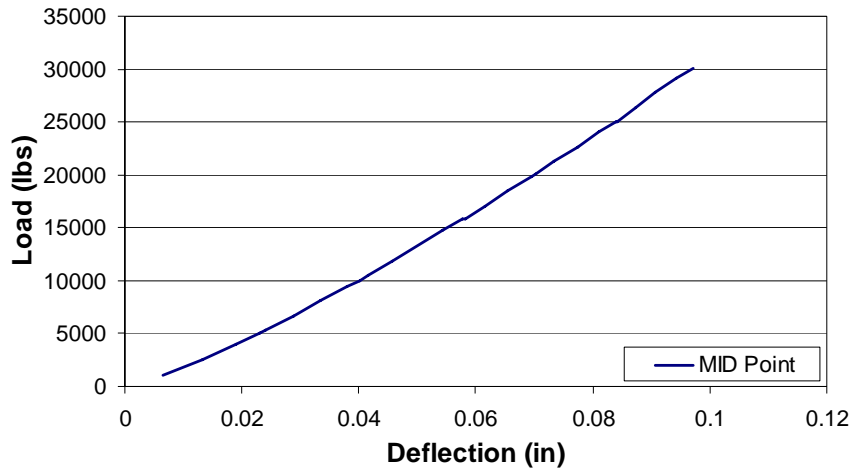
Load vs. Slip for NB14-2 over NB14-1 5' Span



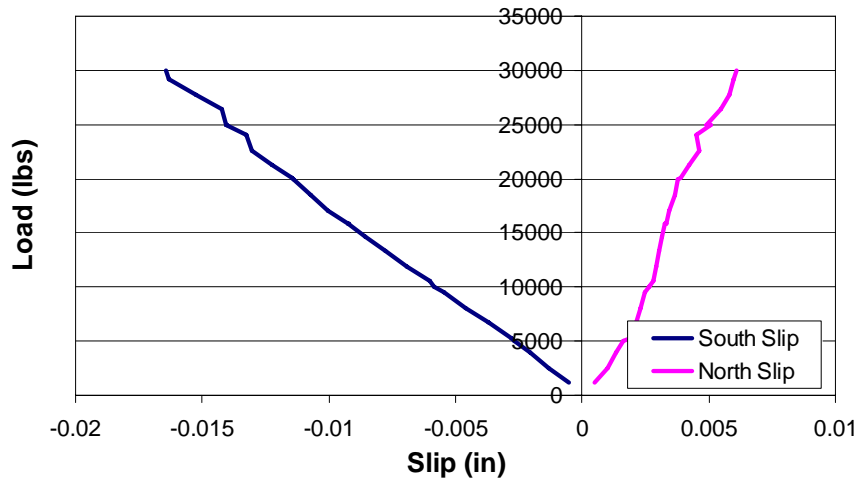
Load vs. Deflection for E14 5' Span



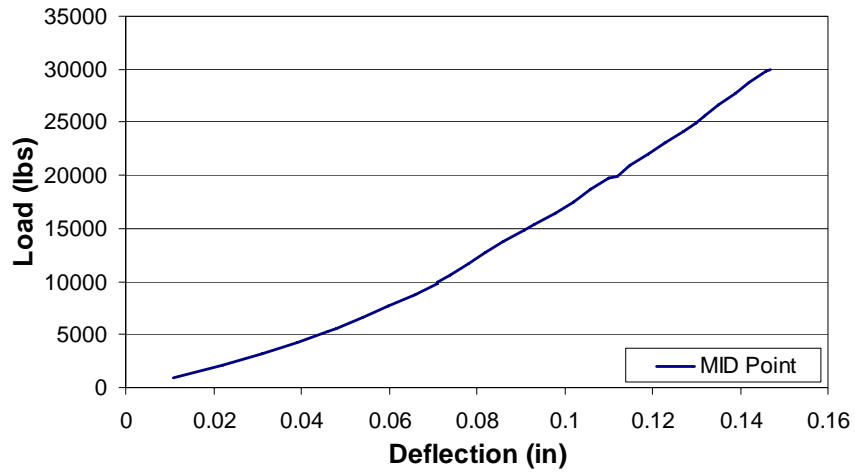
Load vs. Slip for E14 5' Span



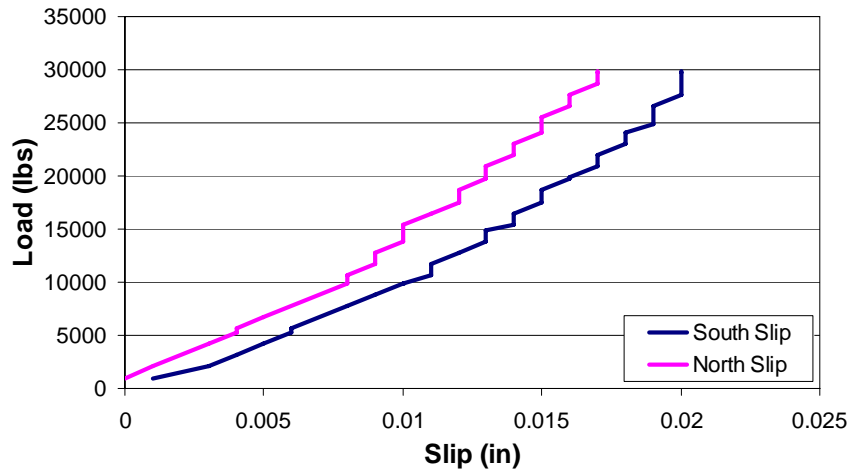
Load vs. Deflection for X14 5' Span



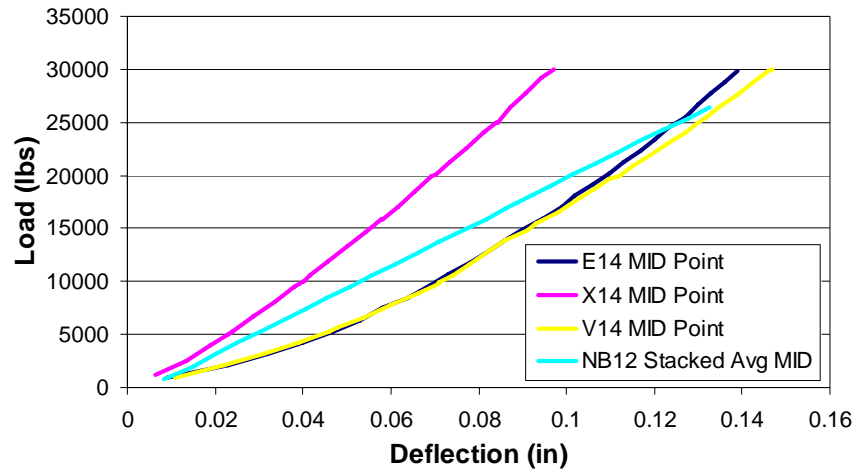
Load vs. Slip for X14 5' Span



Load vs. Deflection for V14 5' Span

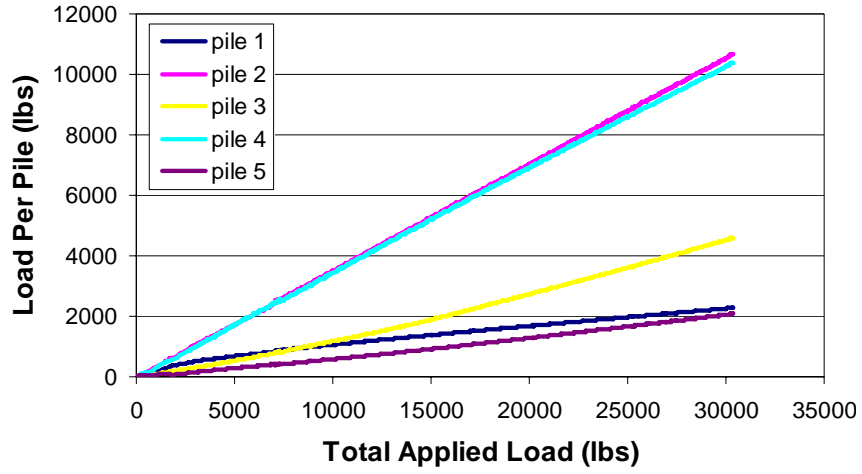


Load vs. Slip for V14 5' Span

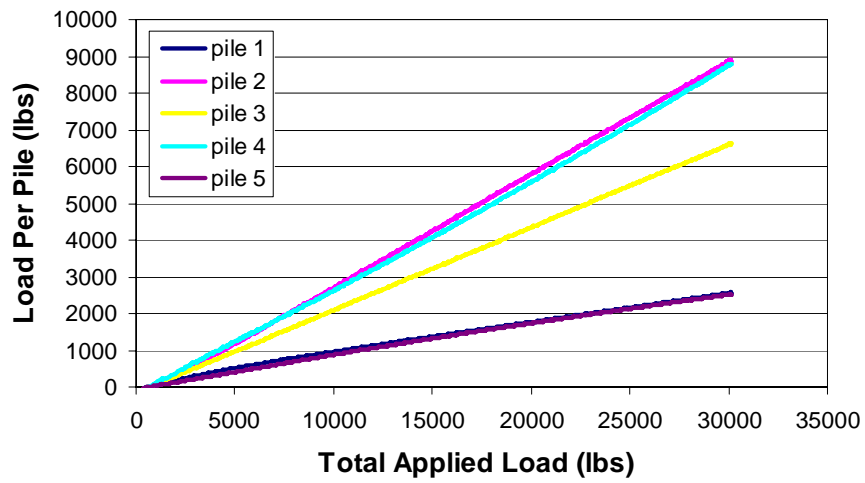


Load vs. Deflection Comparison Across 14 inch Depth Series 5' Span

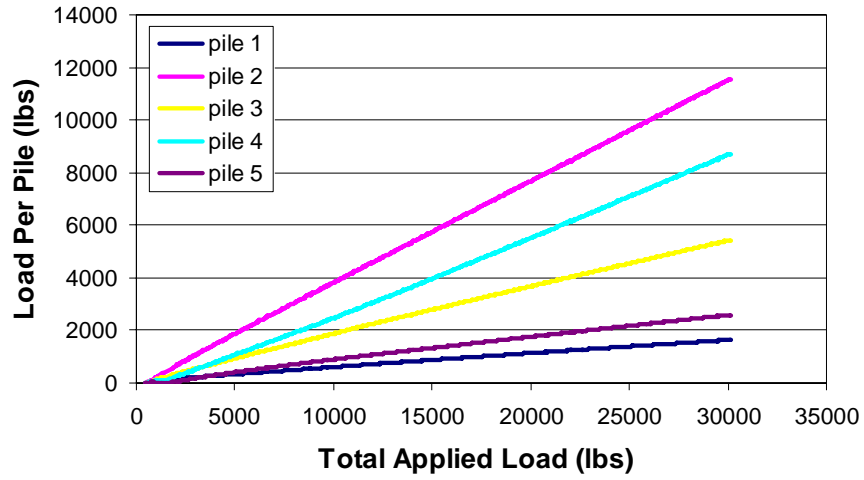
Phase 2: Full Scale Series
Single pile caps



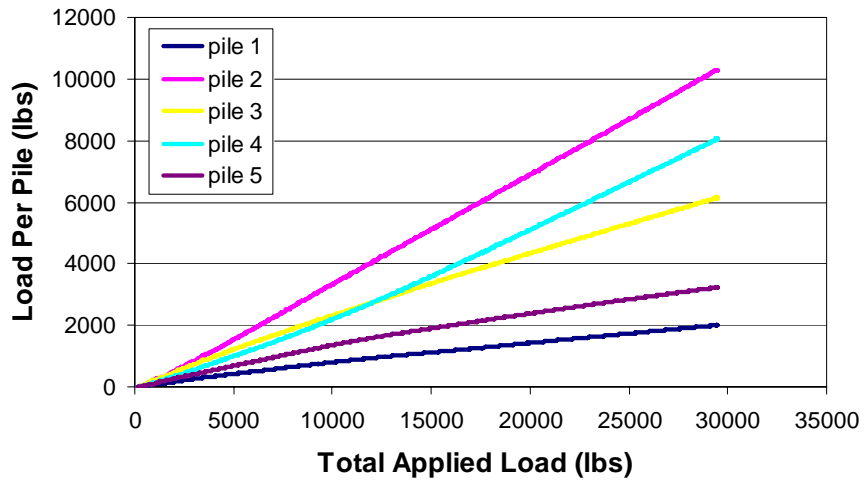
Load Per Pile for NB12x12-1



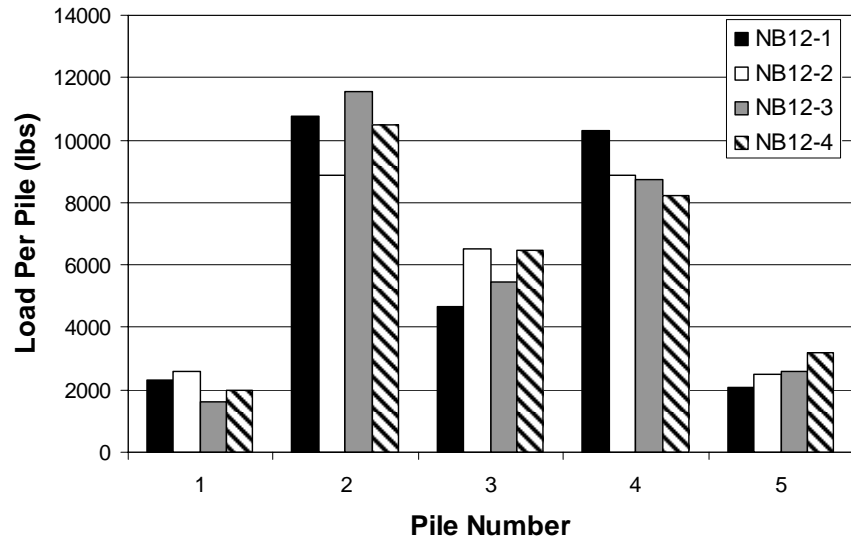
Load Per Pile for NB12x12-2



Load Per Pile for NB12x12-3

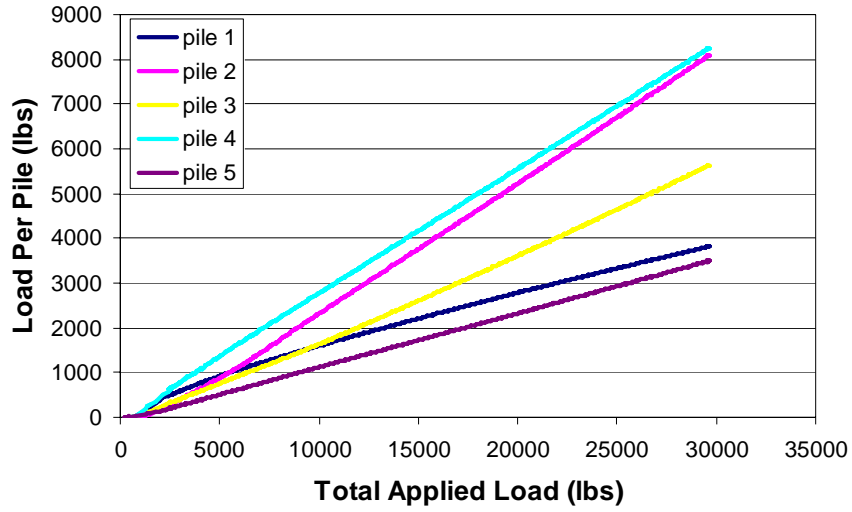


Load Per Pile for NB12x12-4

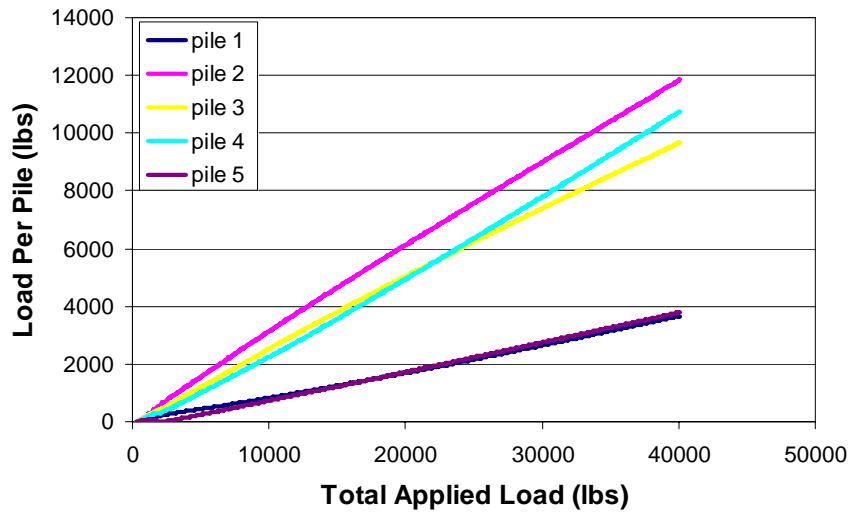


Load Per Pile Comparison Across Single Pile Caps

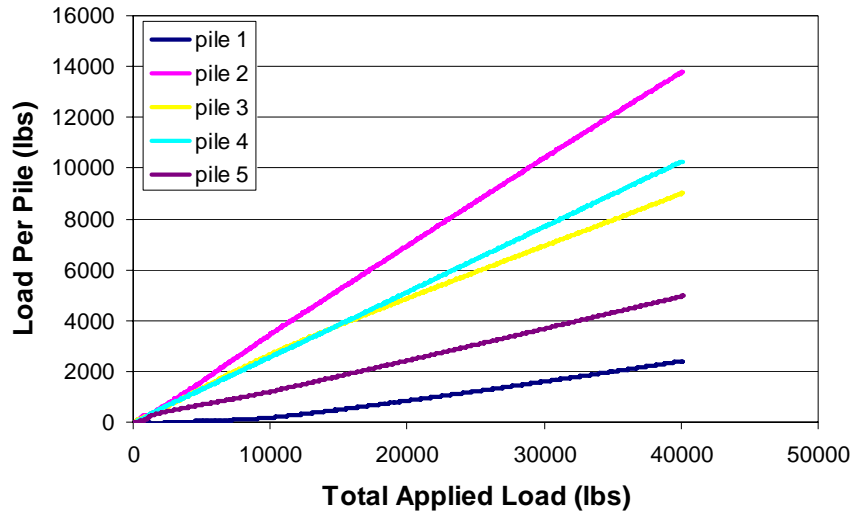
Phase 2: Full Scale Series
Double pile caps



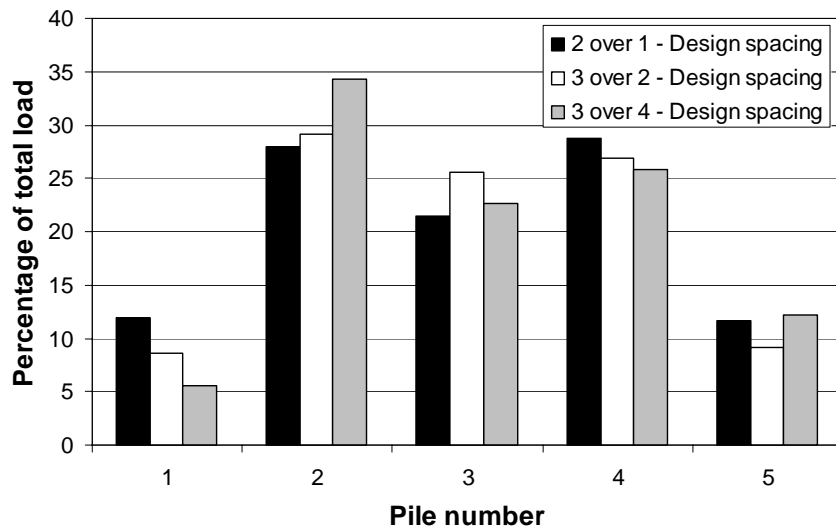
Load Per Pile for NB12x12-2 over NB12x12-1 Design Pile Spacing



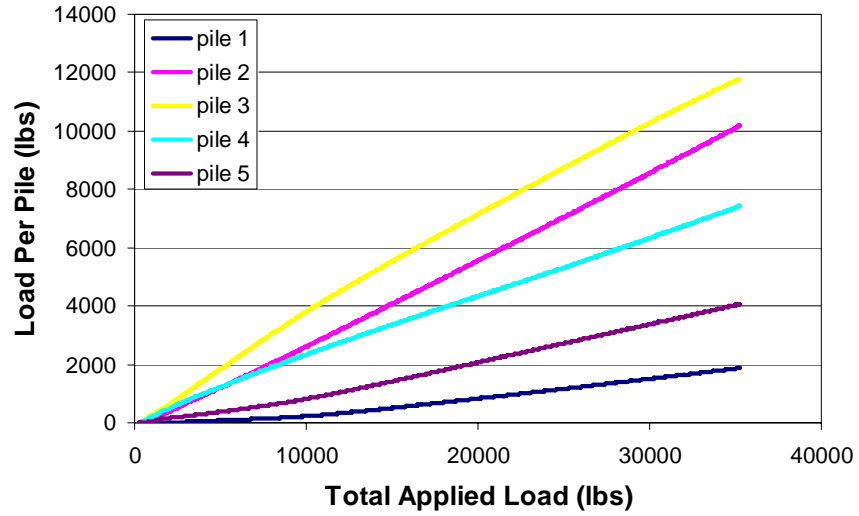
Load Per Pile for NB12x12-3 over NB12x12-2 Design Pile Spacing



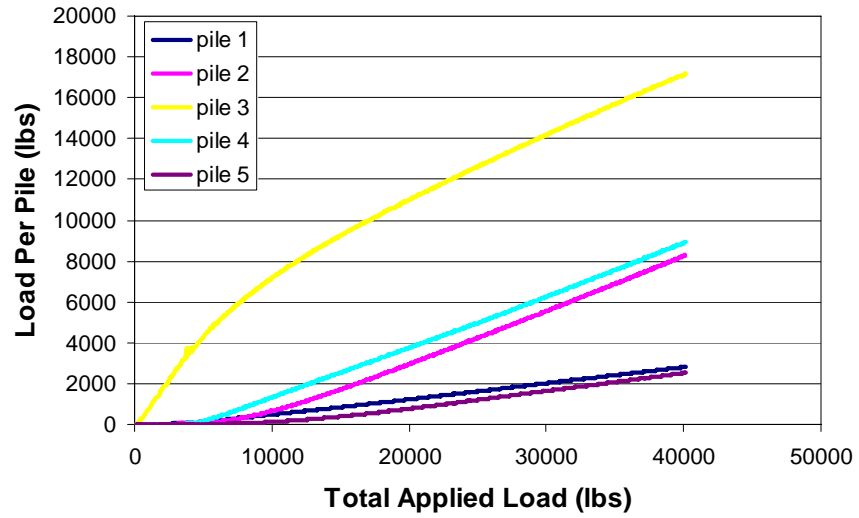
Load Per Pile for NB12x12-3 over NB12x12-4 Design Pile Spacing



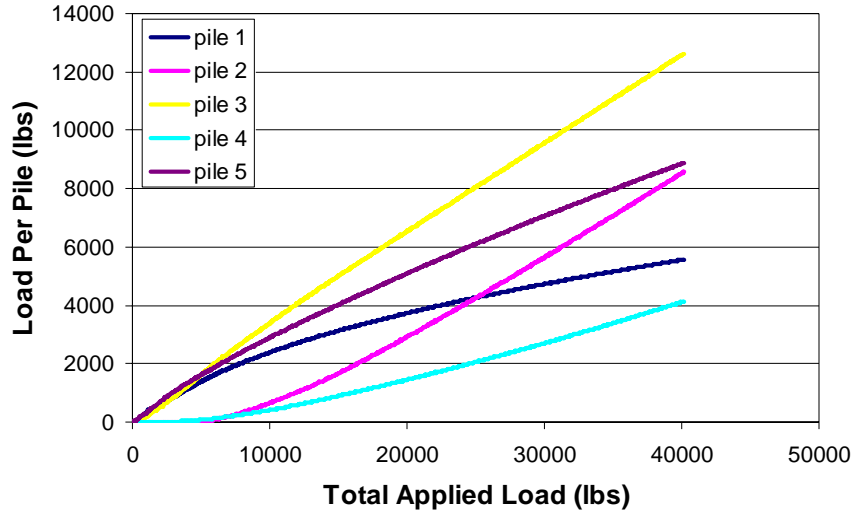
Percentage of Load Per Pile Comparison Across Double Pile Caps Design Spacing



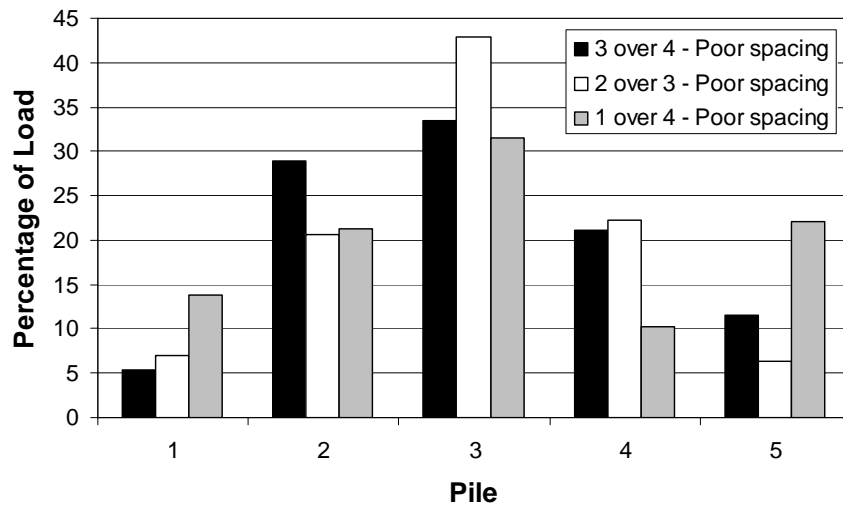
Load Per Pile for NB12x12-3 over NB12x12-4 Poor Pile Spacing



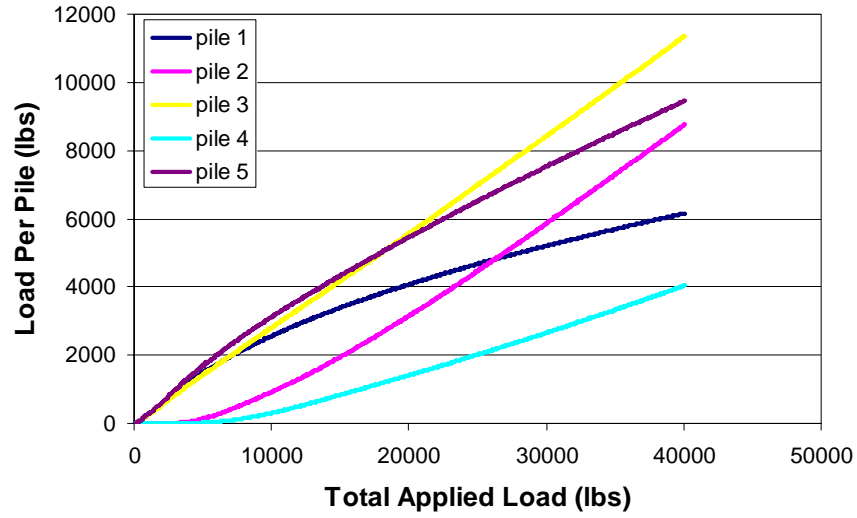
Load Per Pile for NB12x12-2 over NB12x12-3 Poor Pile Spacing



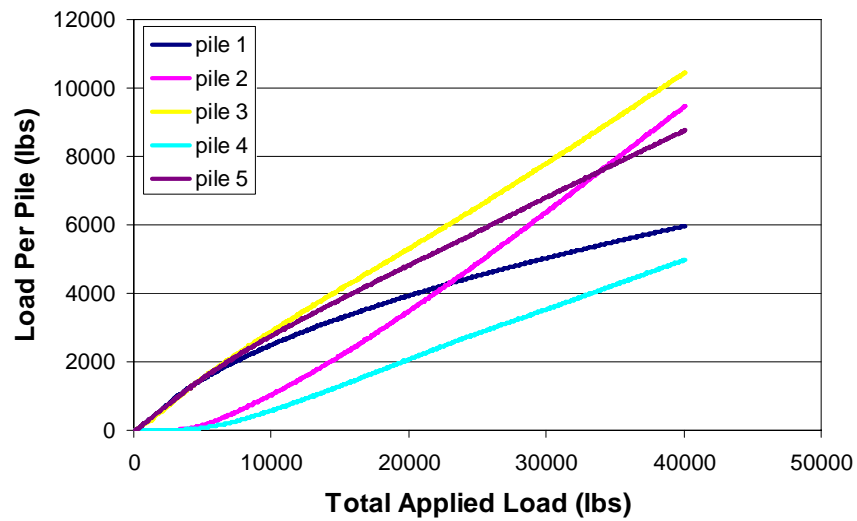
Load Per Pile for NB12x12-1 over NB12x12-4 Poor Pile Spacing



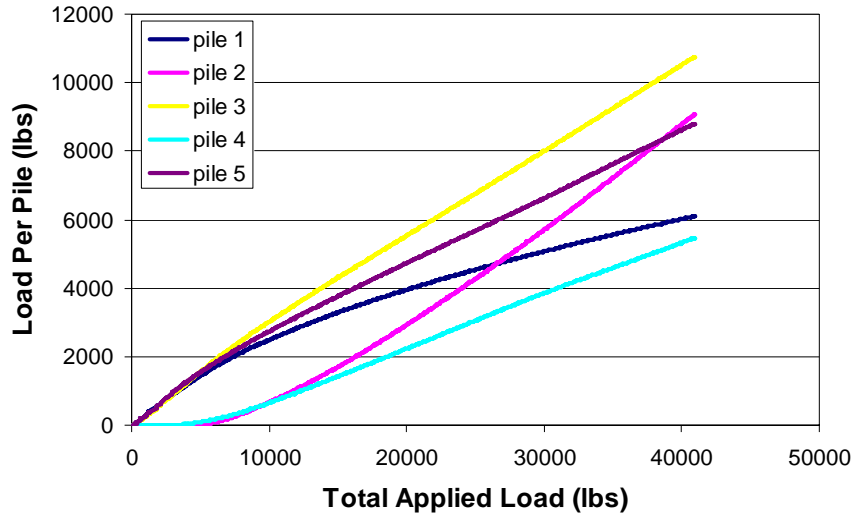
Percentage of Load Per Pile Comparison Across Double Pile Caps Poor Pile Spacing



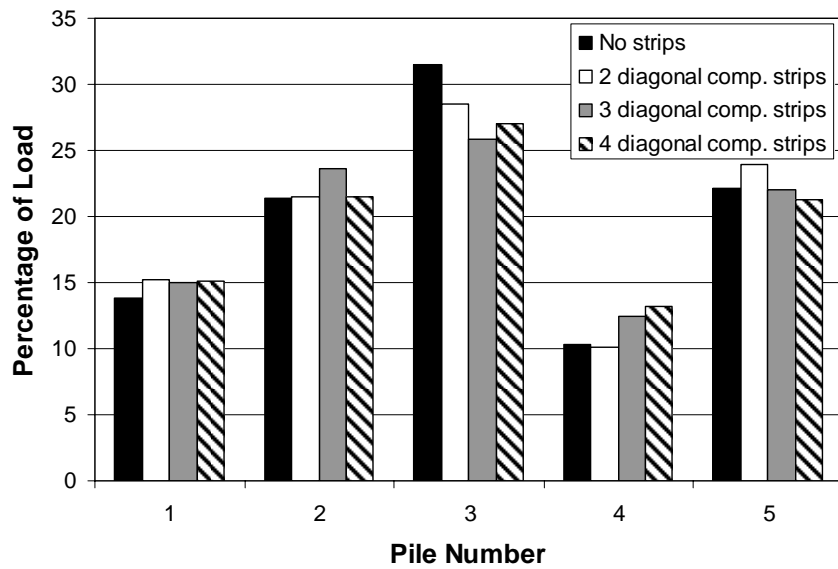
Load Per Pile for NB12x12-1 over NB12x12-4 With 2 Diagonal Strips, Poor Pile Spacing



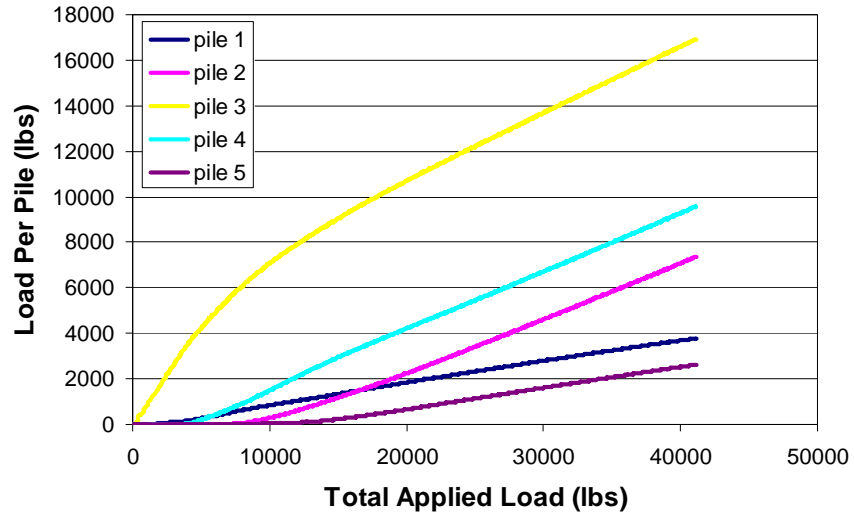
Load Per Pile for NB12x12-1 over NB12x12-4 With 3 Diagonal Strips, Poor Pile Spacing



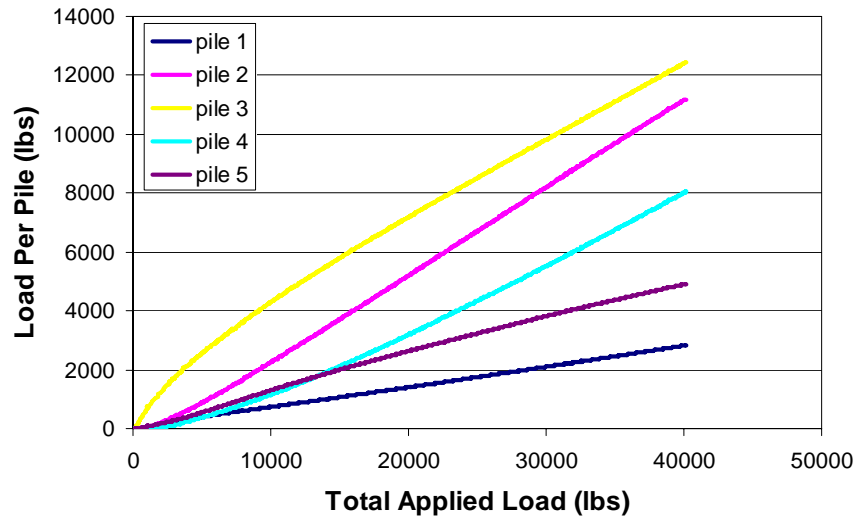
Load Per Pile for NB12x12-1 over NB12x12-4 With 4 Diagonal Strips, Poor Pile Spacing



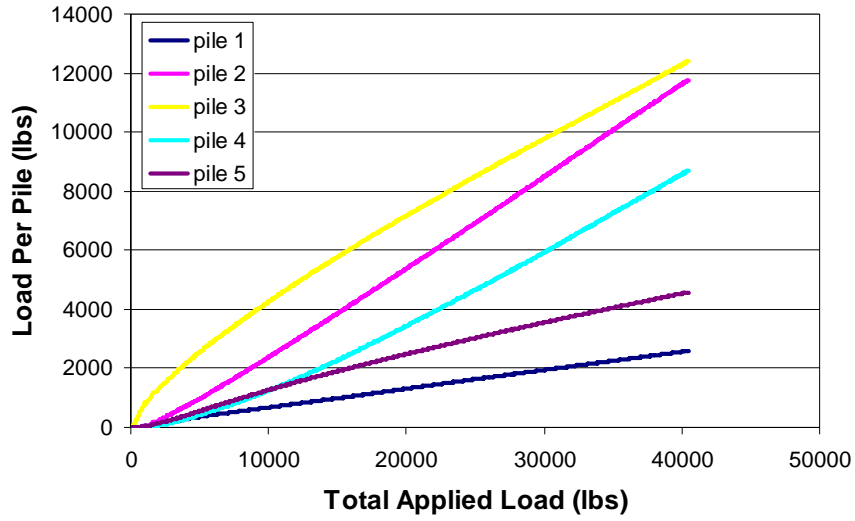
Percentage of Load Per Pile Comparison of Different Strip Combinations on NB12x12-1 over NB12x12-4, Poor Pile Spacing



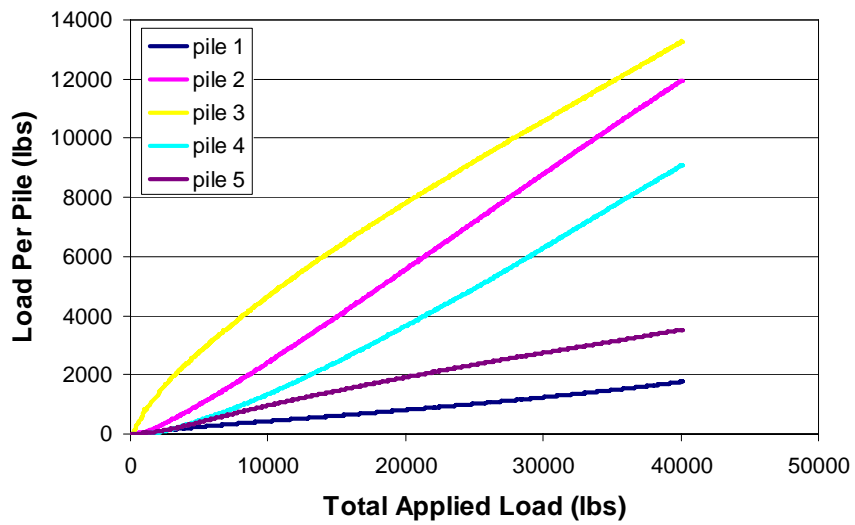
Load Per Pile for NB12x12-2 over NB12x12-3 With 2 Diagonal Strips, Poor Pile Spacing



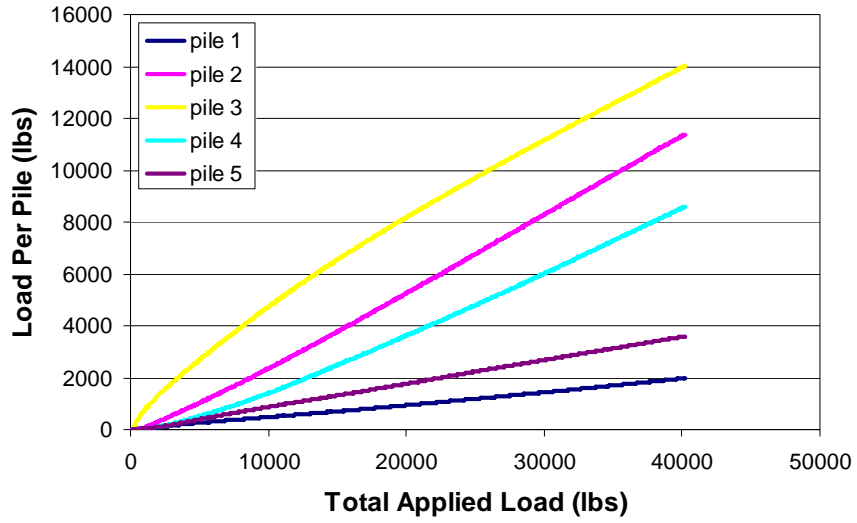
Load Per Pile for NB12x12-2 over NB12x12-3 With 2 Diagonal Strips and 1 Vertical Strip, Poor Pile Spacing



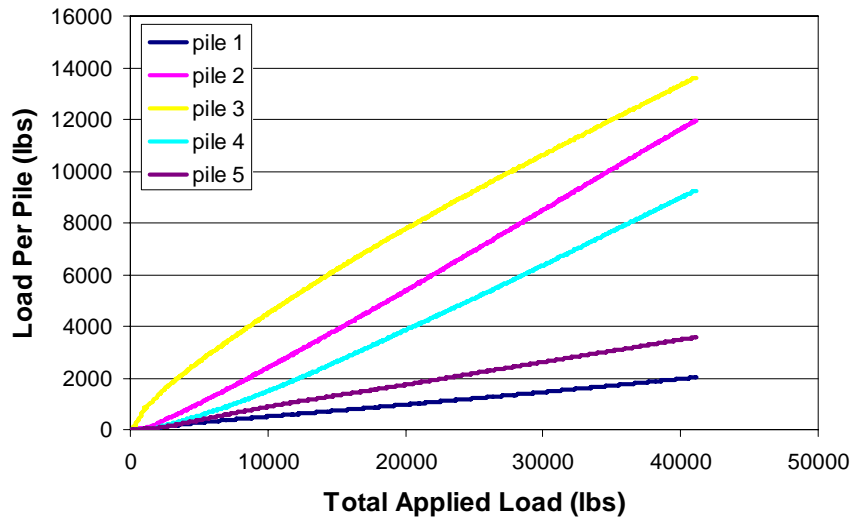
Load Per Pile for NB12x12-2 over NB12x12-3 With 2 Diagonal Strips and 2 Vertical Strips, Poor Pile Spacing



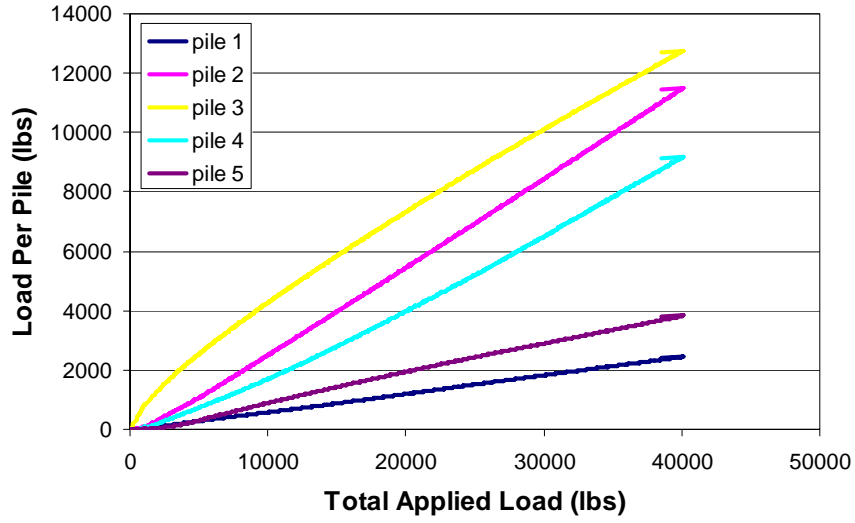
Load Per Pile for NB12x12-2 over NB12x12-3 With 2 Vertical Strips, Poor Pile Spacing



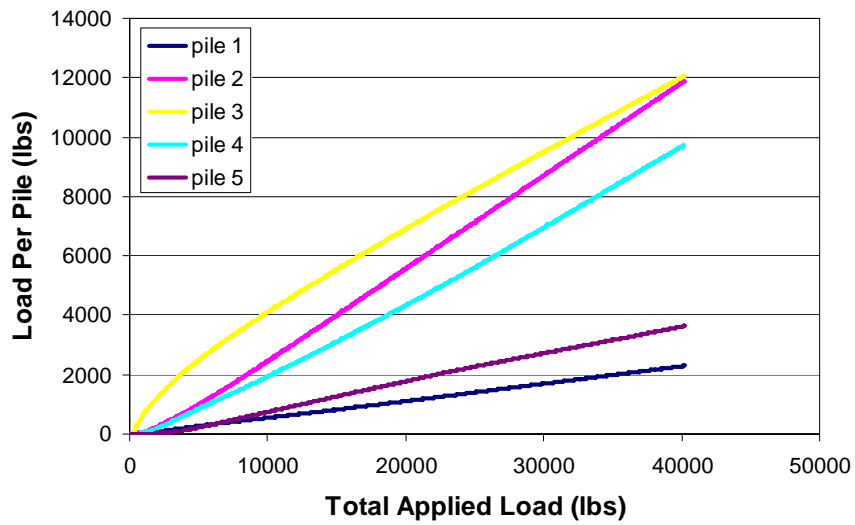
Load Per Pile for NB12x12-2 over NB12x12-3 With 1 Tension Diagonal Strip, Poor Pile Spacing



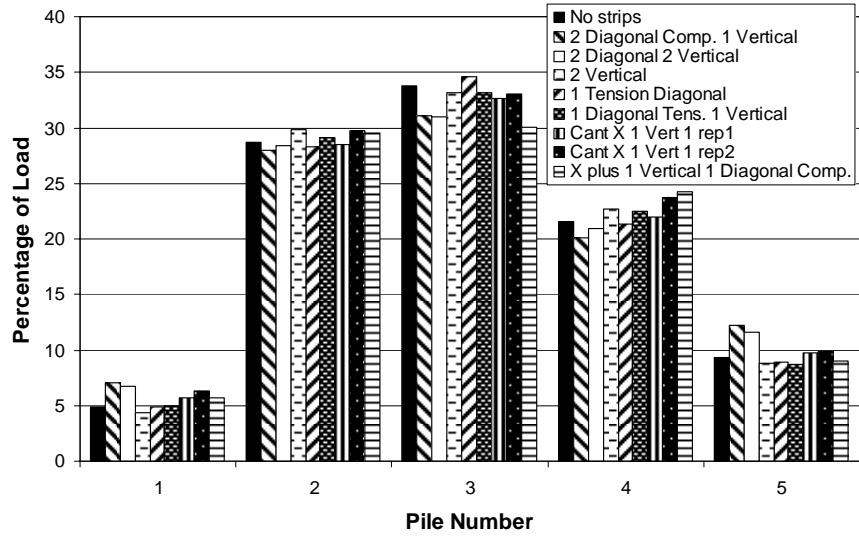
Load Per Pile for NB12x12-2 over NB12x12-3 With 1 Tension Diagonal Strip and 1 Vertical Strip, Poor Pile Spacing



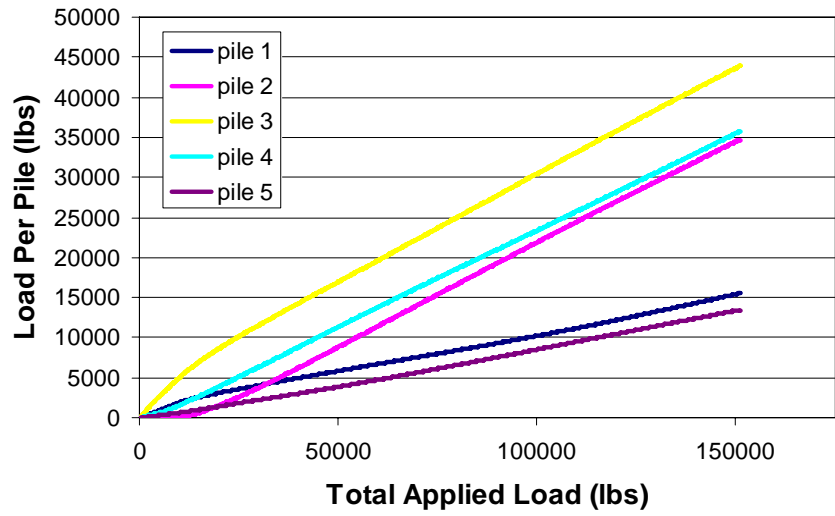
Load Per Pile for NB12x12-2 over NB12x12-3 With 1 X-brace and 1 Vertical Strip, Poor Pile Spacing



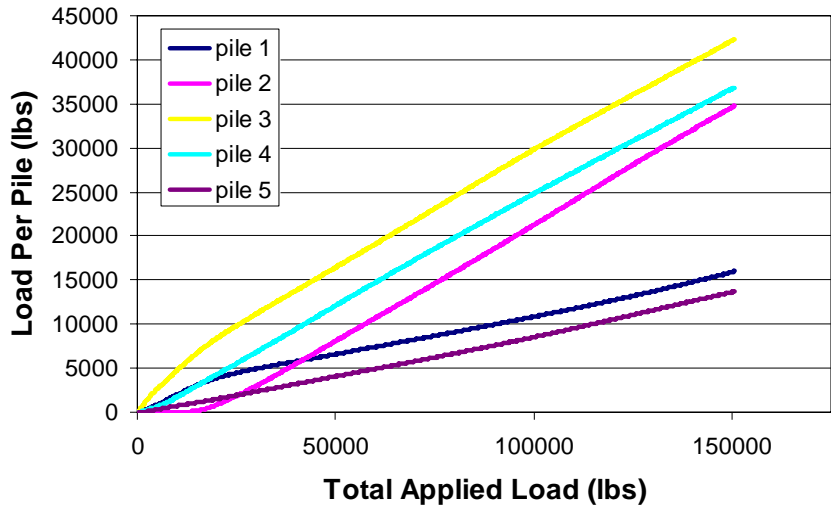
Load Per Pile for NB12x12-2 over NB12x12-3 With 1 X-brace, 1 Diagonal Strip, and 1 Vertical Strip, Poor Pile Spacing



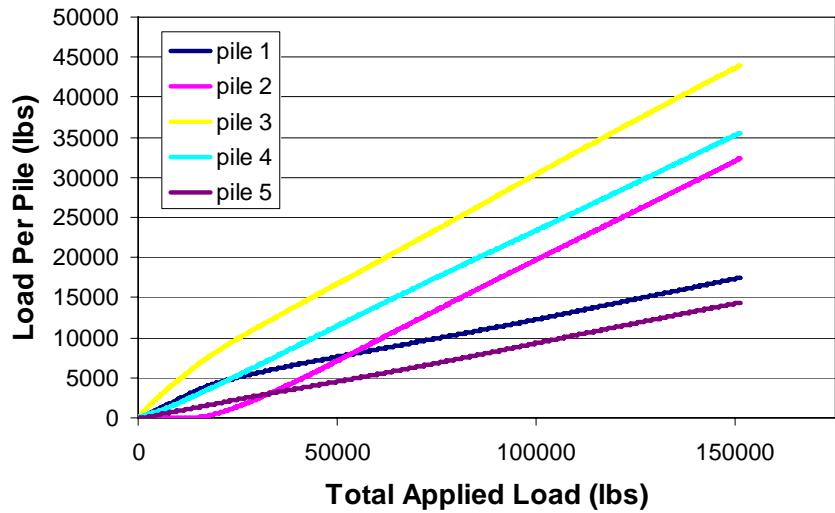
Percentage of Load Per Pile Comparison of Different Strip Combinations on NB12x12-2 over NB12x12-3, Poor Pile Spacing



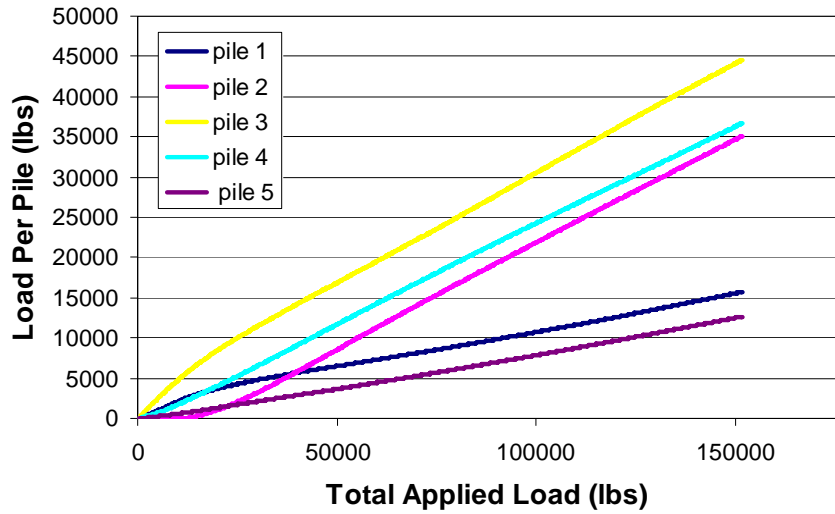
Load Per Pile for NB12x12-2 over NB12x12-3, Poor Pile Spacing, 150 kip Test



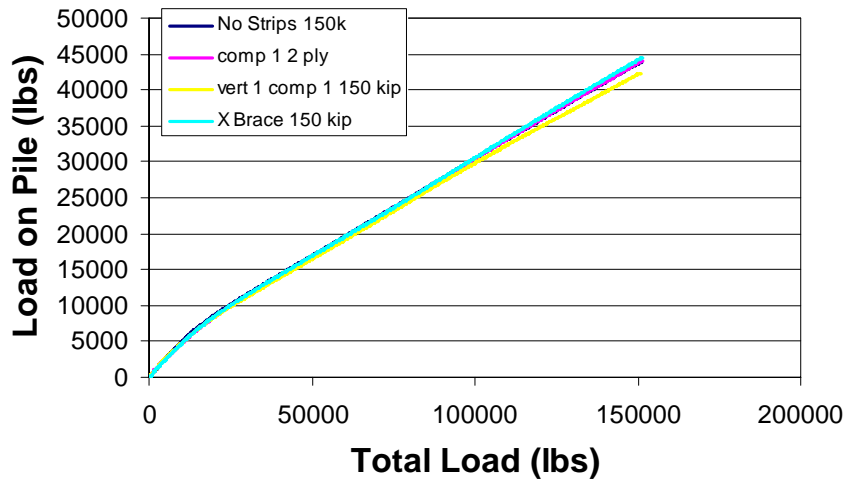
Load Per Pile for NB12x12-2 over NB12x12-3 with 1 Vertical Strip and 1 Diagonal Strip, Poor Pile Spacing, 150 kip Test



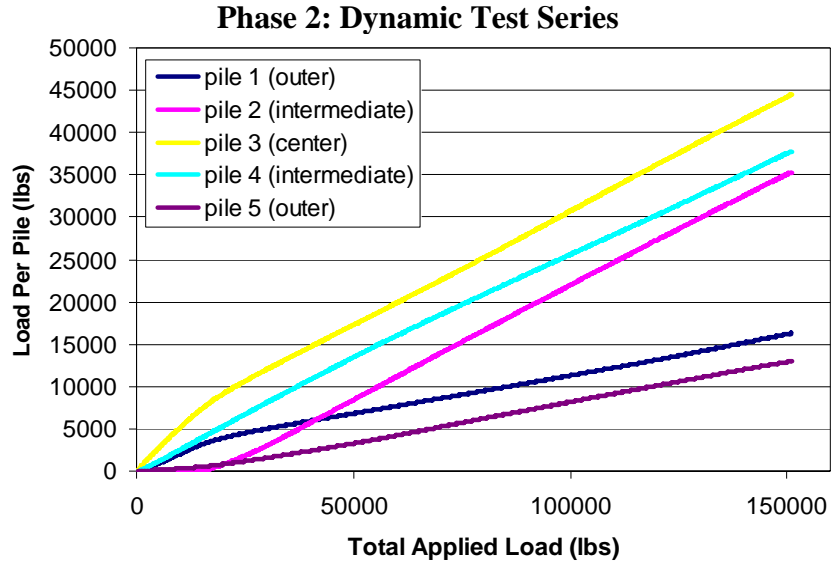
Load Per Pile for NB12x12-2 over NB12x12-3 with 1 Diagonal Strip, 2 ply, Poor Pile Spacing, 150 kip Test



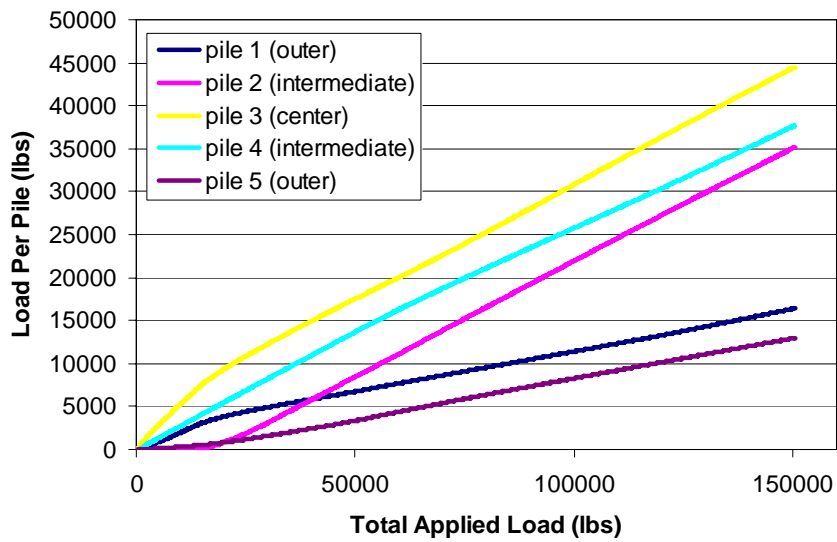
Load Per Pile for NB12x12-2 over NB12x12-3 with X-brace Pattern, Poor Pile Spacing, 150 kip Test



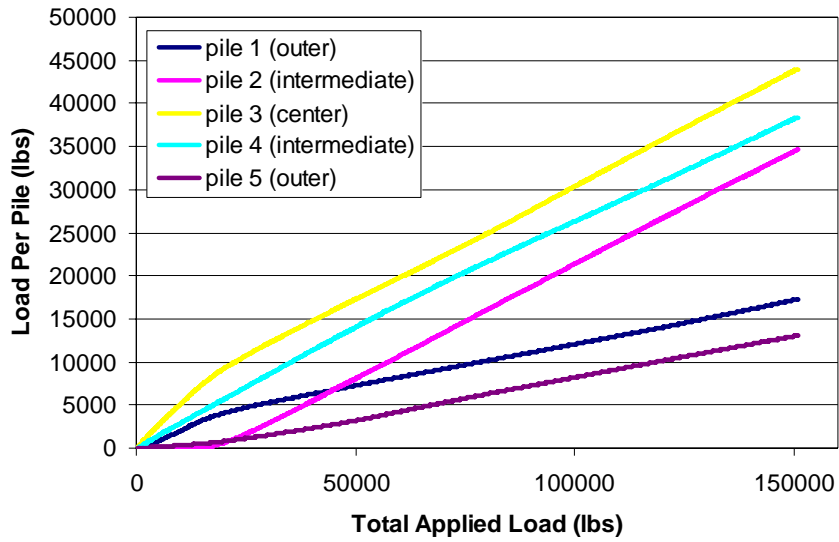
Comparison of Load on Center Pile (Pile 3) for Various Strip Configurations on NB12x12-2 over NB12x12-3, Poor Pile Spacing, 150 kip Tests



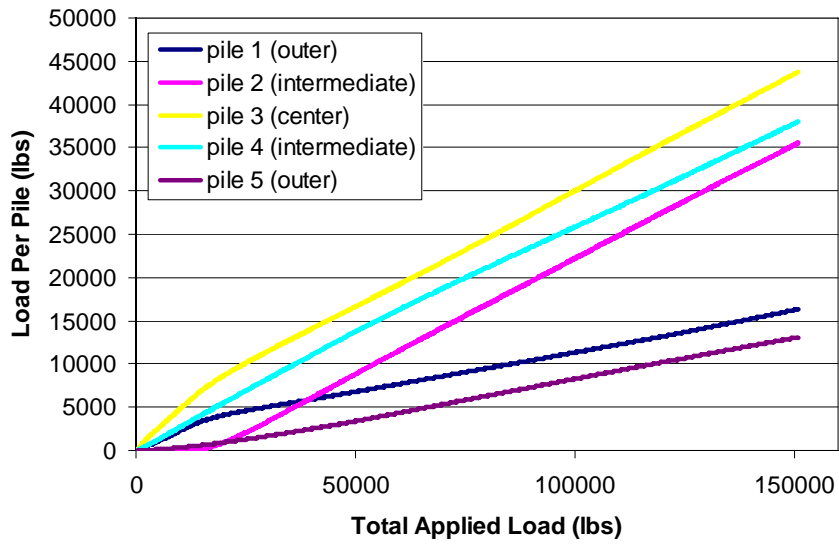
Load Per Pile on X-braced Strip Pattern for NB12x12-2 over NB12x12-3 Dynamic Test, 150,000 cycles



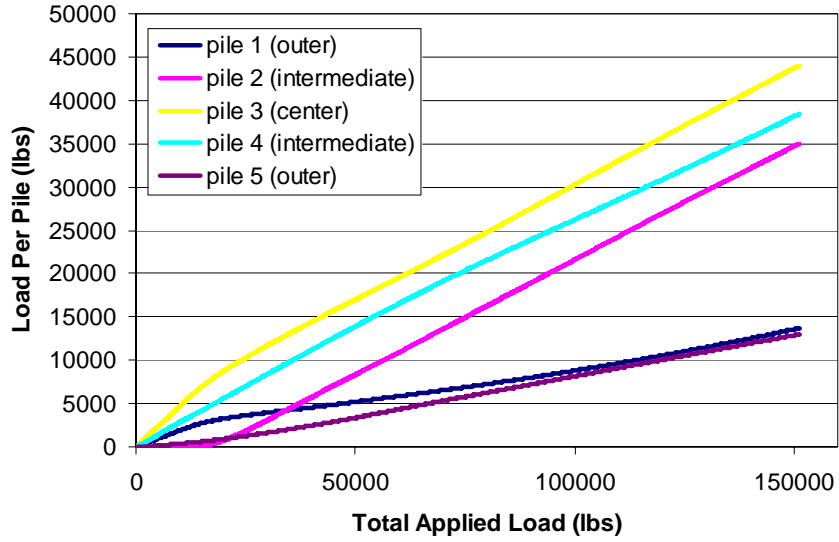
Load Per Pile on X-braced Strip Pattern for NB12x12-2 over NB12x12-3 Dynamic Test, 215,000 cycles



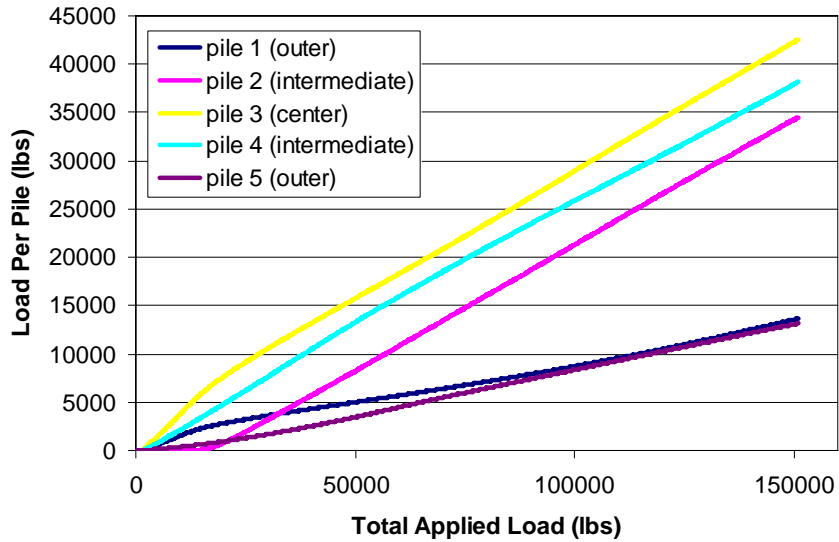
Load Per Pile on X-braced Strip Pattern for NB12x12-2 over NB12x12-3 Dynamic Test, 365,000 cycles



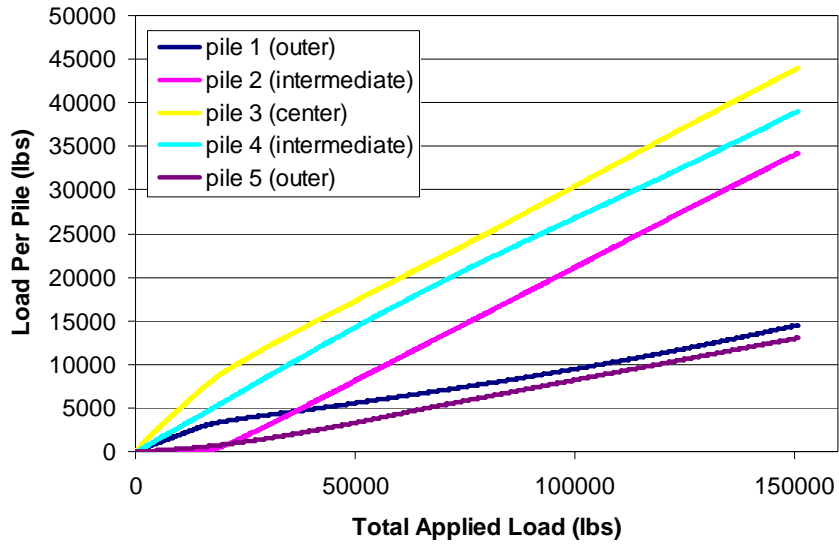
Load Per Pile on X-braced Strip Pattern for NB12x12-2 over NB12x12-3 Dynamic Test, 466,666 cycles



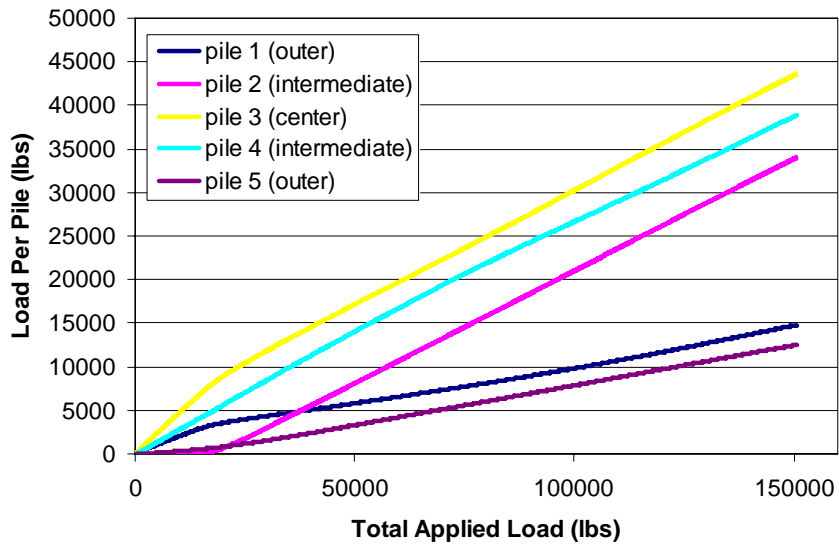
Load Per Pile on X-braced Strip Pattern for NB12x12-2 over NB12x12-3 Dynamic Test, 580,800 cycles



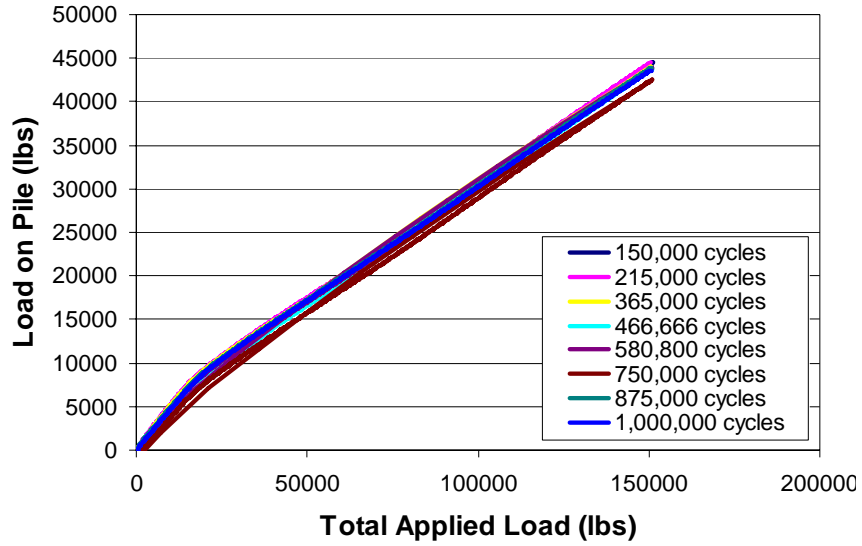
Load Per Pile on X-braced Strip Pattern for NB12x12-2 over NB12x12-3 Dynamic Test, 750,000 cycles



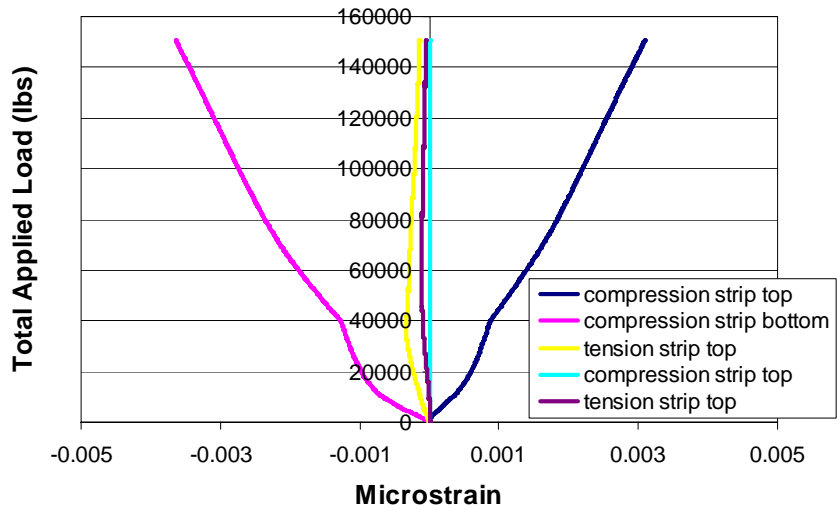
Load Per Pile on X-braced Strip Pattern for NB12x12-2 over NB12x12-3 Dynamic Test, 875,000 cycles



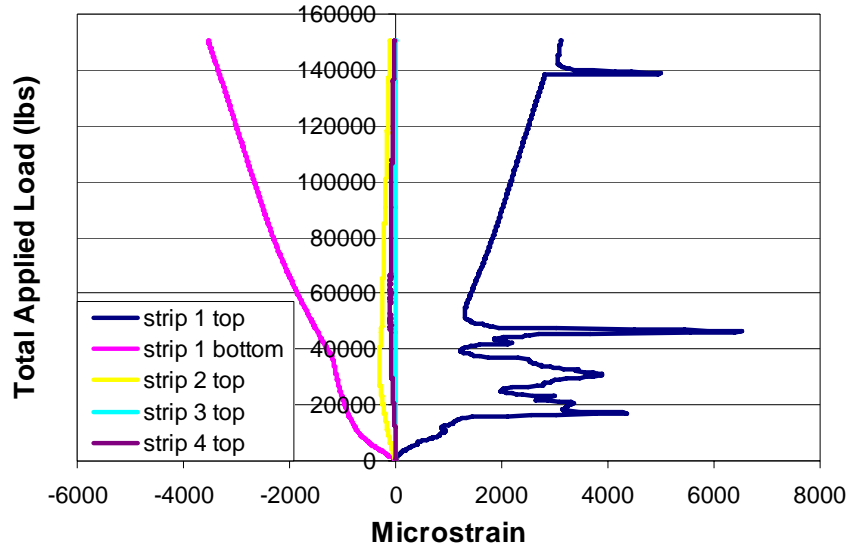
Load Per Pile on X-braced Strip Pattern for NB12x12-2 over NB12x12-3 Dynamic Test, 1,000,000 cycles



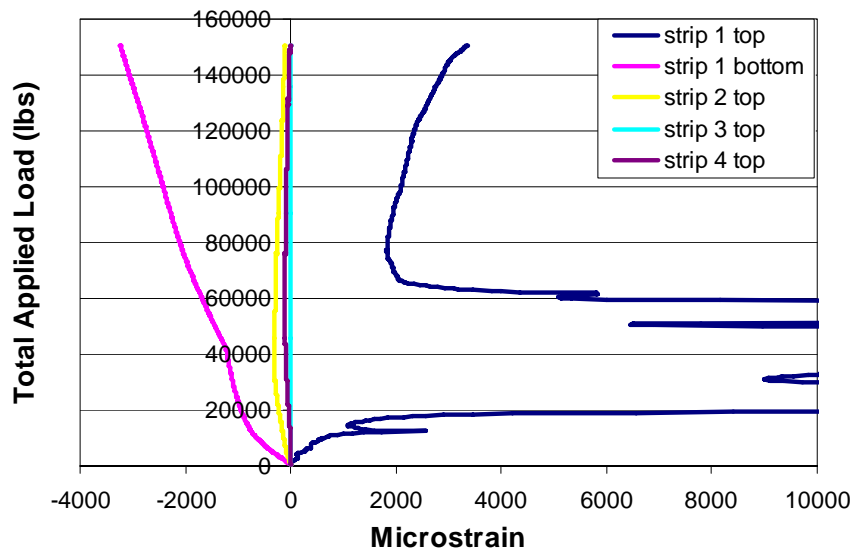
Comparison of Load on Center Pile (Pile 3) Through Progression of Cyclic Loading



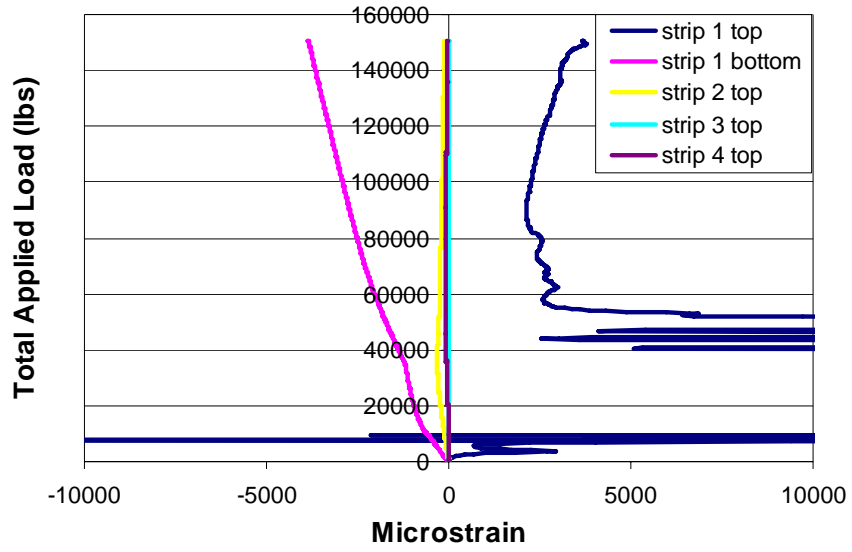
Load vs. Microstrain for NB12x12-2 over NB12x12-3 X-braced Strip Pattern Dynamic Test, 150,000 cycles



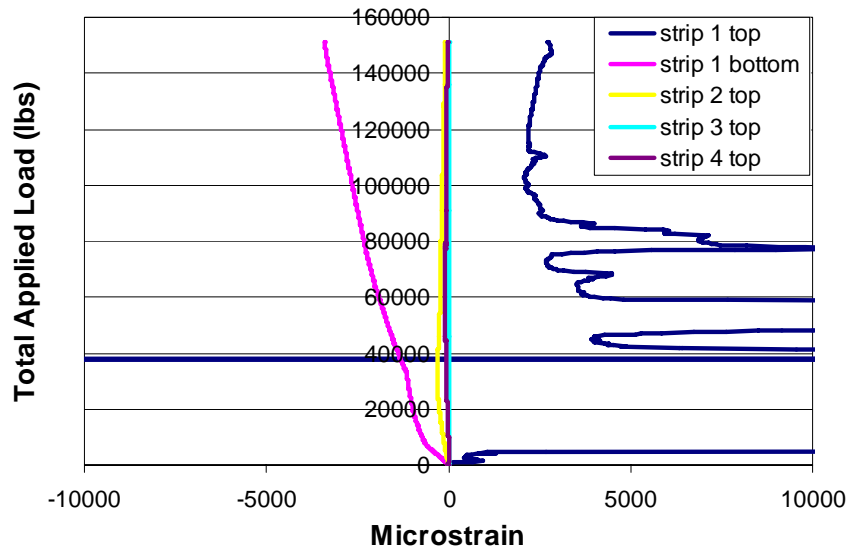
Load vs. Microstrain for NB12x12-2 over NB12x12-3 X-braced Strip Pattern Dynamic Test, 215,000 cycles



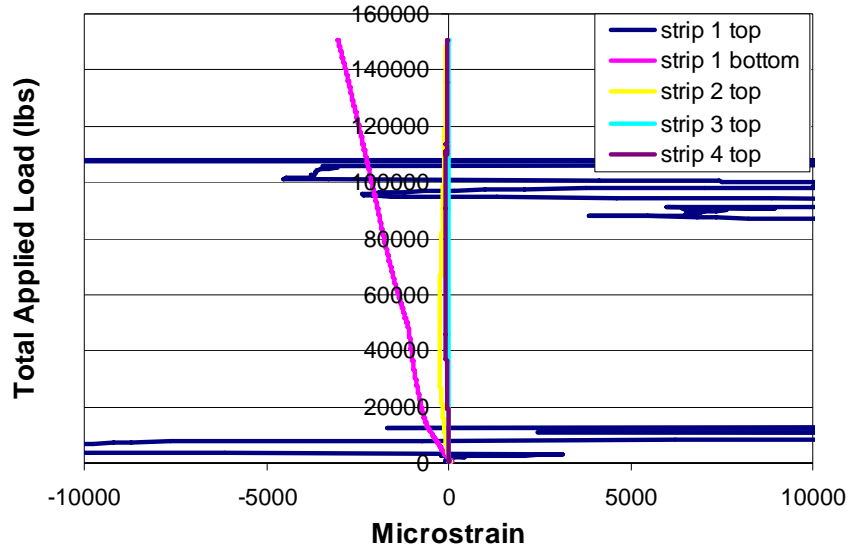
Load vs. Microstrain for NB12x12-2 over NB12x12-3 X-braced Strip Pattern Dynamic Test, 365,000 cycles



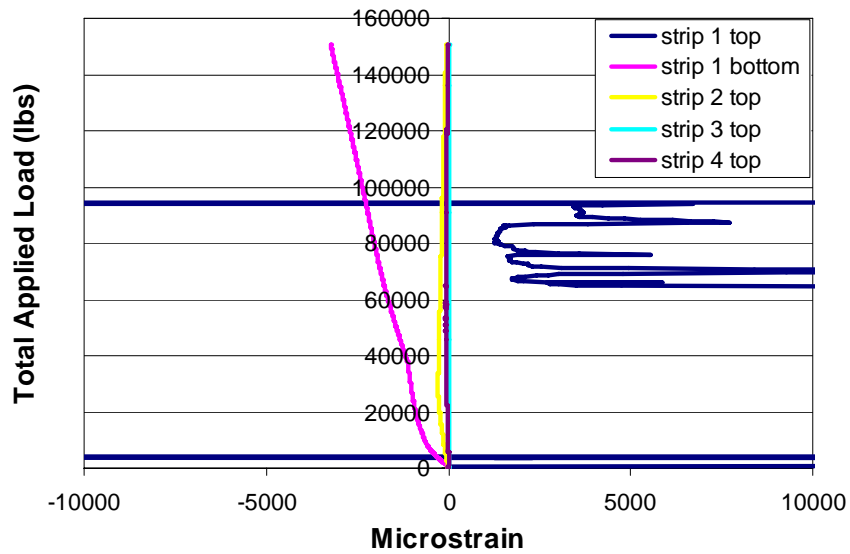
Load vs. Microstrain for NB12x12-2 over NB12x12-3 X-braced Strip Pattern Dynamic Test, 466,666 cycles



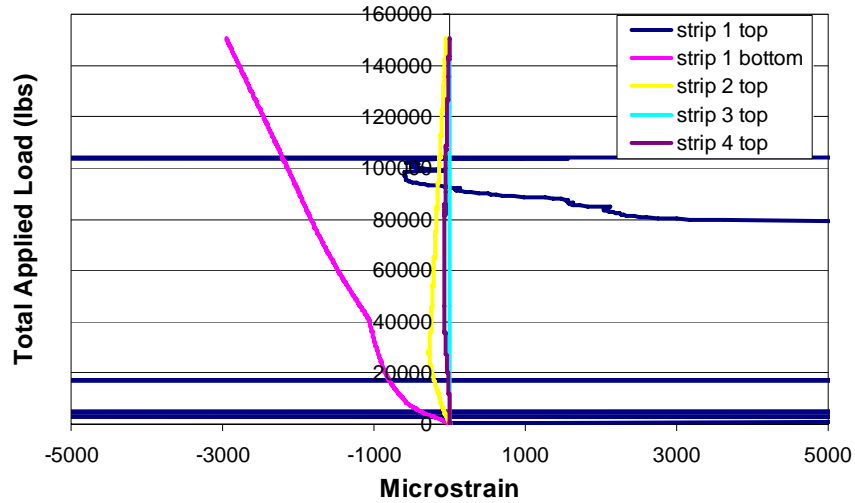
Load vs. Microstrain for NB12x12-2 over NB12x12-3 X-braced Strip Pattern Dynamic Test, 580,800 cycles



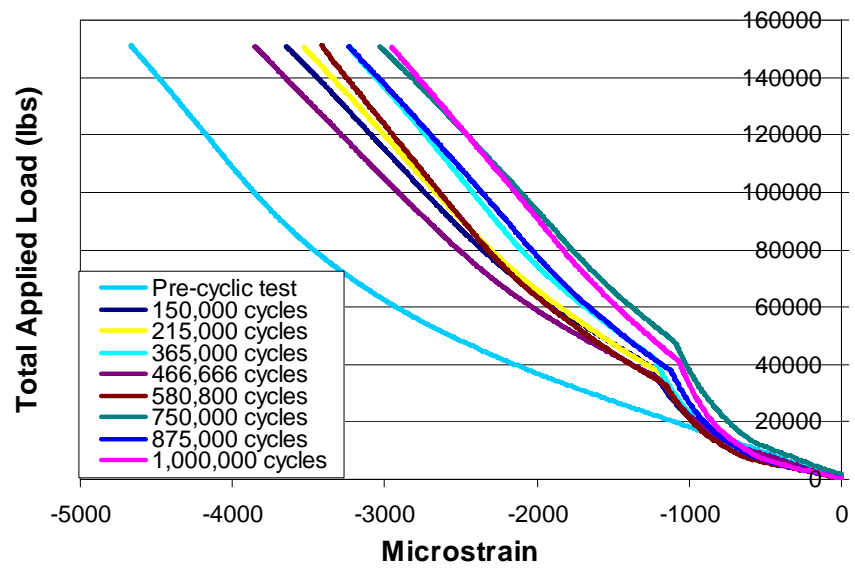
Load vs. Microstrain for NB12x12-2 over NB12x12-3 X-braced Strip Pattern Dynamic Test, 750,000 cycles



Load vs. Microstrain for NB12x12-2 over NB12x12-3 X-braced Strip Pattern Dynamic Test, 875,000 cycles



Load vs. Microstrain for NB12x12-2 over NB12x12-3 X-braced Strip Pattern Dynamic Test, 1,000,000 cycles



Comparison of Strain Through Progression of Cyclic Loading

Appendix C

5-Pile Bent
Taken from AREA 1953 Manual

Define Variables

$D := 12$	depth of pile cap, inches
$B := 12$	width of pile cap, inches
$R := 1$	live load taken by one bent, kips
$c_p := 30$	distance of inner pile from centerline of bent, inches
$b := 126$	distance between outer piles
$a := 29$	width of stringer bearing on cap, inches (assumed uniform)
$I := \frac{B \cdot D^3}{12}$	$I = 1728$ moment of inertia of cap, in ⁴
$A_{cap} := D \cdot B$	$A_{cap} = 144$ cross sectional area of cap, sq.in.
$L_p := 120$	effective length of pile, inches, taken as exposed length plus 1/2 penetration
$E := 1850$	modulus of elasticity, in bending and axial compression, ksi
$E_T := \frac{E}{80}$	$E_T = 23.125$ modulus of elasticity, transverse (taken as E/80)
$G := \frac{E}{16}$	$G = 115.625$ modulus of elasticity, shear (taken as E/16)

DEFLECTION COEFFICIENTS (deflections of cap, due to unit loads)

Due to R=1

$$q_a := \frac{1}{24E \cdot I} \left[b^3 - \frac{b \cdot a^2}{2} - 6 \cdot (30)^2 \cdot b + 30 \cdot a^2 + 4 \cdot (30)^3 \right] + \frac{0.6 \cdot (b - 60)}{A_{cap} \cdot G} \quad q_a = 0.021$$

$$q_b := \frac{1}{24 \cdot E \cdot I} \left[\left[\left[3 \cdot b^2 - a^2 - 12 \cdot (30)^2 \right] \cdot \left(\frac{b}{2} - c_p \right) - 4 \cdot \left(\frac{b}{2} - c_p \right)^3 + \frac{1}{a} \cdot \left(\frac{a}{2} + 30 - c_p \right)^4 \right] \right] \dots$$

$$+ \frac{0.6}{A_{cap} \cdot G} \cdot \left[b - 60 - a + \frac{1}{a} \cdot \left(\frac{3 \cdot a - 60}{2} + c_p \right) \cdot \left(\frac{a + 60}{2} - c_p \right) \right] \quad q_b = 0.016$$

Due to Xa=1

$$r_a := \frac{1}{48E \cdot I} \cdot b^3 + \frac{0.3}{A_{cap} \cdot G} \cdot b \quad r_a = 0.015$$

$$r_b := \frac{1}{48 \cdot E \cdot I} \cdot \left(\frac{b}{2} - c_p \right) \cdot \left[3 \cdot b^2 - 4 \cdot \left(\frac{b}{2} - c_p \right)^2 \right] + \frac{0.6}{A_{cap} \cdot G} \cdot \left(\frac{b}{2} - c_p \right) \quad r_b = 0.01$$

Due to $X_b=1$

$$s_a := 2 \cdot r_b$$

$$s_a = 0.021$$

$$s_b := \frac{1}{6 \cdot E \cdot I} \cdot (b + 4c_p) \cdot \left(\frac{b}{2} - c_p\right)^2 + \frac{1.2}{A_{cap} \cdot G} \left(\frac{b}{2} - c_p\right)$$

$$s_b = 0.016$$

PILE SHORTENING AND COMPRESSION OF CAP

$$u := \frac{114.5}{E} \cdot \left(\frac{1}{14 - 0.011L_p} - \frac{1}{14}\right) + \frac{1}{2 \cdot E_T \cdot B} \cdot (\ln(B + 2 \cdot D) - \ln(B))$$

$$u = 2.44 \times 10^{-3}$$

DEFLECTION EQUATIONS for consistent deformations of cap and piles

Given

$$\left(r_a + \frac{3}{2} \cdot u\right) \cdot X_a + (s_a + u) \cdot X_b = (q_a + u) \cdot R$$

$$\left(r_b + \frac{1}{2} \cdot u\right) \cdot X_a + (s_b + 2 \cdot u) \cdot X_b = (q_b + u) \cdot R$$

$$\text{Piles} := \text{Find}(X_a, X_b) \rightarrow \begin{pmatrix} 0.49675903620887759108 \\ 0.58244666619884880641 \end{pmatrix}$$

RESULTS

Percentage for the middle pile

$$\text{Middle_Pile} := (100 \cdot \text{Piles})_{0,0} \text{ float}, 4 \rightarrow 49.68$$

Percentage for a single intermediate pile

$$\text{Intermediate_Piles} := (100 \cdot \text{Piles})_{1,0} \text{ float}, 4 \rightarrow 58.24$$

Percentage for a single outer pile

$$\text{Outer_Piles} := \frac{100 \cdot 2 - \text{Middle_Pile} - 2 \cdot \text{Intermediate_Piles}}{2} \text{ float}, 4 \rightarrow 16.92$$

5-Pile Bent - Double Capped
Taken from AREA 1953 Manual

Define Variables

D := 12	depth of pile cap, inches		
B := 12	width of pile cap, inches		
$\overset{w}{R} := 1$	live load taken by one bent, kips		
$c_p := 30$	distance of inner pile from centerline of bent, inches		
b := 126	distance between outer piles		
a := 29	width of stringer bearing on cap, inches (assumed uniform)		
$I := \frac{2B \cdot D^3}{12}$	I = 3456	moment of inertia of cap, in ⁴	x 2 for the double cap
$A_{cap} := 2D \cdot B$	$A_{cap} = 288$	cross sectional area of cap, sq.in.	x 2 for the double cap
$L_p := 120$	effective length of pile, inches, taken as exposed length plus 1/2 penetration		
E := 1850	modulus of elasticity, in bending and axial compression, ksi		
$E_T := \frac{E}{80}$	$E_T = 23.125$	modulus of elasticity, transverse (taken as E/80)	
$\overset{w}{G} := \frac{E}{16}$	G = 115.625	modulus of elasticity, shear (taken as E/16)	

DEFLECTION COEFFICIENTS (deflections of cap, due to unit loads)

Due to R=1

$$q_a := \frac{1}{24E \cdot I} \left[b^3 - \frac{b \cdot a^2}{2} - 6 \cdot (30)^2 \cdot b + 30 \cdot a^2 + 4 \cdot (30)^3 \right] + \frac{0.6 \cdot (b - 60)}{A_{cap} \cdot G} \quad q_a = 0.01$$

$$q_b := \frac{1}{24 \cdot E \cdot I} \left[\left[\left[3 \cdot b^2 - a^2 - 12 \cdot (30)^2 \right] \cdot \left(\frac{b}{2} - c_p \right) - 4 \cdot \left(\frac{b}{2} - c_p \right)^3 + \frac{1}{a} \cdot \left(\frac{a}{2} + 30 - c_p \right)^4 \right] \right] \dots$$

$$+ \frac{0.6}{A_{cap} \cdot G} \cdot \left[b - 60 - a + \frac{1}{a} \cdot \left(\frac{3 \cdot a - 60}{2} + c_p \right) \cdot \left(\frac{a + 60}{2} - c_p \right) \right] \quad q_b = 7.871 \times 10^{-3}$$

Due to Xa=1

$$r_a := \frac{1}{48E \cdot I} \cdot b^3 + \frac{0.3}{A_{cap} \cdot G} \cdot b \quad r_a = 7.653 \times 10^{-3}$$

$$r_b := \frac{1}{48 \cdot E \cdot I} \cdot \left(\frac{b}{2} - c_p \right) \cdot \left[3 \cdot b^2 - 4 \cdot \left(\frac{b}{2} - c_p \right)^2 \right] + \frac{0.6}{A_{cap} \cdot G} \cdot \left(\frac{b}{2} - c_p \right) \quad r_b = 5.248 \times 10^{-3}$$

Due to $X_b=1$

$$s_a := 2 \cdot r_b$$

$$s_a = 0.01$$

$$s_b := \frac{1}{6 \cdot E \cdot I} \cdot (b + 4c_p) \cdot \left(\frac{b}{2} - c_p\right)^2 + \frac{1.2}{A_{cap} \cdot G} \left(\frac{b}{2} - c_p\right)$$

$$s_b = 8.173 \times 10^{-3}$$

PILE SHORTENING AND COMPRESSION OF CAP

$$u := \frac{114.5}{E} \cdot \left(\frac{1}{14 - 0.011L_p} - \frac{1}{14}\right) + \frac{1}{2 \cdot E_T \cdot B} \cdot (\ln(B + 2 \cdot D) - \ln(B))$$

$$u = 2.44 \times 10^{-3}$$

DEFLECTION EQUATIONS for consistent deformations of cap and piles

Given

$$\left(r_a + \frac{3}{2} \cdot u\right) \cdot X_a + (s_a + u) \cdot X_b = (q_a + u) \cdot R$$

$$\left(r_b + \frac{1}{2} \cdot u\right) \cdot X_a + (s_b + 2 \cdot u) \cdot X_b = (q_b + u) \cdot R$$

$$\text{Piles} := \text{Find}(X_a, X_b) \rightarrow \begin{pmatrix} 0.51715399875437954844 \\ 0.53371581967511230798 \end{pmatrix}$$

RESULTS

Percentage for the middle pile

$$\text{Middle_Pile} := (100\text{Piles})_{0,0} \text{ float},4 \rightarrow 51.72$$

Percentage for a single intermediate pile

$$\text{Intermediate_Piles} := (100\text{Piles})_{1,0} \text{ float},4 \rightarrow 53.37$$

Percentage for a single outer pile

$$\text{Outer_Piles} := \frac{100 \cdot 2 - \text{Middle_Pile} - 2\text{Intermediate_Piles}}{2} \text{ float},4 \rightarrow 20.77$$

5-Pile Bent - Composite section
Taken from AREA 1953 Manual

Define Variables

$D := 24$	depth of pile cap, inches	dimensions reflect a fully composite shape
$B := 12$	width of pile cap, inches	dimensions reflect a fully composite shape
$R := 1$	live load taken by one bent, kips	
$c_p := 30$	distance of inner pile from centerline of bent, inches	
$b := 126$	distance between outer piles	
$a := 29$	width of stringer bearing on cap, inches (assumed uniform)	
$I := \frac{B \cdot D^3}{12}$	$I = 13824$	moment of inertia of cap, in ⁴
$A_{cap} := D \cdot B$	$A_{cap} = 288$	cross sectional area of cap, sq.in.
$L_p := 120$	effective length of pile, inches, taken as exposed length plus 1/2 penetration	
$E := 1850$	modulus of elasticity, in bending and axial compression, ksi	
$E_T := \frac{E}{80}$	$E_T = 23.125$	modulus of elasticity, transverse (taken as E/80)
$G := \frac{E}{16}$	$G = 115.625$	modulus of elasticity, shear (taken as E/16)

DEFLECTION COEFFICIENTS (deflections of cap, due to unit loads)

Due to R=1

$$q_a := \frac{1}{24E \cdot I} \left[b^3 - \frac{b \cdot a^2}{2} - 6 \cdot (30)^2 \cdot b + 30 \cdot a^2 + 4 \cdot (30)^3 \right] + \frac{0.6 \cdot (b - 60)}{A_{cap} \cdot G} \quad q_a = 3.47 \times 10^{-3}$$

$$q_b := \frac{1}{24 \cdot E \cdot I} \left[\left[\left[3 \cdot b^2 - a^2 - 12 \cdot (30)^2 \right] \cdot \left(\frac{b}{2} - c_p \right) - 4 \cdot \left(\frac{b}{2} - c_p \right)^3 + \frac{1}{a} \cdot \left(\frac{a}{2} + 30 - c_p \right)^4 \right] \right] \dots$$

$$+ \frac{0.6}{A_{cap} \cdot G} \cdot \left[b - 60 - a + \frac{1}{a} \cdot \left(\frac{3 \cdot a - 60}{2} + c_p \right) \cdot \left(\frac{a + 60}{2} - c_p \right) \right] \quad q_b = 2.762 \times 10^{-3}$$

Due to Xa=1

$$r_a := \frac{1}{48E \cdot I} \cdot b^3 + \frac{0.3}{A_{cap} \cdot G} \cdot b \quad r_a = 2.765 \times 10^{-3}$$

$$r_b := \frac{1}{48 \cdot E \cdot I} \cdot \left(\frac{b}{2} - c_p \right) \cdot \left[3 \cdot b^2 - 4 \cdot \left(\frac{b}{2} - c_p \right)^2 \right] + \frac{0.6}{A_{cap} \cdot G} \cdot \left(\frac{b}{2} - c_p \right) \quad r_b = 1.758 \times 10^{-3}$$

Due to $X_b=1$

$$s_a := 2 \cdot r_b$$

$$s_a = 3.516 \times 10^{-3}$$

$$s_b := \frac{1}{6 \cdot E \cdot I} \cdot (b + 4c_p) \cdot \left(\frac{b}{2} - c_p\right)^2 + \frac{1.2}{A_{cap} \cdot G} \left(\frac{b}{2} - c_p\right)$$

$$s_b = 2.935 \times 10^{-3}$$

PILE SHORTENING AND COMPRESSION OF CAP

$$u := \frac{114.5}{E} \cdot \left(\frac{1}{14 - 0.011L_p} - \frac{1}{14}\right) + \frac{1}{2 \cdot E_T \cdot B} \cdot (\ln(B + 2 \cdot D) - \ln(B))$$

$$u = 3.36 \times 10^{-3}$$

DEFLECTION EQUATIONS for consistent deformations of cap and piles

Given

$$\left(r_a + \frac{3}{2} \cdot u\right) \cdot X_a + (s_a + u) \cdot X_b = (q_a + u) \cdot R$$

$$\left(r_b + \frac{1}{2} \cdot u\right) \cdot X_a + (s_b + 2 \cdot u) \cdot X_b = (q_b + u) \cdot R$$

$$\text{Piles} := \text{Find}(X_a, X_b) \rightarrow \begin{pmatrix} 0.46131457129248508745 \\ 0.46977829101440272837 \end{pmatrix}$$

RESULTS

Percentage for the middle pile

$$\text{Middle_Pile} := (100 \cdot \text{Piles})_{0,0} \text{ float}, 4 \rightarrow 46.13$$

Percentage for a single intermediate pile

$$\text{Intermediate_Piles} := (100 \cdot \text{Piles})_{1,0} \text{ float}, 4 \rightarrow 46.98$$

Percentage for a single outer pile

$$\text{Outer_Piles} := \frac{100 \cdot 2 - \text{Middle_Pile} - 2 \cdot \text{Intermediate_Piles}}{2} \text{ float}, 4 \rightarrow 29.96$$